

UNIVERSITY OF NAPLES "FEDERICO II"



Department of Industrial Engineering - Aerospace Section

Doctorate School in Industrial Engineering

Ph.D. Course in Aerospace, Naval and Quality Engineering

XXVIII cycle

Expedient Repair of a Battle-Damaged Composite Fixed-Wing Aircraft

Research Supervisor:

Prof. Leonardo Lecce

The Chairman of the Ph.D. School:

Prof. Luigi De Luca

Candidate:

Marco Barile

May 2016

...to my lovely family

Index

Chapter 1 - Damage and Repair of composite structure (review of literature).....	8
1.1. Damage and Repair of Aircraft composite structures	8
1.1.1. Repair Types	11
1.1.2. Failure Criteria for Composites	12
1.2. Bonded Joint Repair	15
1.2.1. Scarf-Tapered Joint	19
1.2.1.1 Scarf Joint Geometry	20
1.2.1.2. Scarf Adherends and Adhesive	21
Chapter 2 - Aircraft Battle Damage Repairs.....	23
2.1. Aircraft Battle Damage Assessment and Repair (ABDAR) Technical Manual ...	23
2.2. Damage Assessment	24
2.3. Structures Description	24
2.4. Damage Categories	26
2.5. Damage Limitations	26
2.6. Materials	26
2.7. Typical Repairs	26
2.8. Safety Factors.....	27
2.9. Repair Facilities	27
2.10. Material Handling and Storage	28
2.11. ABDR Trailer	29
2.12. Battle Damage Repair Steps.....	29
2.13. Bonded Repairs of Composite Structures in ABDR	31
Chapter 3 - FEA Investigation on Bonded Repairs	37
3.1. Design process and concepts: tensile load transfer.....	37
3.2. FEM of scarf joint developed by Wang [35].....	38
3.3. Theoretical Stress Analysis: Separation of Adhesive Stress Components	38
3.4. Development and Implementation of the FE Model for scarf-patch repaired composite laminates	41
3.5. Parametric study	47
3.6. Elastic-plastic analysis	55

Chapter 4 - Physical demonstrators of the repair efficiency	60
4.1. Identification and redesign of the test articles that will be subjected to battle-field damages	60
4.2. Manufacturing of the test articles using RTM process	62
4.3. Inspection Report.....	66
4.4. Ballistic tests performed by US team, aimed to define the damage scenario..	67
4.5. Relevant considerations about the location of the damage and loading tests	69
Chapter 5 – Design and implementation of the repair for a Battle-Damaged Composite Fixed-Wing Aircraft	70
5.1. Finite Element Analysis and Modeling	70
5.2. Elastic Analysis	72
5.3. Elastic-plastic Analysis.....	73
5.4. FE Modeling of Progressive Failure for Bonded Joints.....	75
5.4.1. Numerical approach.....	76
5.4.2. Undamaged Panel	77
➤ Progressive Failure Analysis (PFA).....	79
➤ Non-linear Static Analysis.....	83
5.4.3. Damaged, Repaired with full accessibility and Repaired with limited accessibility to damaged part	84
5.4.4. Results	91
5.4.5. Implementation of the repair for COMPRIP project.....	93
CONCLUSIONS AND FUTURE DEVELOPMENTS	95
Acknowledgements.....	97
References.....	98

Introduction

The ever-growing application of composite materials on primary and secondary structures of the latest-generation military aircrafts, poses the Expedient Repair (ER) methods in a key position in the outcome of a war conflict.

The concept of aircraft ER, more commonly known as Aircraft Battle Damage Repair (ABDR), dates back to World War I, when the United States Air Service used parts from French farm machineries in order to keep aircraft flying. Despite a continuous evolution in strategy through a subsequent World War, a Cold War, multiple conflicts, and modern irregular warfare, the overall mission of ER remains constant [1].

ER procedures are aimed to ensure to commanders the resources needed to complete their missions, when battle-damages occur. Such techniques should ensure that battle-damaged aircrafts continue to fly, after the repair, up to the next scheduled maintenance, even with some limitations (i.e. limitation in maneuvers and/or maximum speed). Hence, given the evolving demands of combat and technology, ER concepts of operations are constantly required to adjust.

Within this context, the present thesis, based on a numerical-experimental approach, was aimed to assess the effectiveness of ER concepts in case of a fixed-wing composite aircraft, subjected to battle-field damage.

The research was carried out within project called "COMPRIP", a contract between the Department of Industrial Engineering - Aerospace Section and Italian Ministry of Defense - Segretariato Generale della Difesa e Direzione Nazionale Armamenti - Direzione degli Armamenti Aeronautici e per l'Aeronavigabilità - Ufficio Tecnico Territoriale di Napoli.

All activities were conducted following decisions agreed in the frame of "*Aircraft Expedient Repair (AER)*" Program by a Consortium including experts coming from Armed Forces of US, Germany, France and Italy. The objective of AER Project is to develop and exchange aircraft Expedient Repair techniques, procedures, and methodologies that will enhance the ER capabilities of the contributing participants individually and collectively, thus improving operational aircraft performance through restoring full operational capability of composite structures while reducing repair costs.

The part of the AER Program related to the present thesis included mainly the identification, re-design and manufacturing of 6 physical demonstrators by Italian team, the performing of ballistic tests on one of demonstrators by US team in order to identify a damage scenario to agree with all partners, then each partner involved in the program was requested to perform a proper repair on the assigned panel and at last, all the repaired panels will be tested by French team. Loading tests will be performed also on a integer specimen (reference panel) and on a damaged one, in order to assess the efficiency of the repair through an assessment

based on the comparison of experimental tests.

Thesis work starts with a review of literature on the type of damages and conventional/unconventional repair procedures of aircraft composite structures. Several preliminary FE investigations on bonded repairs were performed to define a set of guidelines to use in the design of bonded repairs. It is worth to point out that no Structural Repair Manual (SRM) was available in the test case.

After this phase, following the decisions agreed by partners of AER Program, a set of structural demonstrators (flat composite stiffened panels representative of lower wing skins) were identified, redesigned and manufactured using RTM process. The repair scenario identified concerned a large representative and challenging damage condition that required a structural repair. The numerical assessment involved a relative comparison of four models: pristine, damaged with simulated ballistic damage, repaired with full accessibility and with limited accessibility to the damaged composite structure. For the full access condition, a scarf repair (adhesives and filler composite patch) was taken into account, while for limited accessibility condition, a coupling of bonded patch and bolted substantiation was used. A versatile predictive model applicable to the design of repairs in case of conventional (as reported in common SRMs) and unconventional damages, was herein developed and implemented with the aim to investigate stress and strain concentration, the failure initiation and failure progression mechanisms of involved composite structures. Even if numerical results have shown that damage would cause significant stiffness and strength reduction with respect to the pristine condition, the design of a suitable ER, both in case of full and limited access to the damaged part, has demonstrated the capability to sufficiently restore the stiffness and static strength of the component. Since the partners of AER Program agreed to perform loading tests on the damage condition to repair with the constraint of limited access (sole external access) to the damaged part, such repair was designed and implemented on the assigned demonstrator. At this moment, the numerical results have shown that application of ER concepts returns improved operational aircraft performance through restoring operational capabilities of composite structures while reducing repair costs.

Chapter 1 - Damage and Repair of composite structure (review of literature)

1.1. Damage and Repair of Aircraft composite structures

In recent decades, the knowledge and techniques required for repairs of advanced composite structures (such as boron-epoxy, graphite-epoxy, carbon-epoxy) have increased significantly. The repair processes or instructions for commercial aircraft are available from the commercial aircraft manufacturers (i.e. Boeing, Airbus). In case of a small damage, less than a maximum of 4 in. of the total area, the repair can be conducted using the Structural Repair Manual (SRM) issued by the Original Equipment Manufacturers (OEM) of the aircraft. For damage too large or too severe to be restored by the airline's shop, the advanced repair method and process should be advised or performed by the OEM. Repairs for aircraft structures, outside the scope of manufacturers SRM, have been successfully performed during past years, but in most cases there was almost no systematic studies of the effect of damage size on repair efficiency [2]. Damage analysis is, indeed, a vital step in the repair process and it should be an integral part of the repair process if optimum and cost effective results are to be obtained. Figure 1 depicts a typical repair process.

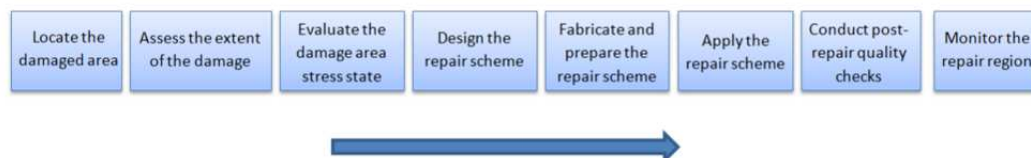


Figure 1 - Typical repair methodology process proposed by Heslehurst [3]

Ideally, main objective of a repair is to restore the damaged structure to its original functional capacity. Such restored capability is evaluated in terms of strength, functional performance, safety, cosmetic appearance and service life. A strength restoration to 80% of the tension ultimate allowable [4] is usually considered sufficient to cover the most unusual cases, while the compression ultimate allowable is rarely used as the critical design allowable. The most common technique used to restore a damaged structure is to repair or reinforce the damaged zone with splice or doubler made of a material having a strength and stiffness higher with respect to the original (parent) material. On the contrary the earlier technique, employed to repair advanced composite materials, was based on an external patch repair method such as adhesively-bonded. Differently from the former type, this kind of repair presents the most efficient results, if they are correctly designed and executed. The principal defect categories for composite

structures, defined by Heslehurst [3], are matrix cracks, in-plane holes and delaminations, as shown in Figure 2. Generally, composite structures experience a local loss in stiffness for transverse matrix cracks whereas holes lead to a reduction in strength due to stress concentration effects and delaminations may lead to structural instability when the component is loaded in compression or in shear.

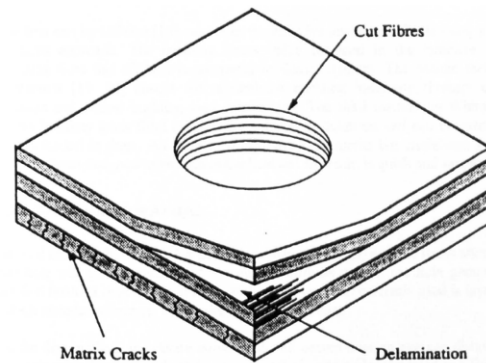


Figure 2 - Principal damages in composite structures

The first step to realize a good repair is the analysis of the stress state around the damaged area and the selection of a suitable failure criteria to use in the design phase. Composite laminates are commonly exposed to combined in-plane and out-of-plane loadings. Given this complexity, it is often very difficult to use closed form analysis techniques to evaluate accurately the stress distribution in the damaged structure, because the stress state in composite materials is in three dimensions. This cause the understanding of failure initiation and progression of components, subjected to common load case encountered in flight, very difficult, but crucial to prevent premature collapse of the structure. Most of the analyses carried out for repair programs were based on closed form semi-empirical solutions. Several examples were presented by Volkersen [5] and Goland-Reissner [6]. Due to the limitations encountered with analytical methods, the need to look elsewhere for better solutions is very strong. For this reason alternative numerical methods were suggested [7] and they include finite elements analyses, finite differences or boundary elements solutions. In general, currently used repair technologies for composite structures based on external patch bonding are mainly of two types:

- 1) The use of 'soft' patches: patches are made up from prepreg layers and cured directly into the underlying structure. An additional co-cured adhesive layer could be included;
- 2) The use of 'hard' patches: patches made of cured prepreg are adhesively bonded to the prepared damaged area.

The 'soft' patch repair procedure is technically more complicated, 'hard' patches, instead, are quicker to install and the quality is more consistent. Gong e al. [8] found the use of a same diameter patch repair by the hard and soft techniques,

returns a difference in failure load of about 6%, in favor of soft patches. Once a few of fundamentals are understood, most composite repairs can be completed successfully, further extending the life of the part. For this purpose a simple key-stages flow chart is presented in Figure 3:

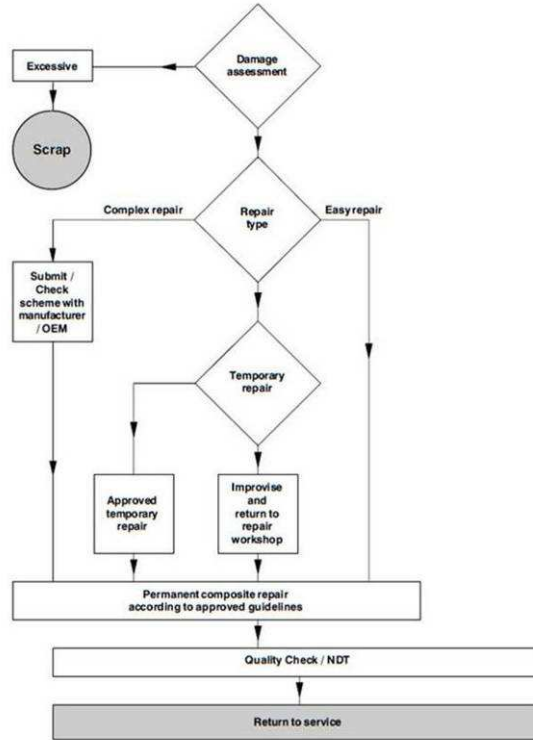


Figure 3 - Composite repair flow chart

The first and most important decision to take when a damage occurred is whether making a repair or scrap the damaged part. This decision is determined by considering the extent of repair needed to replace the original structural performance of the component. Other important considerations are the repair costs, the position and accessibility to the damaged area and the availability of suitable repair materials. The second stage is to evaluate the repair type, an easy repair does not affect the structural integrity of the component, instead a complex repair is needed when the damage is extensive. Best selection of materials would be to use the original fibers, fabrics and matrix resin, but the selection is constrained by the boundary conditions in which the repair has to be performed. Before returning to service, a quality check of the repaired part is always required and for comprehensive inspection of repaired parts a number of Non Destructive Tests (NDT) have to be performed. In addition to strength and stiffness requirements, when designing a repair, the stability is very important, if the structure is loaded primarily in compression or shear. This is the case of components as airframe panels which may buckle between major supports. Other structures such as stabilizers are designed primarily for stiffness, in bending and in torsion, to cope with aerodynamic loading. Repairs for such components will be

designed primarily to restore stiffness rather than strength. Thus the predominant criterion will be closely related to the primary function of the structure. Particular attention need to be paid in abrupt change in thickness and contours, because this will affect the aerodynamic features of any aircraft structure. Although the total weight added by a repair results insignificant compared to the aircraft gross weight, it is worth considering the weight being added in relation to the component functionality. At the end any repair scheme should consider the costs that will be involved in effecting it. These include aircraft downtime which should be minimized, repair personnel skills, facilities, tools and equipment as well as repair material costs.

1.1.1. Repair Types

A typical composite repair usually starts after damage detection. When a composite structure sustains damage in service, one of four levels of repair must be employed. Basic types of composite repair include:

- I. *Non-structural or cosmetic repair:* required when the damage is minor, but environmental protection is necessary to avoid further degradation. This type of repair will not regain any strength and is used only where strength is unimportant. An example of non-structural repair is presented in Figure 4.

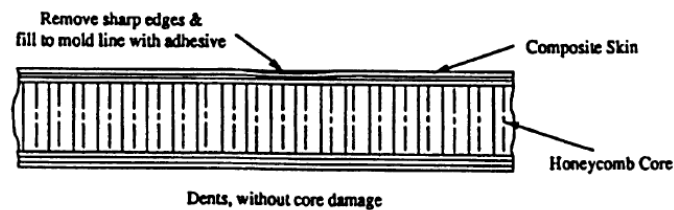


Figure 4 - Cosmetic repair

- II. *Semi-structural repair:* for damages more important than minor scratches. The damaged area is usually filled with an adhesive foam or a core replacement. This type of repair can regain some strength. Figure 5 depicts this repair type.

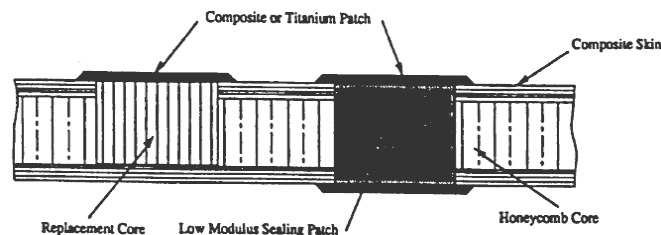


Figure 5 - Semi-structural repair

- III. *Adhesively bonded structural repair*: used for major damage. A patch is adhesively bonded over the damaged area, as illustrated in Figure 6. This repair should restore full structural properties.

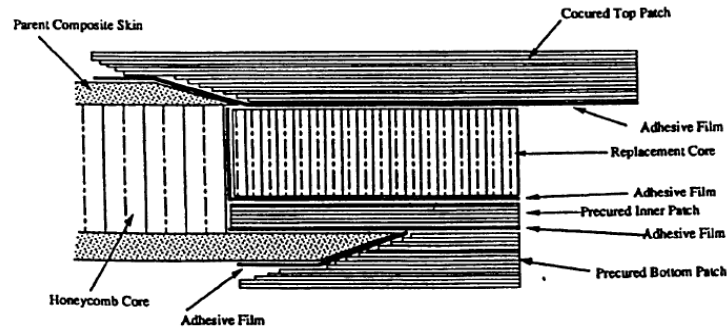


Figure 6 - Adhesively bonded structural repair

- IV. *Mechanically fastened structural repair*: also used for major damage. In this case, the patch is bolted to the parent structure. Figure 7 shows a schematic design of a mechanically fastened repair.

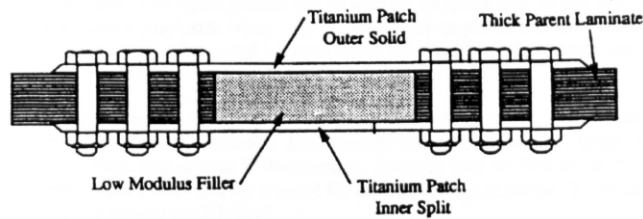


Figure 7 - Mechanically fastened structural repair

1.1.2. Failure Criteria for Composites

While designing a composite structure, it should be considered whether the selected material strength can sustain the estimated load or not. If the applied load level is higher than the capacity of the material to carry the load and if one of the stress in the natural axes exceeds the corresponding allowable stress, then failure occurs in the structure. The main characteristic of laminate strength theories is that they are expressed in term of single lamina strengths. In addition, they assume that the material is homogeneous and linear elastic to failure [9]. Currently, a large number of lamina failure criteria and laminate failure analysis methods are available to predict the response of the structure under applied multi-axial stress states. The accuracy of the failure criterion is the most crucial target to gain. The purpose of a failure criterion is to determine the strength and mode of failure of a unidirectional composite or lamina in a state of combined stress. Up to now, all the existing lamina failure criteria are basically of phenomenological nature. In composite structures, ultimate laminate failure occurs due the

propagation or accumulation of failure which initiate in a ply, as first ply failure, in the form of delamination of two layers, fiber breakage, matrix cracking and fiber-matrix debonding of layers due to the loads applied. Boundary conditions, geometry and the laminate definition also play a key role on the initiation and progression of failure. It should be taken into account that in a laminate, failure mechanisms are more complicated, hence a lamina failure criterion must be flexible enough to accommodate the more complicated nature of laminate analysis. Herein presented study gives emphasis to the effect of non-linearity on the failure initiation and progression. Inter-laminar failure is not considered since most inter-laminar failures are modeled by fracture mechanics based approach. However, delaminations can also be predicted by using strength or strain based failure criteria. Several theories are used to predict failure in composite materials are available in literature and the list of the most commonly used can be found in several works [10-11]. Generally, failure theories can be categorized into three main groups:

- Limit or Mode-Independent Criteria: These criteria predict failure load by comparing each stress σ_{11} , σ_{22} , and τ_{12} (or strains ϵ_{11} , ϵ_{22} , and γ_{12}), acting on a lamina along the principal material axes, to the corresponding strength in that direction. The theory points out that failure is deemed to have occurred if at least one stress component exceeds its corresponding strength. The failure is evaluated without defining the mode of failure, such as fiber or matrix failure. The simplest mode-independent polynomial failure criteria are the maximum stress and maximum strain criteria, they are also non-interactive criteria, since individual tensor components of stress or strain do not interact within the criteria. For example, failure prediction in transverse tension is not influenced by the presence of longitudinal shear [12]. Equations (1), (2) and (3) show an example of Maximum Stress Criteria:

$$\frac{\sigma_{11}}{X} = 1 \quad (1)$$

$$\frac{\sigma_{22}}{Y} = 1 \quad (2)$$

$$\frac{\tau_{12}}{S} = 1 \quad (3)$$

Where X,Y and S are respectively tensile (or compression) strength in fiber direction, tensile (or compression) in transverse direction and shear strength.

- Interactive Criteria: These criteria predict the failure load by using a single quadratic or higher order polynomial equation involving all stress (or strain) components. Their origins go back to von Mises distortional energy

yield criterion for ductile metals which was adapted to account for anisotropy in ductile metals. Failure is assumed when the equation is satisfied and if the failure index is higher than one. An interaction term is reported in the polynomial equation. Most common interactive failure criteria are Tsai-Wu [13] and Hill theories [14]. For further information it should be stated that one of the great drawbacks of the much used interactive criteria is that they lack any connection between failure predictions and physical phenomena. This has been the biggest criticism of the interactive theories which, according to Hart-Smith [15], are better suited to characterize homogeneous anisotropic solids than heterogeneous fiber polymer composite. An example of Hill Criterion is shown in Equation (4):

$$\frac{\sigma_{11}^2}{X^2} + \frac{\sigma_{22}^2}{Y^2} + \frac{\sigma_{11}\sigma_{22}}{X} + \frac{\tau_{12}^2}{S^2} \quad (4)$$

- Separate or Mode-Dependent Criteria: These criteria separate the matrix failure from the fiber failure and they predict a variety of failure modes such as fiber tensile failure, fiber compressive failure, matrix tensile failure, matrix compressive failure, and delamination using stress-based equations. Stress interaction varies from criterion to criterion. The Hashin, the Hashin-Rotem and the Puck are a few examples of mode dependent failure criteria.

It is difficult to determine which theory to use due to the lack of comprehensive experimental results. In wide terms the choice between a criterion and another should be taken considering material properties and load condition of the specimen under the magnifying glass. In this study, Hill failure theory is selected to perform a progressive failure analysis because it seems to be the best when strengths are equal in tension and compression and there is no explicit distinction between tensile strengths and compressive [16].

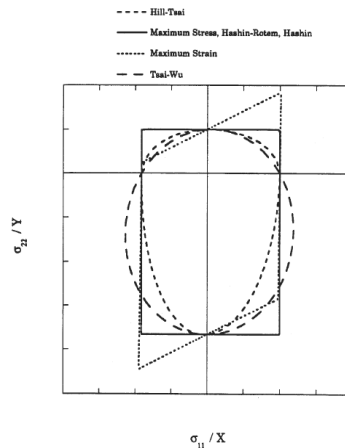


Figure 8 - Comparison of the most common lamina failure criteria

Figure 8 depicts a comparison among the most common failure theories. The Maximum Stress envelope is a simple rectangle bounded by the failure loads and the Maximum Strain envelope is close to that of the Maximum Stress but is slightly skewed due to the effect of Poisson's ratio. Both the Hill and Tsai-Wu criteria allow quadratic stress interactions; therefore, each has a curved failure envelope. As regards failure of adhesives in structural joints, the literature is very extensive, therefore just preliminary considerations will be faced up. It becomes natural to consider the maximum shear stress in the prediction of joint strength [17]. Another approach showed that the maximum peel stress could be used as a failure criterion for single lap joints [18]. Other possible criteria include the maximum shear strain criterion, the effective uniaxial plastic strain criterion and the maximum von Mises stress criterion. For all the maximum stress or strain criteria described, the problem comes from the maximum value of the failure parameter considered. There will always be a singularity at the ends of idealized bonded joints. The maximum strain for such a model will coincide with the value at the singularity and thus will vary greatly with mesh refinement. To overcome this mesh dependency, several researchers have resorted to the application of these criteria at a particular distance from the singularity or over a given zone. Charalambides et al. [19] proposed a weighted averaged maximum stress criterion where the adhesive thickness is used as the distance over which the maximum principal stresses are averaged and compared to the adhesive yield strength.

1.2. Bonded Joint Repair

Adhesive bonding is a material joining process in which an adhesive, placed between the adherend surfaces, solidifies to produce an adhesive bonding. These joints are an increasing alternative to conventional mechanical joints, providing many advantages over the last. They provide a more uniform stress distribution along the bonded area, which gives a higher stiffness and a better load transmission, they also present lower fabrication cost and improved damage tolerance. In addition, the adhesively composite bonded joints contain higher strength-to-weight ratio as to reduce the weight-penalty that usually happens to conventional joints.

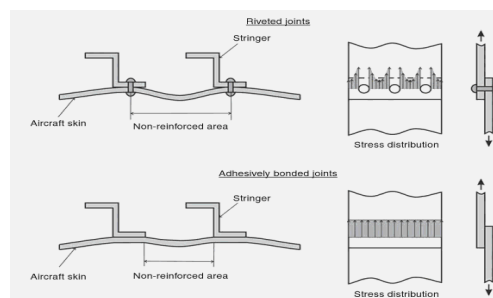


Figure 9 - Improved stiffness and stress distribution of adhesively bonded joints compared to riveted joints [20]

Bonded joints are frequently expected to sustain static or cyclic loads for considerable periods of time without any adverse effect on the load-bearing capacity of the structure and due to the polymeric nature of adhesives, adhesive joints provide good damping properties which enable to have high fatigue strength. The strength of a given type of joint depends, for a given type of load, on the stress distribution within the joint, which in turn depends on the joint geometry and the mechanical properties of adhesive and adherend. Another advantage is that adhesive can bond dissimilar materials with different thermal expansion coefficient because the adhesive flexibility can compensate the difference. Moreover they bond thin plates very efficiently, which is one of the major application of structural adhesives. Adhesive bonding is also associated with some disadvantages, such as the need to reduce peel stress because they concentrate the load in a small area fixing a poor joint strength. Anyway it should be noted that, often, joints made with high strength adhesives are more likely to fail prematurely in the composite before failure in the adhesive occurs. Furthermore the bonding is usually not instantaneous and the hardening needs temperature for many adhesives. This is a big economical issue. A wide variety of joints are available to the designer [21]. Commonly, adhesively bonded structural repairs share similar features with adhesively bonded joints and the prevalent configurations that have been applied to patch repairs in aerospace structures are single-lap joints, double-lap joints, stepped joints, and scarf joints (Figure 10).

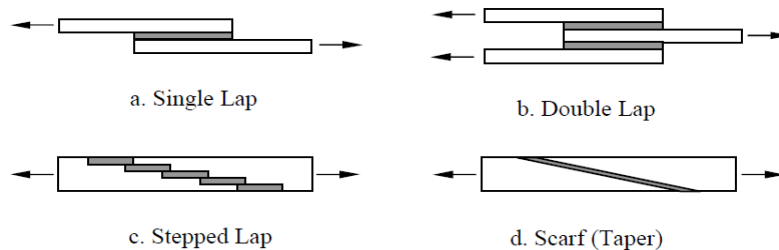


Figure 10 - Common types of joints used in Aerospace industry

Adhesively structural bonded repairs can also be divided into external patch repair (single and double-lap repair joints mainly) and flush patch repair (step and scarf joints). External patch repairs are relatively easy to apply under field conditions because they are less critical in nature. These repairs could be made with prepreg, wet layup, or pre-cured patch. External patches are usually stepped to reduce the stress concentration at the edge of the patch. Strength recovery between 70% and 100% can be achieved. They are used on thin structures and where there is limited back side access or substructure interference. To minimize peel and shear stresses at the ends of the patch, tapering could be used. Flush repairs are more time consuming because of the effort involved in preparing the surfaces. Scarf joints are the most difficult to realize because of their dimensional tolerances but they

provide the highest joint efficiency of all repair types. Comparing to single-lap shear joints, the double lap, the scarf and the stepped joints are designed to decrease the peel stresses. Adherend shaping is also used to decrease the peel stresses in the composite joints.

There are several different repair methods for laminates. The patch can be precured and then secondarily bonded to the parent material. This procedure most closely approximates the bolted repair. The patch can be even made from prepreg and then co-cured at the same time as the adhesive or using a wet layup repair.

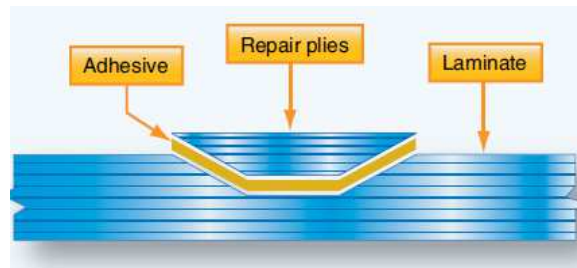


Figure 11 - Example of a pre-cured patch bounded to the parent material

The literature dealing with joining composite structures with adhesives is focused on investigating the bond strength. Topics of particular interest are: surface preparation, joint configuration, adhesive properties, environmental conditions, analytical and finite-element analyses of joints, test methods.

The surfaces play an important role in the bonding process and are, perhaps, the most important process governing the quality of an adhesive bond joint [22]. Bond strength can be significantly improved by surface treating the adherends prior to bonding. Surfaces must always be clean and dry and are often abraded or grit-blasted. However the most common misconception in surface preparation is that the only requirement for a good bond is a clean surface. A clean surface is a necessary condition for adhesion but it is not a sufficient condition for bond durability. Most structural adhesives work as a result of the formation of chemical bonds between the adherend surface atoms and the compounds constituting the adhesive. By increasing surface tension, increasing surface roughness, and changing surface chemistry, a more intimate bond can be formed, which allows for increase in strength and durability. The good design and analysis of the adhesively bonded joints requires inevitably analytical methodology to obtain accurate and truthful stress/strain distributions through the adherends and the adhesive. These analytical techniques were developed from continuum mechanics, plane strain/stress closed form solutions, 2-D and 3-D finite element methods and 2-D and 3-D variational approach based on solution [23]. The simplest analysis concerns the single-lap joint, one of the most common joints found in practice. In this analysis, the adhesive is considered to deform only in shear and the adherends

are considered to be rigid. The adhesive shear stress (τ) is constant over the overlap length and given by:

$$\tau = \frac{P}{b \cdot L} \quad (5)$$

where P is the applied load, b is the joint width and L is the overlap length. The value for the shear stress can be interpreted as the average shear stress acting on the adhesive layer. Volkersen's analysis [5] introduced the concept of differential shear. It was assumed that the adhesive deforms only in shear but that the adherends can deform in tension, because they are considered elastic and not rigid.

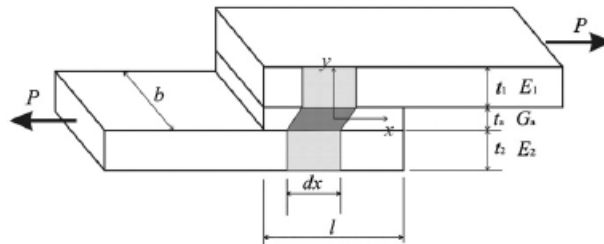


Figure 12 - Single-lap joint analyzed by Volkersen

These analyses are not very realistic due to many simplifications, but they represented a big step forward in the stress analysis of adhesively bonded joints. It is worth to underline some limitations of these analyses. Actually, they do not take into account variations of the adhesive stresses through the thickness direction, especially the interface stresses which are important when failure occurs close to the interface, and for peak shear stress, which occurs at the ends of the overlap and violates the stress-free condition. Earlier studies tried to overcome these issues: the adhesive shear stress was allowed to vary across the thickness, no matter how thin the adhesive may be, but the adhesive peel stress was maintained constant across the thickness. It was concluded that the main difference between the theories that include and those that ignore adhesive thickness effects occurs at the ends of the overlap: the maximum shear stress increases and the peel stress decreases with the inclusion of this effect [24-25]. Wah was the first to consider laminated composite adherends. The laminated adherends were symmetrical about their mid-surface. The adhesive shear stress was constant through the thickness whereas the adhesive peel stress was allowed to vary and it was modeled in two ways, with linear [26] and nonlinear behavior [27]. In the first case, the adhesive was assumed to be a homogeneous, isotropic and linear elastic material, modeled as continuously distributed linear tension/compression and shear springs. In the second case the adhesive plasticity has been included in order to correctly simulate the stress and strain distributions when the adhesive yields. Adherends

can yield too, and the analysis needs to account for this behavior, if realistic failure loads are to be predicted. The Adams and Mallick analysis [28] also considered elastic-plastic adhesive behavior. The authors took into account the influence of the adhesive plasticity by using an iterative procedure. Successive load increments are applied until the maximum stress or strain reaches some failure condition or until the full load has been applied. This brought them to introduce a linear ‘effective modulus’ solution, equating the energy under the stress–strain curve.

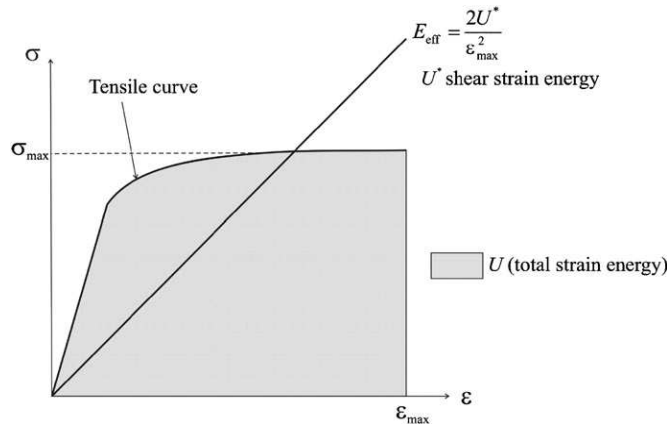


Figure 13 - ‘Effective modulus’ solution proposed by Adams and Mallick

1.2.1. Scarf-Tapered Joint

Scarf repair is the preferred method for repairing composite structures, especially when externally bonded patches can no longer meet the stiffness and strength requirements or when there is the need for a flush surface to satisfy aerodynamic or stealth requirements. Present designs of scarf repairs are based on two-dimensional analyses of scarf joints, assuming a uniform stress distribution along the scarf. The use of a patch material with dissimilar properties to the parent material is normally avoided, it was shown that if the patch materials are different in mechanical properties with respect to the parent materials, a large stress concentration would be introduced into the adhesive layer [18].

A scarf repair can restore a much higher strength than a bonded overlap repair, because the adhesive stresses along the scarf joint do not suffer from the considerable stress concentrations present in overlap repairs. Strain along the bondline of a scarf joint is almost constant, in contrast with that pertinent to an overlap joint. Hence, scarf joints have the advantages of higher repair efficiency and the absence of aerodynamic disturbance.

Disadvantages are the higher costs, due to difficulties inherent to the repair process and a large repair area needed because of the low scarf angles used to obtain high strength values of the repaired joint.

The parameters which more affect the quality of a repair are scarf angle, adhesive thickness, number of plies of adherends and its stacking sequence [29].

The strength capacity of a scarf joint subject to unidirectional tensile loading is highly dependent upon the limit of adhesive bond plastic collapse. This is because all load is transferred through the adhesive. Due to these facts, primary consideration in the design of the scarf joint is the adhesive bondline and associated adhesive parameters.

1.2.1.1 Scarf Joint Geometry

One of the most important parameter that affects the efficiency of a scarf joint is represented by the scarf angle, the acute angle that the adhesive bondline makes with surfaces of adherend material. In this joint, the adherends are mated together with adhesive, forming the adhesive bond line.

The interface between the two is known as the adherend/adhesive interface.

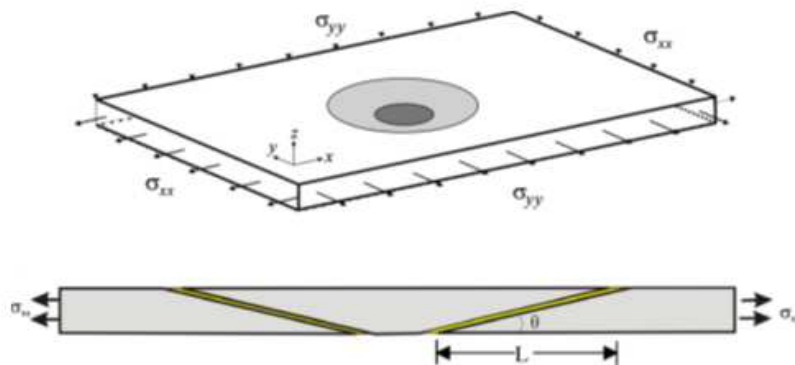


Figure 14 - Typical structural models for a scarf repair and an equivalent scarf joint.

For highly loaded advanced composite structures, taper angles ranging from 3° to 7° are often required to restore a damaged structure to its as-designed ultimate strength, these small angles lead to a large removal of the damaged material, especially in the case of thick laminates, by drilling a conical hole and then adhesively bonding increasing diameter patch layers in order to fill the damaged region. Increasing the scarf angle was found to decrease the joint strength, as the bond length is reduced [18]. Furthermore adhesive stresses cannot be uniform without constant scarf angle for isotropic, identical adherends; only when the scarf angle is constant, adhesive stresses are uniform.

1.2.1.2. Scarf Adherends and Adhesive

Composite scarf joints imply numerous considerations in design of the joint, particularly the non-isotropic adherends behavior makes the analysis more complicated. Current design methodology [30] recommends that a scarf composite repair should match, ply-by-ply, the original structure.

Matched adherends, make the adhesive stresses along the scarf more uniform [31] and the joint is supposed to attain its maximum strength when the average shear stress reaches the ultimate shear strength of the adhesive. For isotropic adherends, the design and analysis of adhesively bonded joints is now a relatively matured discipline [21]. Differently from scarf joints between isotropic metallic adherends, significant stress concentrations have been found to exist in scarf joints between composite adherends of identical lay-up [32], with the maximum stresses occurring adjacent to the ends of 0° plies; since fibers themselves do not cross the bondline, the large stiffness disparity between the adhesive and the composite plies, due to stacking sequence, induces significant stress variations along the scarf even with constant scarf angle. Therefore, the design of an optimum scarf repair for composite structures is complex due to the large number of material and geometric parameters that influence the joint performance.

As it is well known, to achieve a good bonding, first it is necessary to start with a good adhesive. The main components of a structural adhesive usually consist of two compounds which chemically react to produce a polymer. Upon curing, this polymer hardens to form a cohesive solid which is capable of transferring structural load (in the case of the scarf joint, this is from one adherend to the other). The adhesive selection process is difficult as there is no universal adhesive that will fulfill every application, and the selection of the proper adhesive is often complicated by the wide variety of available options. However, adhesive selection includes many factors, such as type and nature of substrates to be bonded, cure method and the expected environments and stresses that the joint will face in service. Thus, general knowledge of the behavior of adhesives must be supplemented. In composite adhesive joints, according to the standard ASTM D5573 [33], there are six typical characterized modes of failure. They are: adhesive failure, cohesive failure, thin-layer cohesive failure, fiber-tear failure, light-fiber-tear failure, stock-break failure or mixed failure.

At the end the increased usage of high-temperature resin-matrix systems for composite materials has necessitated the development of compatible and equally heat stable adhesive systems.

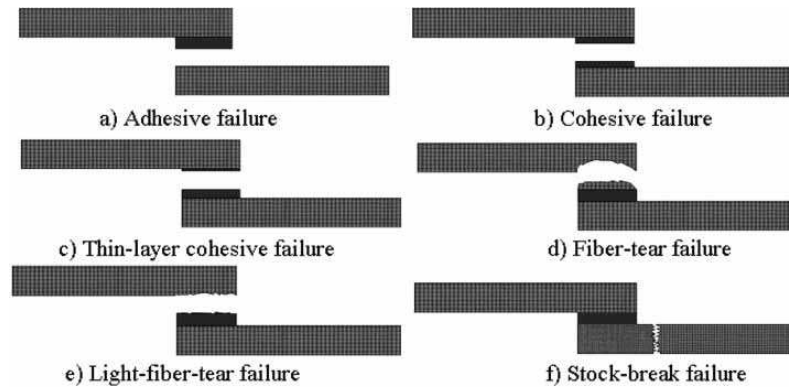


Figure 15 - Possible failure modes in bonded joints between composite adherends.

Epoxy adhesives that are very frequently used for the composite matrixes, are commonly used to bond composites based on epoxy matrix thanks to the compatibility between resin and adhesive.

Chapter 2 - Aircraft Battle Damage Repairs

In this chapter we will focus on the so-called Air Battle Damage Repairs (ABDR), the starting point of the Expedient Repairs (ER). In times of conflict such as the Operation Desert Storm, the damage to loss ratio for the USA Aircrafts A-10 and F-16 was 6:1 and 1.4:1 respectively in absence of any more recent (classified) data from the latest war in Iraq. The ability to effectively repair a critical sized damage without having to remove a primary or secondary aircraft component was considered both desirable and cost effective. Damage inflicted in the course of combat is by its very nature quite different from the encountered during peacetime. The time and logistics constraints during conflict limit the time and extend of repairs that can be implemented. Because of this, ABDR is generally considered separately from other repair activities. Nevertheless, the key decisions that must be made are the same: does the damage need to be repair? And if so, how it can be done in the shortest time span? Generally, the aircraft composite components are subjected to several types of damages including surface thermal blisters, internal voids, delamination, surface punctures, dents and broken fibers, however ballistic (battle) damage may take the form of jagged edged through-thickness holes surrounded by a region containing delaminations, matrix cracking and plies peeled from the back surface. Usually the monolithic carbon/epoxy structures situated in the underside of military aircrafts are prone to ballistic impact.

2.1. Aircraft Battle Damage Assessment and Repair (ABDAR)

Technical Manual

Battle Damage Repair (BDR) can play a key role in the outcome of a war. Promptness, reliability, and effectiveness of repairs affect the availability of aircraft for combat. In an air combat, an efficient Aircraft Battle Damage Repair (ABDR) is a key element in maintaining high sortie rates considering the limited availability of spares. Figure 16 shows the availability of aircraft for combat with and without ABDR, especially it is shown that an excellent repair capability is defined as returning 50 percent of damaged aircraft to combat in 24 hours and 80 percent in 48 hours. Figure 16 shows that a good repair capability can quadruple the number of aircraft after 10 days of combat. As an instance, the Israeli Air Force has developed an efficient system along with repair techniques for ABDR and demonstrated the effectiveness of their ABDR system in 1973 Yom Kippur War. Figure 17 shows the effect of rapid repair on the availability of certain Israeli aircraft for combat. The use of rapid temporary repair techniques enabled Israeli Air Force to return 72 percent of the damaged aircraft to combat within 24 hours [34].

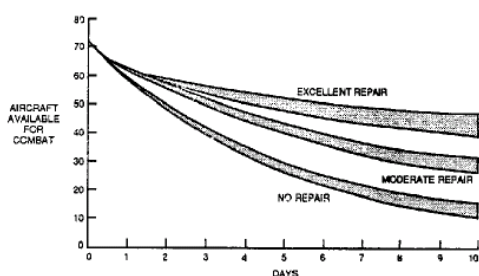


Figure 16 - Aircraft availability with and without repairs

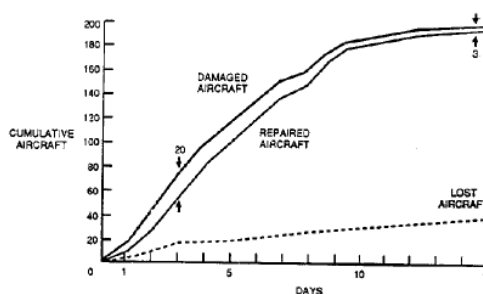


Figure 17 - Battle Damage Repair results of Israeli Air Force

The requirements of Aircraft Battle Damage Assessment and Repair (ABDAR) Technical Manual are discussed in United States Military Specification MIL-PRF-87158B. Various requirements of battle damage repair such as repair of structural components, electrical and mechanical systems, fuel system, wiring, etc., are discussed in the MIL specifications. The Aircraft Battle Damage Assessment and Repair, MIL-PRF-87158B specifies the requirements of ABDAR technical manual so that users can efficiently and reliably take action on the disposition of the damaged aircraft.

Since it is not feasible to discuss all the requirements of the ABDAR manual as per [34], certain essential features and requirements from the reference are mentioned in the next paragraphs because on one hand thanks to their identification, it was easier to perform the design and implementation of the repair foreseen by AER Project, while on the other hand they will be reported to the partners with aim to define a set of suitable experimental procedures to include in a shared document, precursor of an Expedient Repair Manual.

2.2. Damage Assessment

Damage limits, repair guidelines, instructions, and references to applicable documents which enable an assessor to make the correct decision regarding deferment or repair shall be provided to the assessor. Previous data from similar aircraft shall be included in the manual.

2.3. Structures Description

MIL-PRF-87158B specifies that a brief description of the aircraft (rotary or fixed wing) structure shall be given with three dimensional illustrations of various zones. A brief explanation of zones shall be given. These zones shall be selected such that they are essentially repair-independent and physically distinct based on

structural features/equipment commonality. Five separate categories shall be used to categorize all external and internal structural members as follows:

- Category I, primary airframe structure - These members shall include, but are not limited to: bulkheads, main spars and ribs; structural torque boxes in highly stressed areas; stress panels which serve to stabilize tension and compression loads between primary load carrying members; and any group of structural members in which a single failure may result in the immediate loss of an aircraft at the maximum expected load. For this category, limits shall be listed for all three damage classes.
- Category II, secondary structure - This structure serves to transfer aerodynamic and other loads to the primary structural members. This structure primarily consists of external skin panels that are not considered primary stress panels, intermediate ribs, stringers, and formers which only serve to transfer load to primary members. Repair of these structural members does not require restoration of original design strength and stiffness within the content of war time environment. Limits shall be listed for all damage classes.
- Category III, nonessential structure - Nonessential structure such as doors, panels, tips, fairings, etc., which may be extensively damaged or completely missing and no repair or replacement is required to maintain the airworthiness or mission capability. Limits shall be listed for all damage classes.
- Category IV, special structure - These are special structures which are non-structural, but essential for safe flight and aircraft performance. Repair requirements for these structures are based upon considerations other than strength; such as aerodynamics, pressurization or engine performance. Limits shall be listed for all damage classes.
- Category V, repair restrained structure - These structures are not feasible to repair under battle damage restraints due to design and shape. These structures include all complex machined or forged parts and irregular shaped extrusions, channels, etc. Limits shall be listed for A and C damage classes.

2.4. Damage Categories

The damage is classified in the following 3 categories:

- Class A, degraded capability - damage limits that result in establishing operational restrictions when repair is not accomplished. The only purpose of this damage class is to permit the restricted use of the aircraft when time to repair is critical factor;
- Class B, repairable damage - damage limits which permit structural repairs within 24 hours or less, per single repair. Repairs to restore static strength and stiffness of damaged component for Category I, II, and IV structures, shall restore full operational capability of the aircraft for at least one more flight;
- Class C, acceptable damage - Damage limits which do not impose any operational restrictions on the aircraft, when repair is not performed. A minimal cleanup of damage may be required (e.g., stop drill, stress reduction, etc.).

2.5. Damage Limitations

Damage limitations for all Categories I, II, IV, and V structures shall be provided. The limitations shall include the size and location for classes A, B, and C damage up to which repairs can be made under ABDAR constraints. The maximum number of repairs and the limits for the proximity of multiple damages to a given structural component shall be included. Guidelines, instructions and illustrations for accomplishing repair shall be provided.

2.6. Materials

Repairs shall be designed using ABDAR Tool/Material Kits Listings approved by authorities. Preferred materials required for special repairs shall be specified. A consolidated list by part numbers shall be included. Special materials such as bonding materials, primers, sealants, etc. shall be included. All items shall be identified using Military/Federal specifications.

2.7. Typical Repairs

Typical repairs that are common to two or more zones shall be described. Typical ABDAR repairs include repairs that will provide full or partial mission capability.

Such typical repairs shall be provided for all aircraft systems, subsystems, and components. Repair steps influencing survivability, vulnerability or radar cross-section characteristics shall be identified.

2.8. Safety Factors

Analysis supporting battle damage structural repairs shall be based on ultimate strength. Repairs shall have stiffness compatible with original structure. However, service life, corrosion, and aesthetic considerations may be overlooked in exchange for a rapid repair procedure. Strength related calculations for unrepaired structure shall be made to obtain maximum utilization under war time conditions and accommodate worst case contingencies. Calculations shall be made to determine the static strength of the damaged and unrepaired structure. Operations of the aircraft should be restricted to two-thirds of that strength or to restriction engendered by damage tolerance residual strength considerations, whichever is lower. Safety of flight primary structure shall provide for adequate residual strength in the presence of cracks from damage remaining in the structure. The size and types of remaining damage that are to be assumed shall be established for each primary structural member in each zone for each damage category. Structure with assumed remaining damage shall be capable of sustaining limit load or 1.2 times that maximum load associated with any operating restriction. Care shall be exercised to assure that deformation that would degrade the load carrying or operating capability will not occur at the operational restriction.

2.9. Repair Facilities

Having proper repair facilities are perhaps the most important requirements for any repair operation. These requirements are governed by the type of repairs to be performed. For bonded composite repairs the facilities shall include- freezers, ovens, clean room areas, environmental control of the temperature and humidity, electrical and pneumatic power. Necessary equipment such as bonding fixtures, assembly jigs, machining tools, and vacuum pumps should be available. Facilities for handling hazardous materials are needed. Materials for repairs that need to be stocked include prepreg, adhesives, honeycomb core, bagging film, sealants, sheet metal, fasteners, etc. The most important aspect of any repair facilities is having right personnel with necessary knowledge and experience to perform reliable repairs efficiently to meet design requirements. The skills of personnel shall include- machining, bonding of composites, cutting, stacking, bagging, and curing of prepreg.

2.10. Material Handling and Storage

Polymer matrix prepreg materials have to be handled properly and stored in proper environments to assure the quality of the material. The storage requirement and shelf-life are established by the manufacturer based on the chemical composition, and mechanical properties at the time of storage in the controlled environments. Thermoset matrix composites and adhesives are stored in sealed bags at 0°F (-18°C). The storage process retards the “aging” or partial curing of polymer and extends the shelf-life. The sealed containers or bags prevent the condensation during the storage. When the prepreg is removed from the freezer for laminate fabrication, it is allowed to thaw in the sealed containers until it reaches ambient conditions. Polymer matrix prepreg generally has a backing sheet that improves the handling quality and protects prepreg from handling damage. Non-woven unidirectional tapes can otherwise split between fibers. Clean, white lint-free cotton gloves are recommended when handling prepreg material to prevent transfer of skin oil to the material. Splinters are not present in the uncured prepreg; however, caution should be exercised to avoid penetration of small diameter fibers into the hand from prepreg edges. A clean room environment similar to that for bonding process is required when prepreg is to be handled for fabricating laminates. Prepreg must be shielded from impurities and moisture. Fabrication area must be enclosed and doors to remain closed even when area is not in use. Temperature and humidity should be controlled within the limits shown in Figure 18.

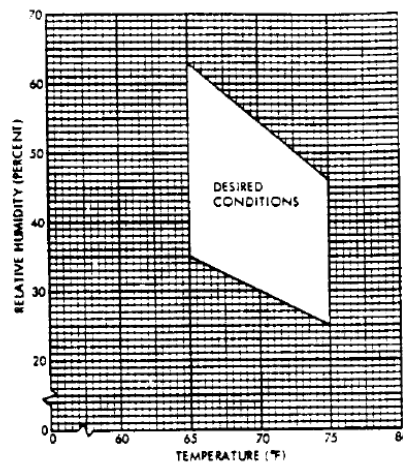


Figure 18 - Composite Fabrication Area Requirements [34].

2.11. ABDR Trailer

United States has developed Combat Logistics Support Squadron (CLSS), designed to provide support in the areas of maintenance, transportation, and supply. CLSS teams train personnel to meet mission requirements irrespective of environmental conditions. To meet ABDR requirements CLSS has established trailers with a limited amount of specialized tools and equipment to support an authorized aircraft. These trailers have been developed with mobility in mind. A typical ABDR trailer has dimensions - L 122" (3.1 m) x W 84" (2.13m) x H 88" (2.24m). The weight is about 5,000 pounds (2,273 Kg) fully stocked plus a 1,300 pound (591 Kg) composite kit. A typical generic ABDR trailer has common hand/power tools, fasteners, hoses, tubing, metal sheets and angles. Composite kit in the trailer contain- hand/power tools, dust vacuum, heat repair bonder, surface treatment material, composite materials, and other materials required for fabrication of specific composite parts.

2.12. Battle Damage Repair Steps

A typical battle damage repair process will involve the following steps [34]:

a. Assess the Damage

Assessing the damage is the first step in any ABDAR process. When an aircraft is identified with ABDR discrepancy, a Debrief Action and a Walk-around Action are created. During the Walk-around Activity zones that contain damage are identified by the walk-around assessor. The Damage Assessor (DA) will debrief the aircraft pilot, diagnose the extent of damage from reported symptoms, assess the physical evidence of the damage, and investigate any secondary damage that might have occurred. After completing the assessment, the DA makes the assessment report which includes repair instructions and priority. In composite structures any non-visible damage present in the form of delaminations around holes or surface indentation is determined by nondestructive inspection. This damage is clearly identified so that it can be cleaned up before a repair is performed. Nondestructive inspection techniques such as tap test, ultrasonic techniques, or digital thickness gage may be used to determine the extent of non-visible damage around the visible damage.

b. Establish Repair Criteria

Next step is to establish criteria to which the repairs have to be designed. If the repair is not a standard repair as per ABDAR manual, the non-standard repair should meet the strength design requirements given in the MIL Spec. If the repair is to be made to an aerodynamic surface, it should meet the aerodynamic smoothness requirements of the surface being repaired.

c. Select Suitable Repair

Depending on the damage category, standard repairs are described in ABDAR manual for an aircraft. If the assessed damage is within the damage category, the standard repairs are selected. However, if the repair to be performed is not a standard one, the type of repair to be performed is governed by several factors. Some of the factors to be considered are:

- Type of structural material to be repaired (metal, composite, sandwich construction);
- Type of structural component to be repaired (skin, spar, rib, longerons, etc.);
- Type and extent of the damage (e.g. cracks, corrosion, impact damage, etc.);
- Load levels and loads spectrum experienced by the structure;
- Material thickness to be repaired;
- Skill of the available labor;
- Availability of repair materials including tools from an established ABDR kit;
- Repair facility.

d. Repair Design/Analysis

Suitable materials are selected to accomplish the repairs. The non-standard repairs are designed to meet the requirements specified in MIL Handbook and any other requirements based on aerodynamic smoothness, radar cross section, etc. A check on the integrity of the repair is done based on the static strength.

e. Perform Repair

The repairs are performed using the established materials and processes for the selected repair design. Prior to performing the repairs, the damage area is cleaned to remove jagged edges and stress concentrators. In composite structures any non-visible damage present in the form of delaminations around holes or surface indentation, identified by nondestructive inspection, is removed before a repair is performed.

f. Post-Repair Functional Checks

Nondestructive inspection of repair is carried out to verify the integrity of repair. The integrity of the aircraft structure to meet the operational usage requirement is verified. Any limitations on the aircraft, systems or performance are identified.

2.13. Bonded Repairs of Composite Structures in ABDR

Repairs of composite materials are similar to those for metallic materials for mechanically fastened repairs. However, the repairs of composite materials are different from those of metals for bonded repairs.

Bonded repairs are stronger than bolted repairs due to more uniform load transfer through the joint compared to bolted repairs where load transfer is at discrete points. Bonded repairs do not have stress concentrations as in bolted repairs, and are usually lighter. A bonded repair has more aerodynamic smoothness. Major advantages of using bolted repairs are- less equipment, facilities and personnel skills as compared to bonded repairs. The major steps involved in bonded repairs are discussed here.

➤ **Selection of Repair Method**

The selection of a repair method for a damage situation is matter of judgment due to variables such as damage size and shape, structural configuration, and accessibility. The criteria to be met by a repair are based on the damaged component, capabilities of repair facility, availability of time and material, and personnel skills. Procedures discussed here are not intended to replace repair techniques discussed in Structural Repair Manuals (SRM) for a particular aircraft. Sometimes damage configurations are not covered by SRM and maintenance engineering personnel have to make decisions on repairs. Guidelines provided here are intended to assist these personnel in making repair decisions. A check list is prepared to identify the repair criteria to be met. The following requirements provide the guidelines:

- Strength, stiffness, stability and durability.
- Aerodynamic smoothness
- Weight (or mass) balance for control surfaces.
- Service temperature of the component
- Service environment
- Effect of repair on operating systems such as fuel tank, sealing etc.

➤ **Flush Patch versus External Patch**

External repairs are faster and cheaper than flush repairs. For large area repairs, a flush patch is desirable as load path eccentricity is minimized with a flush patch and maximum strength and durability are achieved. A flush repair minimizes changes in the stiffness of the repaired component and is smoother and lighter than external patch, hence, ideal for control surfaces. In honeycomb construction where skins are generally thin and are stabilized by the core, an external patch is acceptable.

➤ **Cured-in-Place versus Pre-cured Repair Patch**

Tests have shown that cured-in-place or co-cured patch results in significantly higher strength of the repaired part as compared to pre-cured patch. Pre-cured patches are easier to use but may have fit-up problems and are not suited for curved surfaces. A cured-in-place patch must be staged or partially cured in advance to get a void free patch. Complex structural details or the presence of substructure can act as a heat sink and degrade the quality of co-cured repair. However, for large area repairs co-cured repairs are recommended.

➤ **Scarf Joints versus Step-Lap Joints**

Well-made step-lap and scarf joints have similar strength. A typical scarf repair is shown in Figure 19.

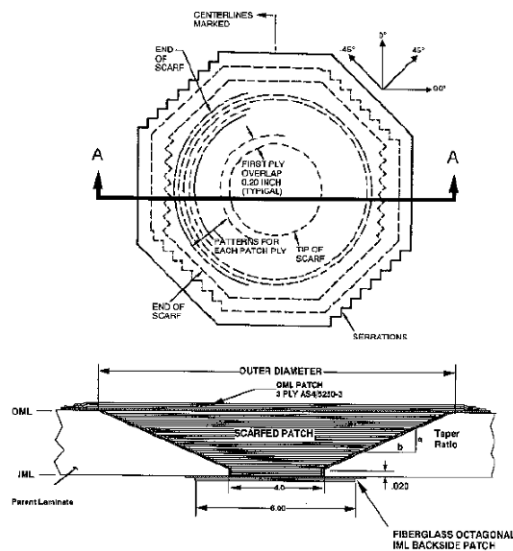


Figure 19 - Scarf Joint Repair

The patch material is within the thickness to be repaired, with additional external plies added for strength. This configuration can restore more strength than an external patch as it avoids the eccentricity of the load path and provides smooth load transfer through gradually sloping scarf joint. A properly designed scarf joint can usually develop the full strength of an undamaged panel. The patch material is usually cured in place, and therefore must be supported during cure. While the patch material can be cured and then later bonded in place, it is generally difficult to get a good fit between the pre-cured patch and the machined opening. A step-lap joint has the advantage of idealized ply orientations on each step for maximum load transfer for a specified loading direction. The steps allow the load to be transferred between specific plies of the patch and parent material. This advantage increases the joint strength; however, it is offset by the peaks in the adhesive shear

stress at the end of each step. This repair concept is shown in Figure 20. Additional external plies are added on the surface for strength.

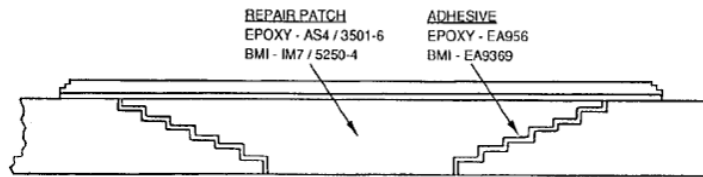


Figure 20 - Step Lap Repair

A disadvantage of step-lap joint is the difficulty in machining the steps to the depth of the exact ply that is desired on the steps. This is a time consuming process and unrealistic for curved surfaces.

➤ **Repair Design and Analysis**

Repair design involves selection of materials, repair configuration, analysis, and repair procedures. Below are listed the design guidelines:

- Minimize the bending effects and peel stresses by avoiding the eccentricity in the load path. If possible an internal doubler may be used to balance the repair. A backside doubler provides a tool surface and a vacuum seal for a co-cured patch for structures having access on one side only.
- Minimize the stress concentration at the edge of a patch by tapering the thickness of the patch to a minimum at the edge or serrating the ends of external plies which are oriented in the direction of the load.
- Locally stiff or soft spots that would change the load distribution in the repair should be avoided in the design. Match ply orientations in the patch with those of the original part.
- Surface plies should be at 45° to the primary load direction.
- Corner radii should be at least 0.5 inch (13 mm) when removing damaged material from the skin to minimize stress concentrations.
- Length of machined scarf should be at least 0.1 inch/ply (2.5 mm/ply) for efficient load transfer while keeping the size of the repair to a minimum. For highly loaded skins or sandwich face sheets, length of scarf should be kept at 0.125 inch/ply (3.18 mm/ply).
- Gaps between adhesive strips (Figure 21), are used as paths to remove trapped air in the bondline.
- Pre-stage thick patches in “books” of plies, as shown in Figure 22, to limit the maximum number of plies for good conformability.

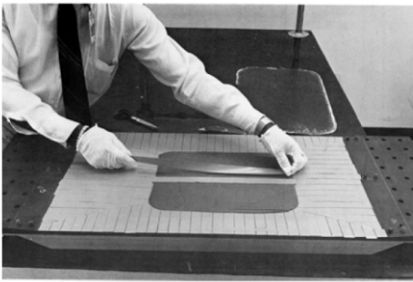


Figure 21 - Gaps in Adhesive Strips

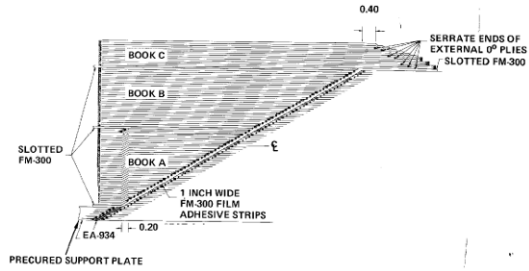


Figure 22 - Books of Repair patch Plies for scarf Repair

The analysis methods for bonded joint repairs are not easy and are based on computational codes. These codes are not well suited for battle damage repair environments. However in the next chapters we will discuss with more details the approach to use in case of a specific load condition.

➤ **Repair Procedures**

The following steps are adopted in performing repairs:

1) Damage Identification

In composites, the actual damage is generally larger than the visible damage due to matrix cracking and delaminations around the visible damage.

2) Damage Removal

Proper tools are necessary to remove the damage in composite without damaging any surrounding material or substructure. A clean opening is left after the damage removal. Figure 23 shows a hand held router used to cut out damage material. The operation on the aircraft may be done without a coolant. A carbide router bit with diamond shaped chisel-cut protrusions is effective at speeds of 1,000 to 6,500 surface feet (305m to 1981m) per minute. Diamond coated routers may also be used. Remove paint beyond scarfed surface for additional area to bond plies. Use light hand sanding with 80 grit paper and finish with 240 grit paper.



Figure 23 - Damage Removal with Hand Held Router

3) Scarf Joint Machining

Scarf repairs are the most commonly used repairs. The material around the opening is machined to provide a scarfed surface which slopes from a feather edge at the opening to the full skin thickness at a specified distance from the opening edge. The distance from the opening edge is determined from the joint design. Tools such as drum sander or disk sander can be used to machine a scarf surface. Machining of a scarf joint with a disk sander, attached to the end of an air-motor, is shown in Figure 24. Such an arrangement is especially useful for fairing in at corners.



Figure 24 - Machining of Scarf Joint with Disk Sander

4) Drying

Composite laminates with organic matrix materials absorb between 1 to 2 percent moisture by weight. Under normal service environment these materials are expected to have about 1% moisture. Moisture absorption causes reduction in the strength of composite materials. The presence of moisture can cause problems during the high temperature cure of a repair. If moisture is not removed, it may cause porosity in a bondline, in honeycomb construction it may cause skins to separate from the core, and it may cause internal damage to the laminate. Drying before repair, which requires bonding at elevated temperature, is necessary. The amount of drying necessary before repair is not well established.

5) Patch Ply Preparation

A pattern of patch plies on vellum or Mylar is prepared. The first patch ply should overlap the tip of the scarf by a minimum of 0.2 inch (5 mm). The patterns for the rest of the plies are traced from the machined surface of the joint. External plies are generally trimmed normal to the fiber direction with pinking shears to provide serrations for added strength. Film adhesive is put on the surface of the patch that will be against the laminate being repaired. Do not trap air pockets between the adhesive and the patch. Adhesive is trimmed slightly larger than the largest patch ply.

6) Bagging and Curing

For the repair of thick composite laminates or curved surfaces a prestage repair patch may be used. The cure cycle for prestage depends on the type of composite laminate and is developed from experience. A staged patch may be stored at room temperature in a sealed vacuum bag until cured in place on the damaged part. Patch and adhesive are placed in position on the laminate being repaired, aligning the centerlines. Bleeder plies, breather plies and other layers are placed and vacuum bagged as per prescribed lay-up procedure. A typical bagging lay-up is shown in Figure 25. The patch and adhesive are cured using a heater blanket or an oven. For on the aircraft repair, care needs to be exercised to make sure that the temperature is maintained within specified limits for required duration. For large area repairs, surrounding structure acts as heat sink and separate heat blankets may be necessary.

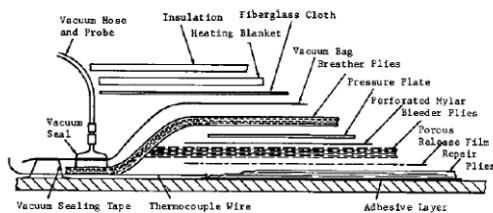


Figure 25 - Schematic Cross-Section of a Bagging Lay-up

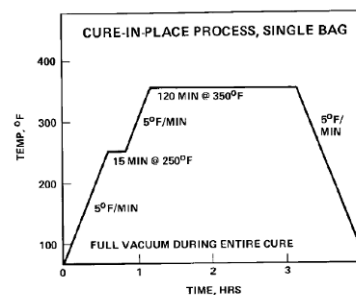


Figure 26 - Typical Vacuum Bag Cure Cycle

7) Repair Quality Acceptance

After a repair is completed, it is inspected to verify its integrity. An inspection is made to make sure that the repair is free of disbonds, blisters or other visually obvious defects. The bonded repairs are inspected by tap test by lightly tapping with a special hammer or a coin. A solid ringing indicates an acceptable repair, while a dead or flat sound generally indicates a disbond or delamination. Nondestructive inspection of repairs can be made using the ultrasonic methods. The pulse echo A-scan is commonly used as it requires access from one side only. This technique is capable of locating disbonds, delaminations and porosity. The use of pulse echo A-scan technique requires the operator to interpret the results displayed on an oscilloscope. Hence, the accuracy of the results depends on the skill and experience of the operator. Standards with known disbond and flaw sizes are commonly used to interpret the results.

Chapter 3 - FEA Investigation on Bonded Repairs

3.1. Design process and concepts: tensile load transfer

As illustrated in previous chapters, one of the most important aspects to take into account in the design of a scarf joint is the adhesive bondline and interface with the adherends. Therefore, a thorough understanding of the adhesive load transfer behavior along the bondline is required.

The maximization of the strength in a scarf joint is obtained through a minimization of the adhesive peak stress; ideally, the adhesive stress should be uniform along the scarf. Any variation of scarf geometry from constant scarf angle introduces large stress concentrations in the adhesive layer, leading to premature adhesive failure. This illustrates the importance of adhesive stress uniformity in load transfer analysis and the consequences of geometric modification of the scarf joint. The strength capacity of a scarf joint subjected to unidirectional tensile loading is highly dependent upon the limit of adhesive bond failure. This is because the entire load is transferred through the adhesive bondline. In the ideal case, whereby the adhesive stress is uniform, no part of the adhesive will fail until all parts are subjected to the maximum stress. With this ideal load transfer case considered, the most complex analysis of composite load transfer needs to be explored. As mentioned before, scarf joints involving laminated composite adherends can involve significant stress variation in the adhesive, this is due to the variation in adherend elastic properties along the adhesive bondline. This variation in elastic properties associated with the adherend arises from the directionally dependent material properties of the lamina orientation. The orientation is dictated in the composite material layup. The resulting non-uniform adhesive stress distribution is undesirable, as it will lead to premature adhesive failure. It was shown that the ply stacking orientation of the composite adherend significantly affects the ultimate strength of the joint and it can be attributed to the non-uniform adhesive stress. Local variations in adherend stiffness due to stacking sequence (result of fiber orientation) result in non-uniform adhesive stress, even in case of constant scarf angle. This occurrence is a further complication that shows the different behavior with respect to the simple isotropic case, complicating the pursuit of the ideal load transfer case of the scarf joint in the application of composite material in the aerospace industry.

3.2.FEM of scarf joint developed by Wang [35]

A Finite Element model of the scarf joint, based on MSC.Marc software, was developed by Wang [35], it is characterized by the variation of adhesive stresses in a scarf joint between non-isotropic composite laminates with an elastic-plastic adhesive bondline. The model investigated several quasi-isotropic layup sequences. Several composite layups were analyzed in order to identify the influence of stacking sequences and orientation of composite plies within certain laminates. Analyses were run assuming that the layup was symmetrical and balanced with respect to the mid-plane of the laminated. The meshing was developed minimizing the number of elements, whilst maintaining sufficient resolution along the area of interest, the scarf joint itself (i.e. along the adhesive bondline). Each ply of the composite specimen was modeled using four rows of elements situated close to the bondline and only one row of elements in areas displaced from the immediate vicinity of the adhesive bondline. Wang specified a generic scarf angle of 5 degrees for the analysis through FE model and each ply thickness was 0.2 mm, as for the adhesive. The length of the entire model was 100 mm, approximately three times the length of the scarf joint. Upon specifying the material properties of the modeled scarf joint adherends and adhesive such as Young's modulus, Poisson's ratio, the analysis started firstly focusing on parameters such as adhesive/adherend stress distribution and variation of mechanical properties with temperature. Wang attempted validation of the FEM results through experimentation and discovered good agreement between the two. Conclusions to be drawn from Wang's study utilizing FEA and experimentation of the scarf joints are that the load bearing plies for a quasi-isotropic adherend layup are those with greatest stiffness. Additionally, the FEM was found to have significant inaccuracies under numerous conditions such as very small scarf angles. These findings will be herein examined in order to define a set of rules that will be later used for designing the repair agreed by partners of AER Project.

3.3.Theoretical Stress Analysis: Separation of Adhesive Stress Components

To take full advantage of the obtainable data produced by tensile testing, appropriate theoretical data analysis need be conducted upon the completion of experimentation. Closed form solutions for adhesive shear stress and adhesive normal stress were developed for the analysis of output data. These solutions are based upon a number of assumptions. The solutions assume that the adherend, when under tensile loading, is in a state of plane stress. Additionally, the solutions give an average of stress within the adhesive, neglecting any non-uniformity. First, a geometric relationship must be defined between the load applied to the

adherends, and how this load is transferred through the adhesive bondline. This can be achieved through resolving the axial force acting upon the test sample into two components transferring load within the adhesive. These components are to be derived as a shear component of force, and a normal component of force. The normal component resolved to be acting perpendicular to the adherend adhesive interface and the shear component parallel. This breakdown from uni-axial applied force, into adhesive force components can be seen in Figure 27. Through simple force resolution and trigonometry, the force components relationship can now be defined in terms of scarf joint geometry and applied uni-axial force.

$$\mathbf{F\sigma=Fsin(\alpha)} \quad (6)$$

$$\mathbf{F\tau=Fcos(\alpha)} \quad (7)$$

$$\mathbf{A=A_{adherend}/sin(\alpha)} \quad (8)$$

Once obtained equations representing average adhesive shear force and adhesive normal force, these equations can be taken a step further and adapted to include the area of action to give a closed form solution to shear and normal adhesive average stress. This is achieved from the basic stress equation, stress equals force on area, the area of which is taken to be the area of adherend adhesive interface. The interface area is found as a function of the adherend cross sectional area and the scarf angle. The interface area of action equation is described by Eq.(11).

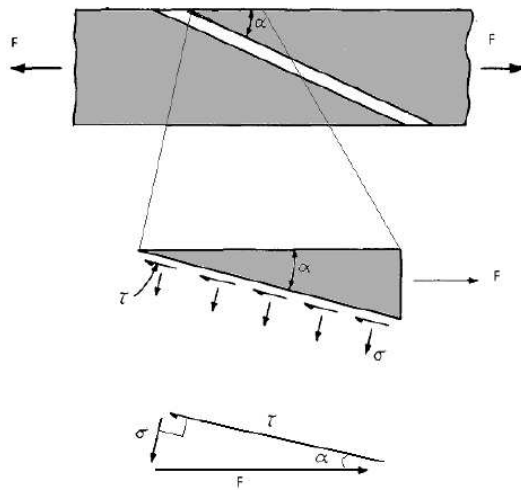


Figure 27 - Separation of Applied Axial Force into Shear and Normal Force Components.

Having shown the derivation for expressions of adhesive force components (Eqs. (6),(7)) and area of action of these force components Eq.(8), these expressions can be substituted into the basic stress equation, force on area, bearing expressions representative of average adhesive stress components. It should be noted that

trigonometric identities are involved in the evaluation of Eqs. (11),(12), from Eqs. (9),(10).

$$\sigma_{AV} = \frac{F_{\sigma}}{A} = \frac{F \sin(\alpha)}{\left(\frac{A_{adherend}}{\sin(\alpha)}\right)} \quad (9)$$

$$\tau_{AV} = \frac{F_{\tau}}{A} = \frac{F \cos(\alpha)}{\left(\frac{A_{adherend}}{\sin(\alpha)}\right)} \quad (10)$$

From which we obtain the average adhesive stress component equations:

$$\sigma_{AV} = \frac{F}{A_{adherend}} \sin^2(\alpha) \quad (11)$$

$$\tau_{AV} = \frac{1}{2} \frac{F}{A_{adherend}} \sin(2\alpha) \quad (12)$$

Having obtained simple closed form average stress solutions for adhesive shear and adhesive normal stress, consideration needs to be given to the relevance and application of the derived stress solutions. The solutions assume that both the adhesive shear and normal stress is uniform and constant along the scarf length. This adhesive stress uniformity, as mentioned, is the case of identical isotropic adherends with constant scarf angle. However, due to the lamina properties of composite materials, particularly the in plane stiffness, adhesive stress varies along the adhesive bond line. This closed form solution does not consider this effect and subsequently overlooks adhesive stress variation. As the solutions gives an average of stress, rather than an accurate representation of adhesive stress of the composite scarf joint, the solutions will overlook peak adhesive stresses, and will rather give a simple average. This is an important fact to note, in that adhesive stress concentrations in adhesively bonded composite scarf joints could be present due to lamina material properties, it may be overlooked in theoretical stress component analysis.

3.4. Development and Implementation of the FE Model for scarf-patch repaired composite laminates

The aim of this study is to assess the range of validity of the current design approach of scarf repairs in composite structures by means of elastic-plastic finite element modeling and mechanical tests comparisons. In attempt to increase the structural adhesive repair efficiency, potential changes to current aerospace industry scarf repair techniques were investigated. With previously discussed knowledge of scarf joint behavior at hand, substantial numerical study were conducted through investigating the variation of the scarf joint through the variation of geometry. The strategy followed in the present study is based on a theoretical analysis of resulting data, compared with literature studies and practical experimentation for validation. The intention is to subsequently investigate the effect of changes to scarf joints and the resulting ramifications. The work has produced useful data for the application of analytical techniques involving theoretical stress analysis, including the previously mentioned closed form adhesive stress solutions. The activity was also useful to provide a complete understanding of the trends that coincide with variation in the parameters of a scarf joint. Investigation into joint behavior, such as stress concentrations and adhesive stress behavior of the scarf joint, is conducted. This was predominantly based upon the stress distribution in the adhesive, the effect of scarf upon ultimate strength and the stress components within the adhesive bondline. The study is additionally extended to involve the examination of new conceptual changes.

In more detail, firstly elastic finite element analyses of scarf joints were run, then a parametric study was performed in order to investigate the stress concentration in composite-to-composite scarf joints, especially highlighting the influence of stacking sequence, laminate thickness and adhesive yielding on the distribution of the stresses in the bondline. The analyses were extended to three-dimensional scarf repairs, focusing on the load shedding phenomenon of scarf repairs, as the surrounding laminate provided multiple load paths. Finally, a non linear finite element analysis of a more refined scarf model was developed. FEM representation was tailored to have analogous geometric and material properties of experimental test samples to enhance potential for correlation. This approach was also taken in the development of the FEM tensile test simulation, in which the conditions of practical experimentation of the uni-axial tensile test were attempted to be reproduced as closely as possible to reality. The models for simulation tensile testing had a scarf angle of 5 degrees. Quasi-isotropic laminates with a stacking sequence of $[45/0/-45/90]_n$, where n was equal to 1, 2, and 4, for three different laminate thicknesses, were modeled. The analysis used solid elements and was performed using MSC. Patran/MSC.Nastran. The models were created using a bottom up approach. It was decided that in order to replicate the experimental tensile test at the best, the adherends were created at replicated

geometry. The two dimensional models were then built as a skeleton based upon a Cartesian coordinate system (Figure 28). This was representative of the symmetrical through sample width, the transverse cross section of the adherends and adhesive bondline. The skeleton was created through the input of key point coordinates, which acted as nodes for creation of end points of lines. Key points were then joined to form lines, then lines joined to form surfaces. This process of bottom up model design produced the skeletal structure of the adherends. The adherends were modeled in the vertical 'y plane' respectively as 1.04, 2.08, 4.016 mm considering three different laminate stacking sequences, these dimensions relating to the thickness or depth of the adherends, and 65 mm long, this dimension relating to the overall length in the 'x plane'. The main issue surrounding the geometric construction of the model was on how to create the scarf joint adhesive bondline. The adhesive bondline was created using an internal Patran geometric function, which created 2D arc angles with respect to the specimen axis of symmetry, particularly 5 degree angle. The end point of the arc and the central point of symmetry were connected in order to create a line, this line was extended through the boundary line of the model, finally this line was offset in opposite directions obtaining the adhesive area. At this point of progress, the complete geometric skeleton of the scarf joint was developed. Consistent geometrical parameters were employed, including adherend size, scarf angle and adhesive bondline thickness. All the geometrical data are collected into the Table 1.

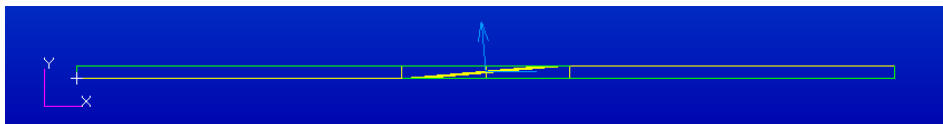


Figure 28 - Specimen geometry

Geometry	
Ply thickness [mm]	0.13
Adhesive thickness [mm]	0.13
Model length [mm]	65
Scarf angle [deg]	5
Slice Model thickness $tp/2$ [mm]	0.065

Table 1 - Specimen geometry

Model	Scarf length [mm]
8 ply	11.89
16 ply	23.77
32 ply	47.55

Table 2 - Scarf length for each model

The properties of the UD composite material and adhesive used in the finite element model, are presented in Table 3.

AS4-3501	E11	E22=E33	v12	v23	v31	G12=G13	G23
	128GPa	13GPa	0.3	0.3	0.03	7.2GPa	5GPa
Adhesive	E	G	v				
	1.014GPa	0.39GPa	0.3				

Table 3 - Material properties

The adherend plies were specified into Patran Material application form to be three-dimensional orthotropic materials with the adhesive specified to be an isotropic material. In order to create a material property for each ply orientation, different oriented coordinate frames were set and each ply property was associated with the corresponding one. The 3-D orthotropic properties for the plies were obtained also using the matrix transformation method and the two methodologies values resulted very close so that the former was preferred for easiness and quickness.

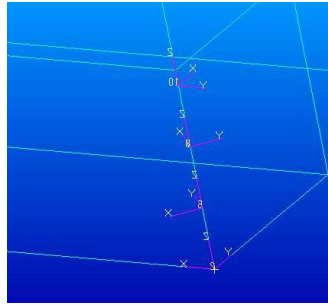


Figure 29 - Example of reference coordinate frames associated to each ply

The joint was modeled by firstly creating a mesh of two-dimensional elements, QUAD4 and TRIA3, then extruding them normally with respect to the surface plane to create three dimensional elements, HEX8 and WEDGE6. Meshing parameters for 2D model are shown and summarized in Figure 30 and Table 4. It can be noticed that four rows of elements were employed to model the adhesive and adherend.

Stacking sequences		Total t	Meshing and Refinement		
N ply	stack	mm	Pl elem	Adhes elem	N. thick. Elem.
8	[45/0/-45/90]s	1.04	4	4	32
16	[45/0/-45/90]2s	2.08	4	4	64
32	[45/0/-45/90]4s	4.16	4	4	128

Table 4 - Mesh parameters

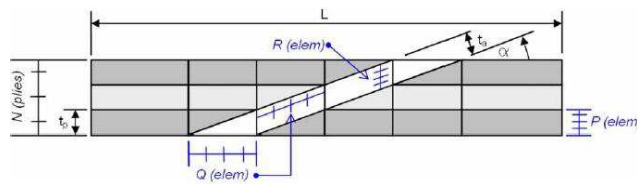


Figure 30 - Mesh parameters

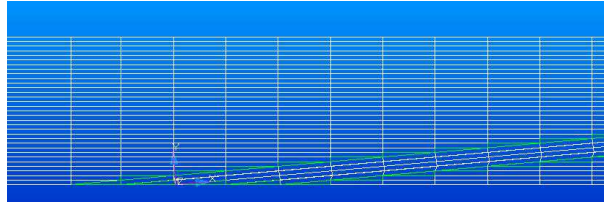


Figure 31 - Side view of the meshed specimen

The same procedure was executed for all the models, moreover to better manage the different ply properties it was useful to regroup elements having the same ply orientation into specific group name. The following figure illustrates an example of group color-angle association.

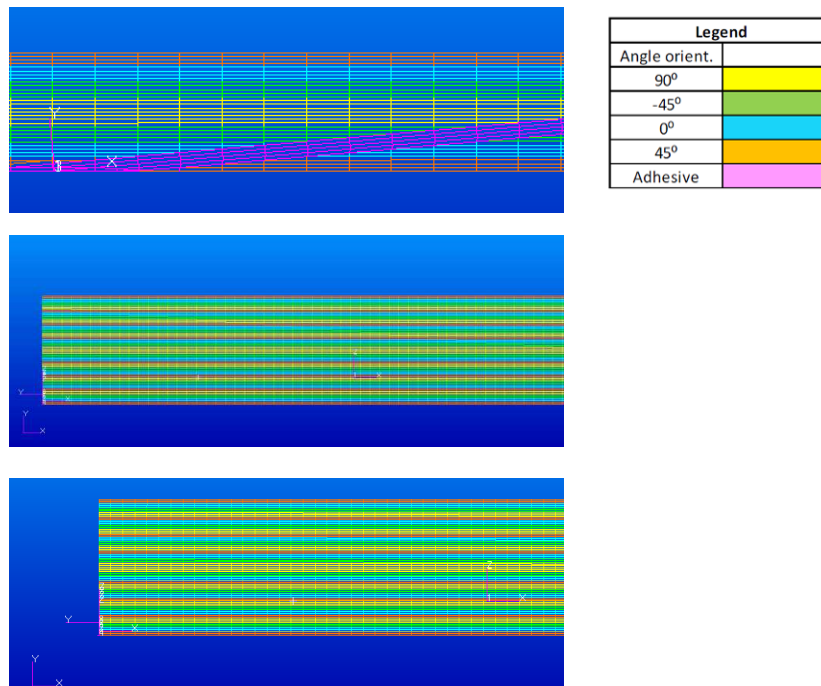


Figure 32 - Side view of the 8,16 and 32 plies specimens

The focus of this investigation was on the adhesive normal (*peel*) and shear stress distribution along the bondline of the scarf joint. Therefore, a line of nodes was always maintained in all models down the centerline of the adhesive, extending to the free surfaces of the joint. A group was created containing the centerline nodes in order to have a target entity to show analysis results. A local coordinate system was set in order to extract the values of shear and normal stresses (Figure 33).

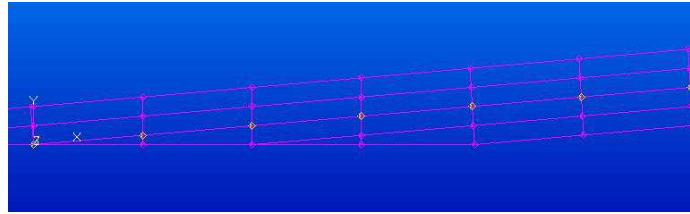


Figure 33 - FE mesh close to the bondline of a 5° scarf joint

The meshing of the adhesive must be created separately to that of the adherends. Considering that a special focus was placed upon the analysis of the adhesive bondline stresses and the relative size of the adherend bondline, a high mesh resolution was required in the area of the adhesive bond line. This was achieved through manually setting the size of the elements by manually creating node divisions on the lines surrounding the adhesive bond line area.

➤ **Tensile Test Simulation:**

The last stage before final analysis was the design of the simulated uni-axial tensile test. A scenario was set to simulate the conditions of experimental tensile testing. This was achieved in the FE environment through the application of simulated loads and boundary conditions.

Boundary conditions on the scarf model were applied as reported in Figure 34. On one edge all degrees of freedom were constrained in attempt to simulate a static grip clamp, while on the other edge a constant uni-axial nominal force of 8kN was applied to the adherend. Regarding the load, particularly it was applied a nodal force as shown in Table 5 depending on considered model.

Nr. ply	Nodal Load (N)
8 ply	11.89
16 ply	23.77
32 ply	47.55

Table 5 - Nodal forces

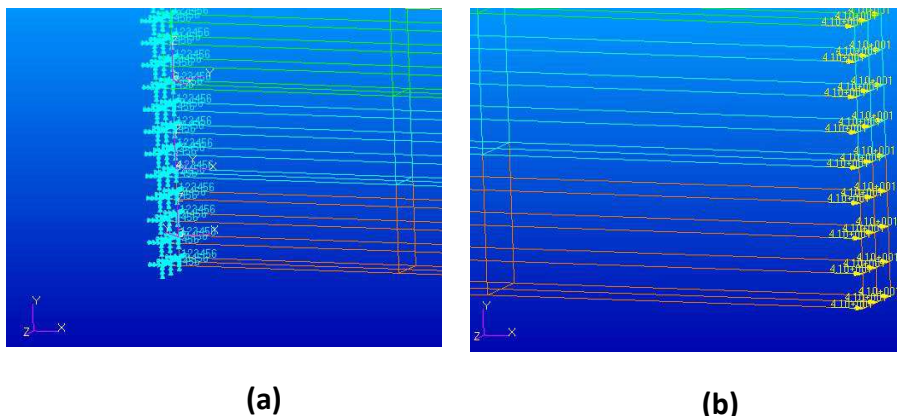


Figure 34 - Boundary conditions and loads applied to the scarf model

This setup simulated the conditions of a clamping attached to a crosshead, enabling un-axial loading and extension of the sample in the direction of the applied force. The points of application of the simulated load and boundary conditions can be seen in Figure 34. The tensile test simulation conditions were applied to all developed models and modifications. This included the 5 degree orthotropic adherend scarf joint for 8, 16 and 32 plies. Linear static analyses were performed using SOL101-MSC.Nastran.

Another interesting aspect deals with the mismatching in ply properties, in fact, there are many triple-point singularities where two adjacent plies intersect the adhesive but this aspect was in the next analyses. The attention was focused on the stresses and strains along the mid-plane of the adhesive layer. This approach is equivalent to the stress-(or strain)-over-a-critical-distance method, with the distance being equal to half the bondline thickness. Shear and peel stress were normalized to the average shear stress and the bondline abscissa to the scarf length respectively of the analyzed models.

Figure 35 illustrates the normalized shear stress and peel stress, clearly showing the existence of significant stress concentrations in the bondline of a scarf joint between identical quasi-isotropic laminates. As expected, very high shear stresses occur at the ends of 0° plies. Even for moderately thick composite laminates of 32 plies, the maximum stress concentration factor exceeds 1.5. It is important to point out that these stress concentrations may cause shear failure (if the maximum shear stress criterion is applied) at a load much lower than if the average shear stress criterion is used.

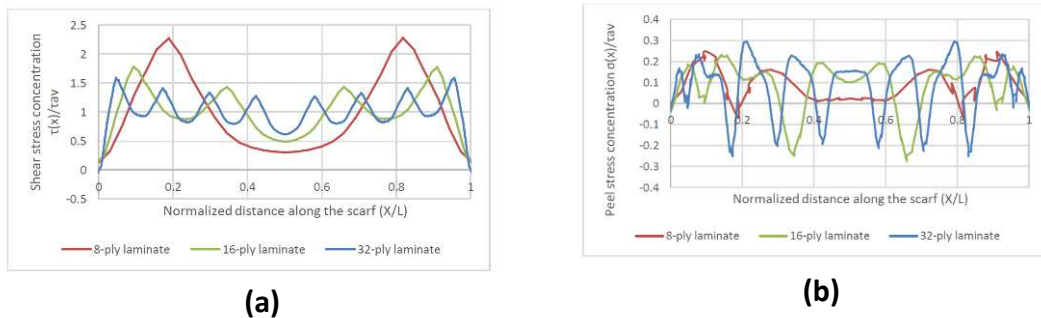


Figure 35 - Shear stress (a) and Peel stress (b) concentrations in a scarf joint ($\theta=5^\circ$) for quasi-isotropic composite laminates. Stacking sequence are respectively $[45/0/-45/90]_s$, $[45/0/-45/90]_{2s}$, $[45/0/-45/90]_{4s}$

3.5. Parametric study

To investigate more in detail the stress distribution along the bondline of the scarf joint, a parametric was performed varying several parameters, such as layup sequence, laminate thickness, adhesive thickness and scarf angle. In such cases the shear and peel stresses have been normalized to the far-field applied stress and then multiplied by 1000 to allow direct comparison of the relative magnitudes.

- **Stacking sequence**

Analysis about the stress within the adhesive was conducted for bi-directional quasi-isotropic and unidirectional layups. Stacking sequences investigated are $[0/90]_{2s}$, $[90/0]_{2s}$, $[45/0/-45/90]_s, [0]_8$. Figure 36 shows the normalized stresses computing the average normalized shear and peel stress, it can be pointed out the significant effect of the stacking sequence on the local stress concentration. As expected, very high shear stresses always occur at the ends of 0° plies. The peak values can reach up to 170% and 330% of the average values, respectively. Adhesive portion close to the free surface does not have any capability of carrying load, in fact the peel and shear stresses tend to zero after the peaks. Analysis was repeated doubling the number of plies. Figures 37-40 show the bondline stress distribution pointing out the same trend of previous analysis, but with more peaks.

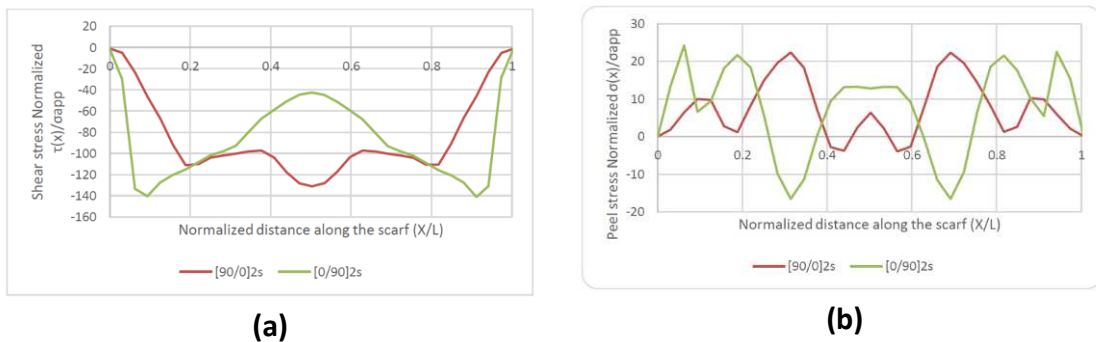


Figure 36 - Normalized shear stresses (a) and peel stresses (b) along the adhesive bondline for $[0/90]_{2s}$ and $[90/0]_{2s}$ laminates

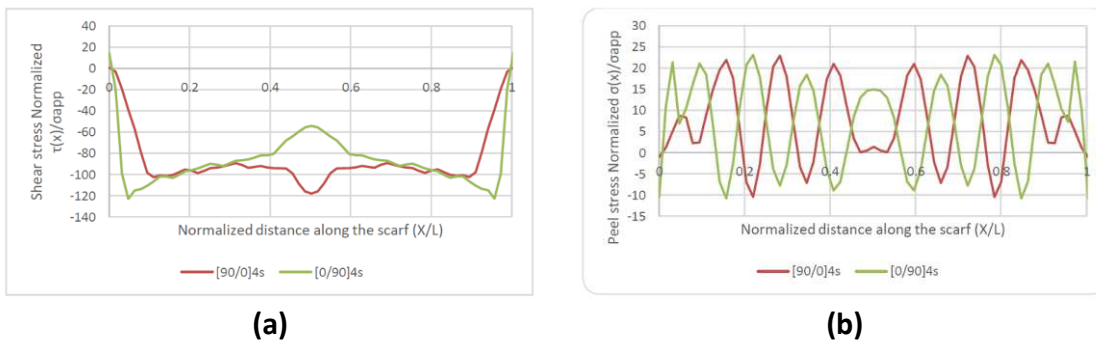


Figure 37 - Normalized shear stresses (a) and peel stresses (b) along the adhesive bondline for $[0/90]_{4s}$ and $[90/0]_{4s}$ laminates

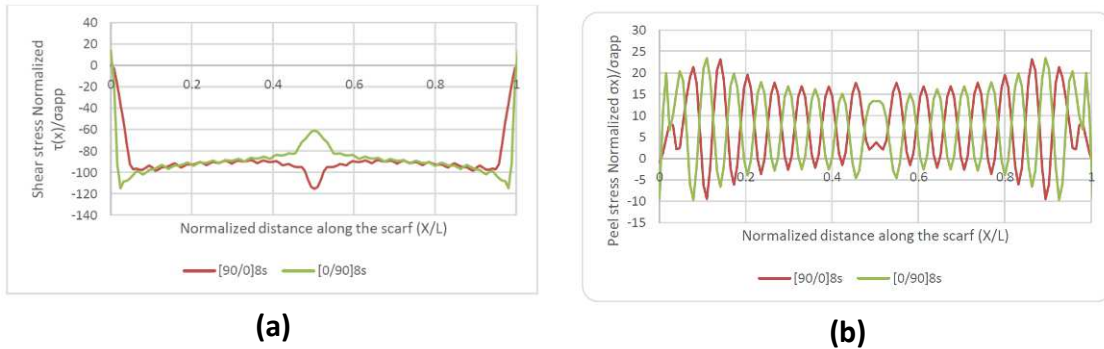


Figure 38 - Normalized shear stresses (a) and peel stresses (b) along the adhesive bondline for [0/90]8s and [90/0]8s laminates

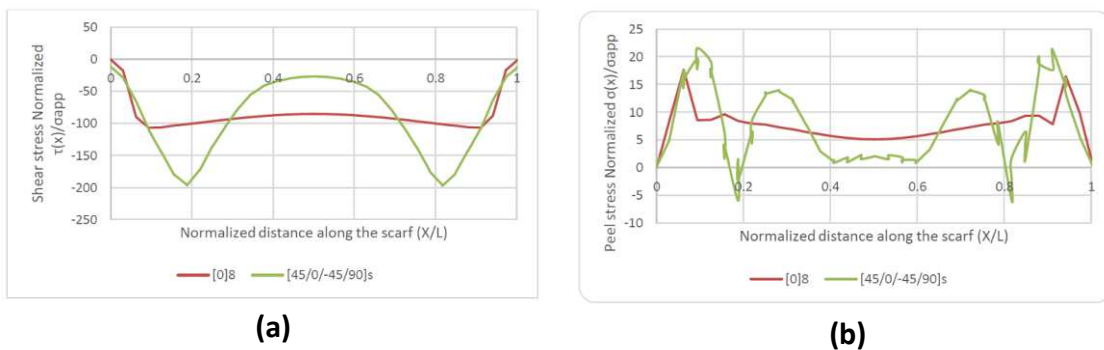


Figure 39 - Normalized shear stresses (a) and peel stresses (b) along the adhesive bondline for [0]8 and [45/0/-45/90]s laminates

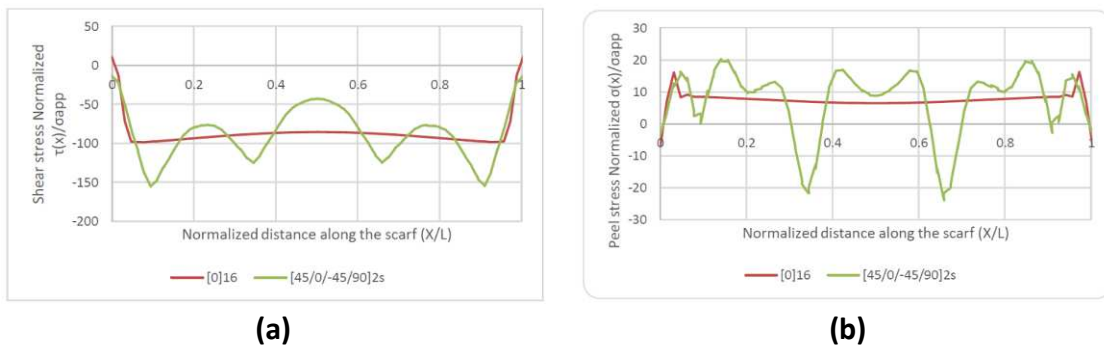


Figure 40 - Normalized shear stresses (a) and peel stresses (b) along the adhesive bondline for [0]16 and [45/0/-45/90]2s laminates

- **Mismatched lay up**

An investigation was performed to assess the effect of mismatched adherend layups in order to evaluate alternative repair schemes.

The influence on bondline stress distribution under in-plane loads was analyzed using [0/90]4s and [90/0]4s lay-ups on either side of the bondline, and repeated with [45/0/-45/90]2s and [-45/90/45/0]2s. The results are shown in Figure 41, while Figure 42 shows the results for the same lay-up sequence but with 32 plies. For all

laminates investigated, the ply orientation changed 90° across the scarf joint. Little changes in the peaks of peel and shear stress in the bondline result from the comparison with stress distribution of matched laminates having equivalent thickness although the different shape (Figures 42-43).

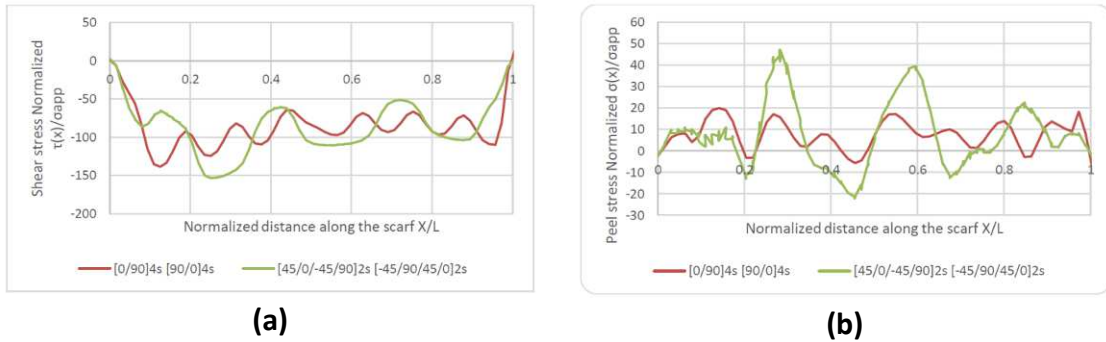


Figure 41 - Normalized shear stresses (a) and peel stresses (b) along the adhesive bondline for mis-matched (MM) adherend pairs; [0/90]4s with [90/0]4s and [45/0/-45/90]2s with [-45/90/45/0]2s laminates

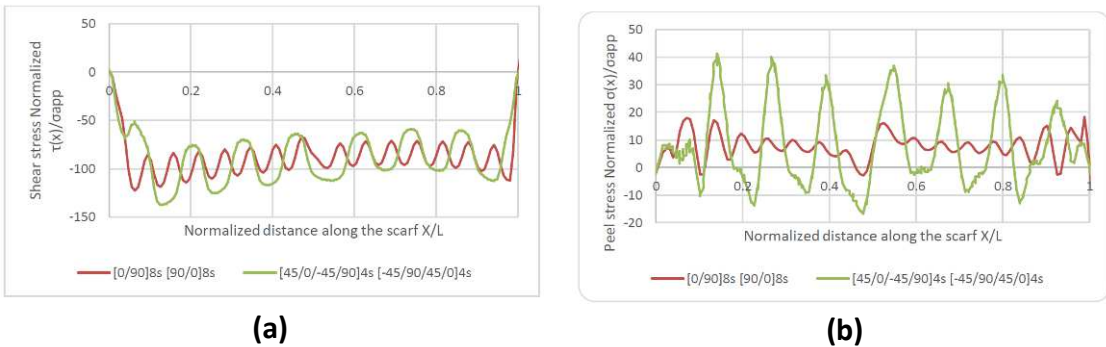


Figure 42 - Normalized shear stresses (a) and peel stresses (b) along the adhesive bondline for mis-matched (MM) adherend pairs; [0/90]8s with [90/0]8s and [45/0/-45/90]4s with [-45/90/45/0]4s laminates

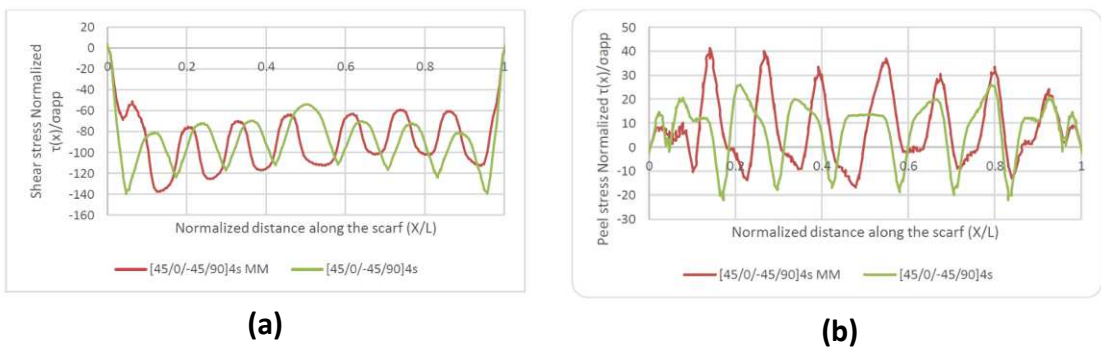


Figure 43 - Normalized shear stresses (a) and peel stresses (b) along the adhesive bondline for mis-matched (MM) adherend pairs; [-45/90/45/0]4s with [45/0/-45/90]4s laminates

- **Laminate thickness**

Another parameter with a significant influence on the adhesive stresses along the bondline is the number of plies for quasi-isotropic laminates having 8, 16 and 32 plies. Figure 44 clearly shows how increasing the number of plies, the peak peel stresses near the ends of the bondline decrease and reach the levels experienced away from the free surfaces. Finally, it can be pointed out that the results obtained are influenced by two local factor, the number of 0° ply and the location of the outer-most 0° ply. The 0° plies carry the main part of the load because their stiffness is significantly more than the other plies in the loading direction. Consequently the increasing of the 0° plies number implies a decrease of the load carried in the outer-most 0° plies. It results in lower and lower peak stresses near the surface relative to the average stress. Outer-most 0° plies on the extremity of the laminate involve the reduction of the load path across the scarf joint, resulting in higher adhesive stresses than when a $\pm 45^\circ$ or 90° ply is at the surface. This aspect can be seen in Figure 45.

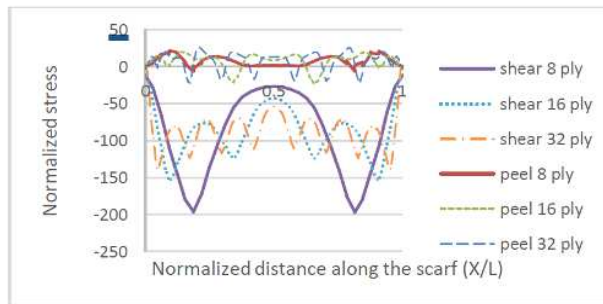


Figure 44 - Normalized shear and peel stresses along for quasi-isotropic laminates with 8,16 and 32 plies

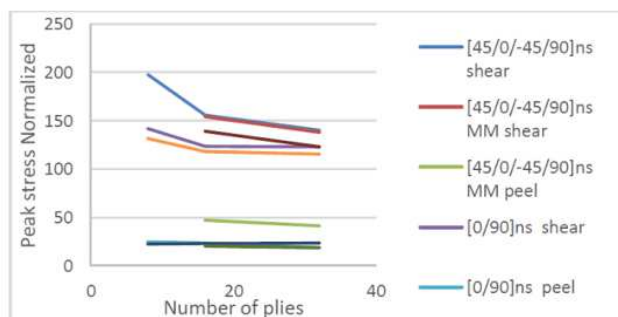


Figure 45 - Peak normalized shear and peel stresses as a function of number of plies for different laminates

- **Scarf Angle**

A specific analysis about the influence of scarf angle on bondline was not conducted, however being an important aspect of the problem it can be interesting to report the results obtained by Gunnion and Herszberg [36]. They investigated the stress distribution on bondline varying the angle (α) between 3 and 15 for a cross ply lay-up $[0/90]_{2s}$. It has been pointed out the significant sensitiveness to scarf angle. In fact, changes to the scarf angle influence the theoretical average stress along the bondline, whose ratio depends on scarf angle by:

$$\frac{\sigma_{yav}}{\tau_{yxav}} = \tan[\alpha] \quad (13)$$

The general trend is an increase of peel stress and a reduction of shear stress as the scarf angle grow. Furthermore, the scarf angle has also a strong effect on the peaks of stress whose sensitivity decreases as the thickness of laminate increases. Lower scarf angles lead higher joint strengths due to greater adhesive joint area of action.

- **Over laminate**

Considering a cross ply laminate with 16 plies, over-laminate plies of equivalent material and thickness have been added to the scarf joint model. These plies run the full length of the model on either surfaces. The purpose was to investigate the effect of the over laminates on scarf joint peel and shear stress. A tensile test was performed in the same way of previous test, still applying the boundary and load conditions only to the original scarf joint plies. Figure 46 shows the models for 4 and 8 over laminate plies.

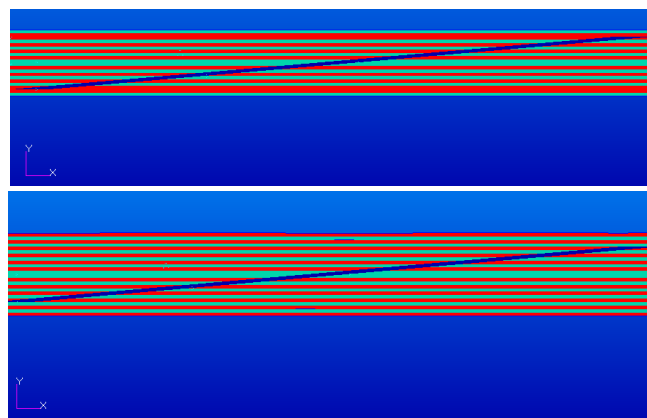


Figure 46 - 4 and 8 plies over laminate models

The results of the tests (Figure 47) pointed out that the addition of over laminate plies to the scarf joint implies a relevant decrease of peak peel and shear stresses. Considering two stacking sequences ([0/90] and [90/0]) of over laminates it did not produce appreciable effect on the stresses within the scarf joint adhesive. It can also be asserted that the increasing the number of over-laminate plies from 4 to 8 does not produce significant advantage in peak stress reduction, although an overall reduction is due to the local increase of the cross-sectional area.

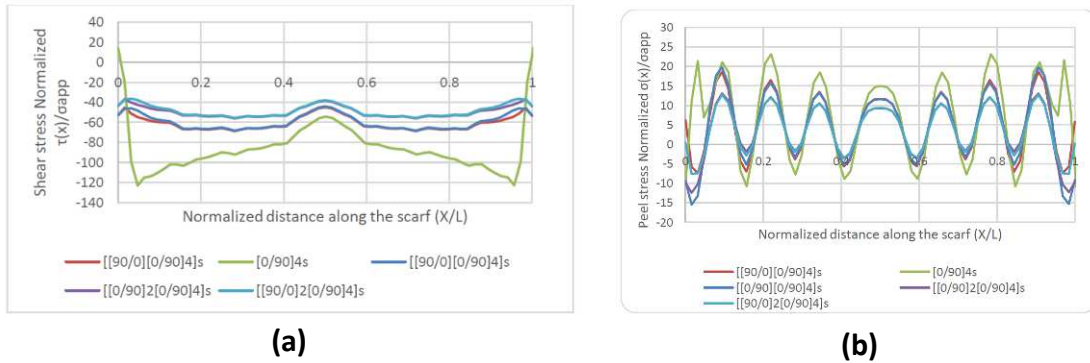


Figure 47 - Normalized shear stress (a) and peel stress (b) along the adhesive bondline for [0/90]4s laminates with 4 and 8 plies over laminate of [0/90] and [90/0]

▪ **3D Circular patch linear analysis**

A finite element model was developed to characterize the variation of the adhesive stresses in a three-dimensional scarf repair. Individual plies were discretely modeled, thus allowing the analysis to capture local variations in the bondline stress distribution. In order to provide high mesh refinement around the scarf joint still keeping the overall model size manageable, a quarter model of the repair and panel was developed. Figures 48-49 show the 3D circular model. Geometrical data are collected into Table 6.

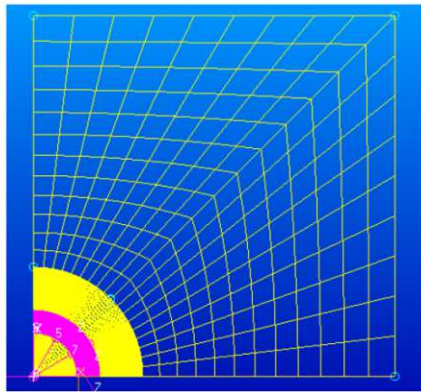


Figure 48 - One quarter panel mesh

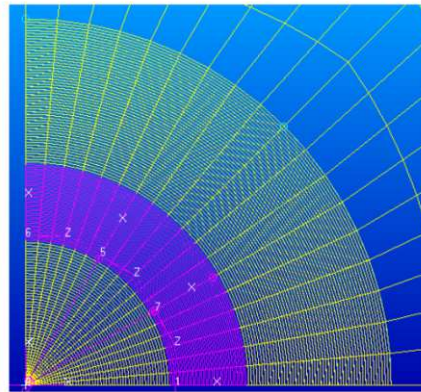


Figure 49 - Refined region

Geometry	Quarter model panel
Half-width [mm]	215
Lower radii [mm]	25
Upper radii [mm]	39
Loaded Area [mm ²]	223.6

Table 6 - 3D Circular patch geometric data

Panel lay-up configurations were limited to 0° and 90° plies only because ±45° plies are incompatible with the application of symmetric boundary conditions. As shown in Figure 50 local coordinate systems were made around the adhesive with 30° steps, where the peel and shear stresses in the bondline were extracted. Boundary conditions were applied fixing the nodes along x edge in d_y, r_x, r_y, r_z and the nodes along y edge in d_x, r_x, r_y, r_z . Load was applied to the right free edge of the model. Figure 51 show the results for lay-up $[0/90]_{2s}$ while Figure 52 show $[90/0]_{2s}$ results. The direction 0° represents the loading direction and 0°-fiber orientation. It can be seen that as the angle to the load increases, both the peak and average shear and peel stresses decrease. Added to this the comparison between the 3D circular model and scarf joint 2D results reveals that the trend of peel and shear stress distributions are identical. This implies the validity of 2D models for investigating joint parameters. A more detailed comparison shows in term of magnitude that peel and shear stresses in 0 for the 3D circular are 6.5 and 80 respectively, clearly inferior to the 2D results 7.5 and 85. This implies a reduction of stresses of 10% because of load by-pass. However, a true comparison of the reduction cannot be made in this case due to a change in element size for the 3D circular patch analysis.

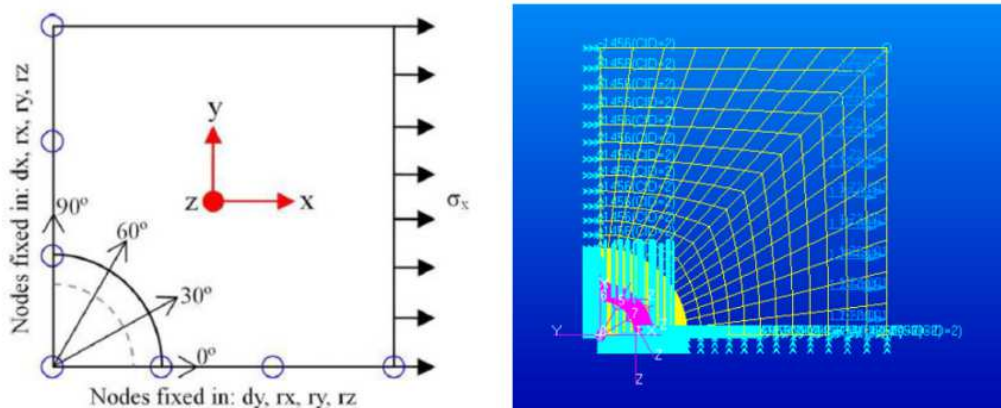


Figure 50 - Reference systems and LBCs

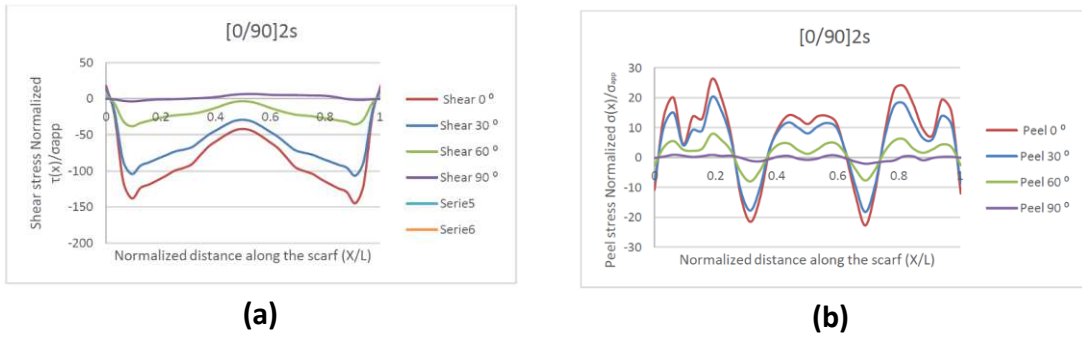


Figure 51 - Normalized shear stresses (a) and peel stresses (b) along the adhesive bondline for [0/90]_{2s} laminate at 30° intervals around a 3D circular scarf joint

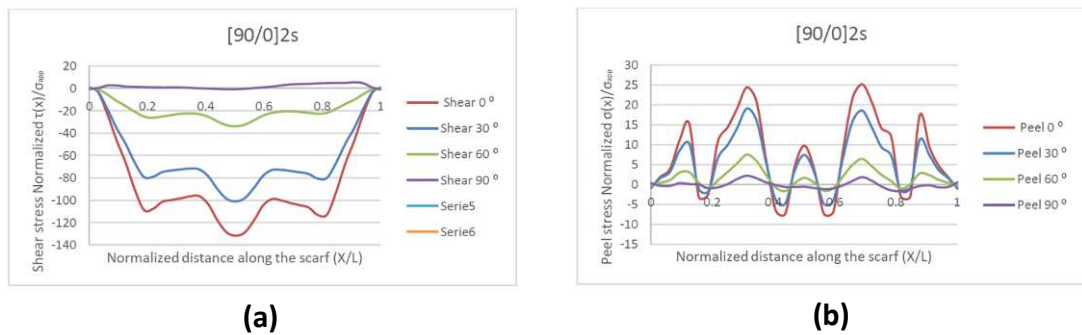


Figure 52 - Normalized shear stresses (a) and peel stresses (b) along the adhesive bondline for [90/0]_{2s} laminate at 30° intervals around a 3D circular scarf joint

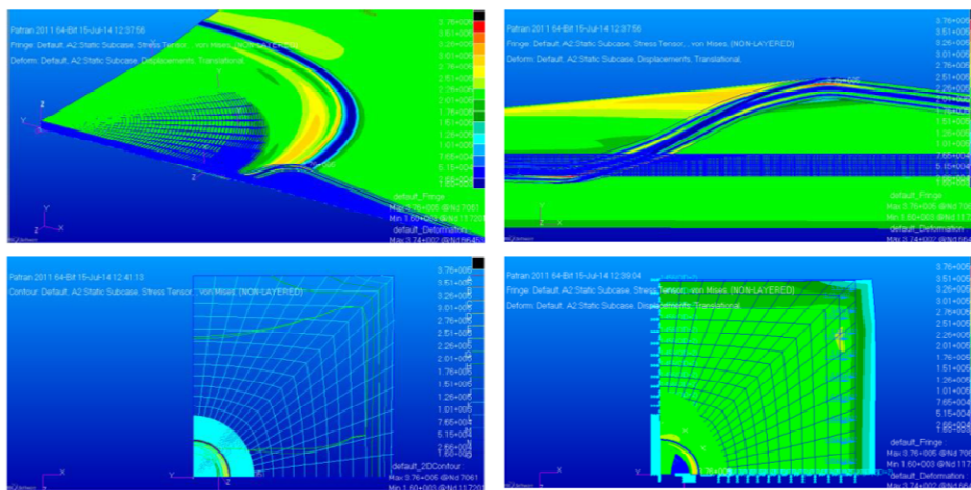


Figure 53 - 3D scarf repair elastic analysis: deformation and stress results plots

3.6. Elastic-plastic analysis

- **2D Scarf joint**

Taking into account that structural adhesives can deform plastically before reaching the failure, particularly under shear deformation, it was needed to model the elastic-plastic deformation behavior of the adhesive in strength prediction. Therefore, elastic-plastic finite element analysis was performed to quantify the resulting stress redistribution, as the adhesive reached plastic yielding.

A model to characterize the stress variations of an elastic plastic adhesive between two orthotropic composite laminates was developed. The layup investigated was $[0/45/-45/90]_{2s}$. The geometrical characteristics of the scarf joint are summarized in Table 7. The length of the model is 100mm, about three times the scarf length; ply thickness is 0.2 mm, the same for the adhesive thickness; the 3D model is a thin-slice model with a thickness of $tp/4$ made up of 3D solid elements.

Geometry	
Ply thickness [mm]	0.2
Model length [mm]	100
Scarf angle [deg]	5
Slice model thickness $tp/4$ [mm]	0.05
Loaded surface [mm ²]	0.16
Scarf length	36.58

Table 7 - Scarf joint geometry data

A refined mesh was developed to reduce computational time still ensuring a good consistent mesh in the region of interest for all the analyses, i.e. the interfaces along the scarf. Each ply was modeled by four rows of elements close to the bondline and by one row of element away from the joint region. The Figure 54 shows a portion of the finite element mesh.

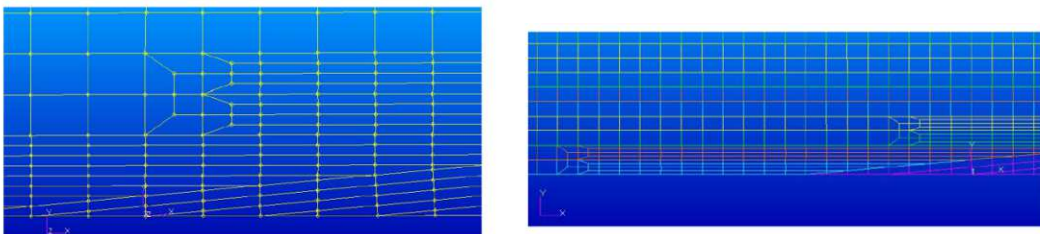


Figure 54 - FE mesh near the scarf region

The ply and adhesive material properties were kept constant throughout this investigation and they are provided in Table 8.

CYCOM 970/T730 12K	E11	E22=E33	v12	v23	v31	G12=G13	G23
	120GPa	8GPa	0.45	0.02	0.45	5GPa	2.7GPa
CYCOM FM300-2	E	G	v	Yield stress			
	2.27GPa	0.84GPa	0.35	0.05GPa			

Table 8 - Adhesive and adherend material properties

The adhesive properties were considered at room temperature. Aimed at computational simplification, the adhesive stress-strain curve was idealized to be elastic-perfectly plastic, as shown in Figure 55. Therefore, only yield stress and ultimate shear strain parameters are required.

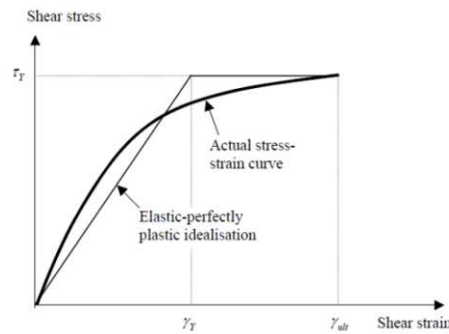


Figure 55 - Elastic-perfectly plastic idealization of adhesive shear-strain relationship

Non linear static analyses were performed using SOL106-MSC.Nastran. Taking account for the loaded area the scarf angle and the derived shear stress at the adhesive interface, different loads with progressive increments were applied to the model in such a way to observe how the shear stress approaches the yield stress along the scarf. Figures 56-57 show for two different orthotropic laminate the normalized shear stress along the bondline due to the incremental applied loads. It can be seen that, once the load overwhelms a certain level the shear stress reaches the yield stress over the entire scarf. The load is indicated by average shear normalized by yield stress.

	Load factor	Applied load (N)
Case1	0.3	15
Case2	0.5	25
Case3	0.7	35
Case4	0.8	40
Case5	0.9	45
Case6	0.98	49
Case7	1.005	50.25

Table 9 - Incremental applied loads

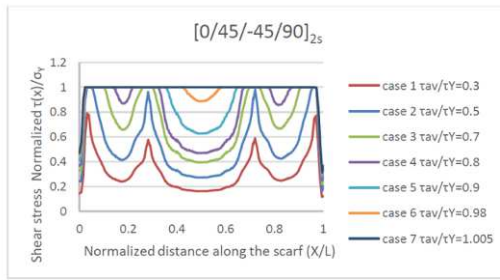


Figure 56 - Shear stress distribution for [0/45/-45/90]_s

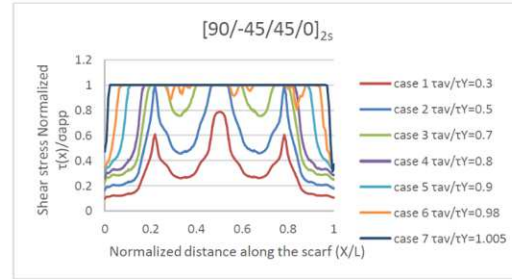


Figure 57 - Shear stress distribution for [90/-45/45/0]_s

- **3D Circular patch non linear analysis**

A finite element model was developed following the same procedure of the 3D Circular patch linear analysis, but the aim was to characterize the variation of adhesive stresses in a three-dimensional scarf repair of an orthotropic composite laminate having an elastic-plastic adhesive. Geometrical data of the circular scarf repair with a scarf angle of 5° are summarized in Table 10. The mesh used for the elastic-plastic analysis was swept in an arc to produce the circular scarf, thus guaranteeing consistent mesh resolution around the adhesive for the two- and three- dimensional elastic-plastic analyses. A quarter of the finite element mesh is shown in Figure 59. The panel can be considered sufficiently large with respect to the repair for this analysis, with $W/D \approx 4.28$.

Geometry	Quarter model panel
Half-width [mm]	300
Lower radii [mm]	30
Upper radii [mm]	70
Loaded Area [mm ²]	960

Table 10 - 3D circular patch geometric data (elastic-plastic)

The adhesive and adherends material properties are the same used in the two-dimensional elastic-plastic analysis. The analysis methodology applied to the two dimensional joint was repeated. About boundary conditions the nodes along x-edge were fixed in d_y , r_x , r_y , r_z and the nodes along y-edge in d_x , r_x , r_y , r_z . Load was applied to the right free edge of the model (in front view - Figure 58). The FE model with load and boundary conditions are presented in Figure 58.

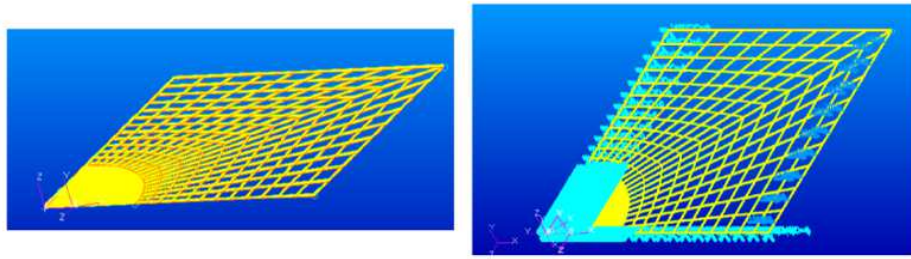


Figure 58 - 3D circular patch model with LBCs

The adhesive stresses and strains for the three-dimensional model were taken in the 0° (loading) direction. The normalized shear stress along the radial line that is parallel to the loading direction are shown in Figure 59.

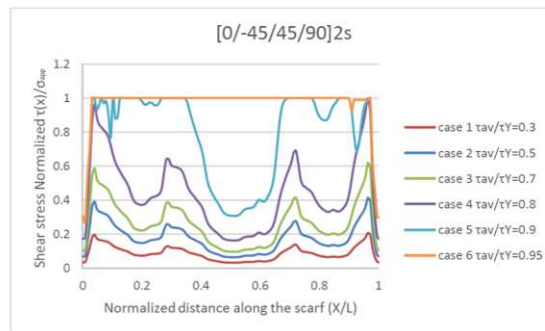


Figure 59 - Shear stress distribution along 3D scarf (shear stress normalized by yield stress) for [0/-45/45/90]

From Figure 60 illustrates the stress distribution plot for incremental load case 1, 4 and 5. The different stiffness of the plies implies a variation in load transfer through the adherends and consequently it induces non uniform stress distribution within the adhesive bondline.

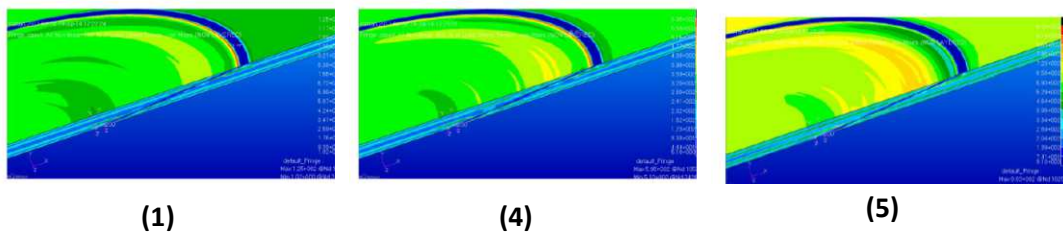


Figure 60 - 3D Von Mises Stress distribution for case 1 4 5

▪ Results

This part of the work investigated with FE linear and non linear analyses, different aspects of the scarf joint in attempt to increase the structural adhesive joint efficiency and better understand the bonded joint behavior.

Using linear FE analyses of 2D and 3D scarf joints, a parametric study was performed, varying several parameters, such as stacking sequence, laminate thickness, adhesive thickness, scarf angle, mismatched adherends, load by-pass and angle with respect to the loading direction. Table 11 displays the obtained results. Relevant aspects are the quite low sensitivity of adhesive stress to mismatched adherend layups and the reduction of peak stresses due to few over laminates adding. Furthermore, over laminates can have positive effect on repair durability giving environmental and impact protection. Another important influence from this investigation is how the stacking sequence of the composite adherends affects the scarf joints. The adhesive shear stress distribution along the scarf is not constant, local variations in adherend stiffness, corresponding to changes in ply orientation, result in peak shear and peel stresses in the adhesive bondline adjacent to the stiff plies of the adherends. This feature shows the potential for elastic tailoring of the scarf joint to dictate load transfer through adherend ply orientation. The stress components of a single scarf angle joint was shown to be dominated by shear. Further development may led to prediction in terms of adhesive stress of the joint behavior. It was shown by analysis that peak local stresses arise at stress concentrations around the termination of 0° plies, away from the adhesive centerline.

Effect of scarf joint parameters on bondline average and peak stresses				
Parameter	Average peel	Peak peel	Average shear	Peak shear
Stacking sequence	No	Increases when 0° plies are on the outer surfaces	No	Decreases with more 0° plies. Increases with increasing distance between 0° plies across the scarf.
Laminate thickness	No	Decreases with increasing laminate thickness	No	Decreases with increasing laminate thickness
Mismatched adherends	No	Slight increase or decrease depending on lay-up	No	Slight increase or decrease, depending on lay-up
Over laminate	Decreases with increasing over laminate number of plies	Slight decrease with increasing over laminate number of plies	Decreases with increasing over laminate number of plies	Slight decrease with increasing over laminate number of plies
Scarf angle	Increases with increasing scarf angle	Strongly decreases with increasing scarf angle	Decreases with increasing scarf	Slightly decreases with increasing scarf angle
Allowing load by-pass of patch	Decreases if there is an alternate load paths	Decreases if there is an alternate load paths	Decreases if there is an alternate load paths	Decreases if there is an alternate load paths
Angle to loading direction for a 3D circular patch	Decreases with increasing angle from loading direction	Decreases with increasing angle from loading direction	Decreases with increasing angle from loading direction	Decreases with increasing angle from loading direction

Table 11 - Parametric analysis results

Chapter 4 - Physical demonstrators of the repair efficiency

4.1. Identification and redesign of the test articles that will be subjected to battle-field damages

As previously described, in the first phase of AER Program, the Italian partner was in charge of identifying, re-designing and manufacturing nr.6 composite panels, representative of components part of military aircraft that will be then used by each participating nation for performing a particular repair, once the damage scenario was agreed by the Consortium. To perform this activity, in agreement with what was done in previous years in collaboration with the offices of the Directorate of Air Armaments, several configurations were assessed and, in compliance with the requirements of the contract, a demonstrator suitable for research purposes was selected. In particular, in collaboration with CIRA, partner of the project, a flat composite stiffened panel, designed as part of the SMAF project (SMart AirFrame) and used as lower wing skin for an unmanned vehicle UAV –MALE 1, was identified.

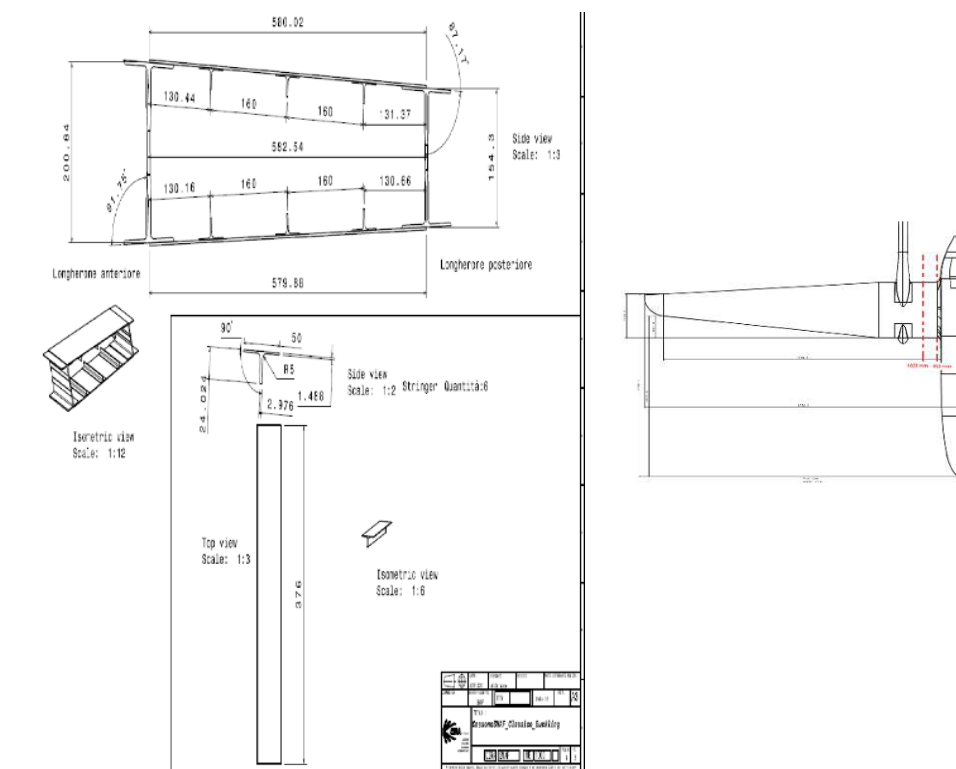


Figure 61 - X-MALE aircraft

Taking into account the above-mentioned purposes of International Research (PA No.3 - AIRCRAFT REPAIR EXEPEDIENT), it was decided to set the external dimensions of the panel to [mm] 750x750, leaving all other geometrical characteristics and lay-up unchanged if compared to what obtained from studies coming from CIRA, except of course the number of stringers that was increased from 3 (on the original CIRA panel) to 4 (COMPRIP panel). For more details see Table 12. An additional simplification was considered in our case, especially a flat panel, rather than curved one. The curvature of these panels is irrelevant to the achievement of the purposes of the project. This simplification was in line with the requirements of COMPRIP project. Geometry, materials and layup used for the structure are reported in the following tables.

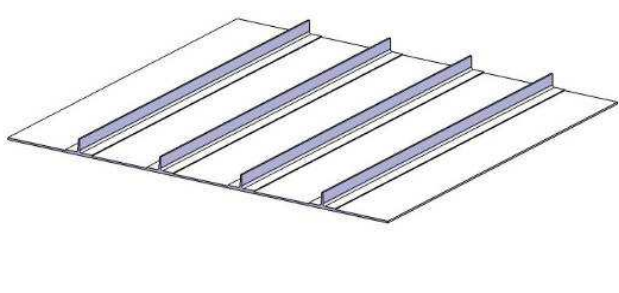
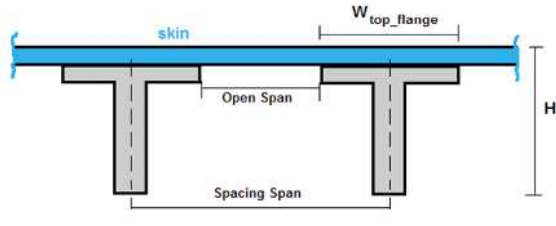
Geometrical parameters	Length [mm]	
Panel Dimensions	750x750	
Height of the Stringer	25.1	
Wtop Flange	52	
Spacing Span	160	
Height Panel	28.5	

Table 12: Panel Geometry

Element		n° ply	Layup	Thickness [mm]
T-section Stringer	Web	8	[+45/0/90/-45]s	2.96
	Flange	4	[+45/0/90/-45]	1.48
Skin		8	[+45/0/90/-45]s	2.96

Table 13: Panel Layup

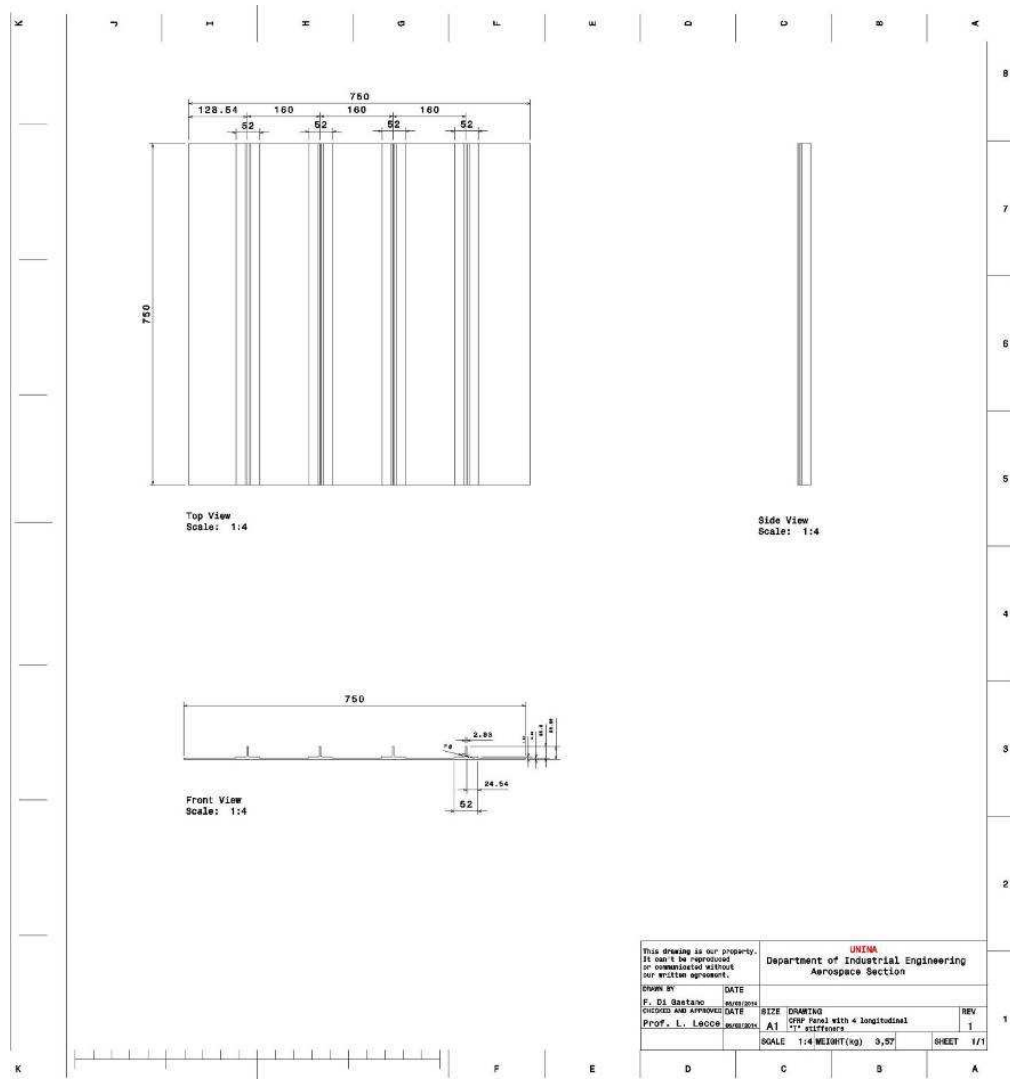


Figure 62 - Views as designed of the CFRP stiffened panel

4.2. Manufacturing of the test articles using RTM process

The manufacturing of composite panels was performed using Resin Transfer Molding (RTM) process, an innovative manufacturing technique, very promising in terms of capability to faithfully reproduce the test articles, as well as the possibility to have duplicates with discrete cost savings. RTM is a process with a rigid closed mold. Figure 63 summarizes the main steps for a simple case. The lamination sequence (preforming phase) is draped in a half mold, then the mold is closed and the preform compacted. After that, the resin is injected using a positive gradient pressure through the gate points replacing the air entrapped within the preform. Usually, vacuum is applied at dedicated vents in order to

favorite the air escape from the mold. When the resin reaches the vents, the gates are clamped and the preform is impregnated. At this point, the cure phase is considered to start. Finally, the mold is opened and the part removed. Especially for aerospace structures, an additional free-mold post-curing phase can be necessary in order to guarantee the polymerization of the matrix and release the internal thermal stress. The closing mold step is characterized by the compaction of the fiber reinforcement, which permits to reach the desired thickness and design fiber volume fraction. The compaction changes the microstructure and the dimensions of the preform, producing large deformations and nonlinear viscoelastic effects. These effects are accompanied by a change in energy within the material, which causes the residual stresses due to the viscoelastic behavior of the fibers. However, during the impregnation phase a release of stress, probably due to the balance, occurs. The injection phase must guarantee the complete impregnation of the preform: a bad impregnation of the fibers results in dry spot areas with missing adhesion between the layers, which makes the surface rough and irregular. If partial impregnation occurs in the proximity of a connecting zone among elements, it can cause a bad integration with a consequent loss of mechanical properties.

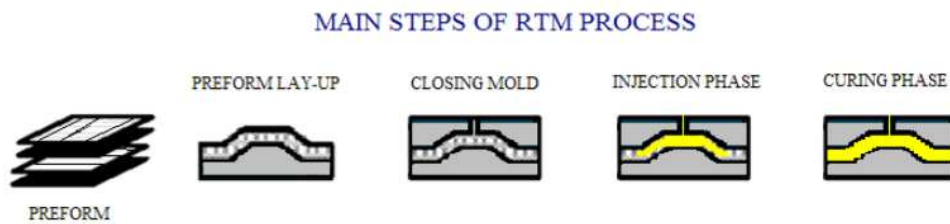


Figure 63 - Sequence of the main steps of RTM process.

The RTM process is governed by variables and parameters that are dependent on each other. Their combination affects the process and the quality of the finished product. Consequently, they need to be carefully determined. The most important parameters, which can't be neglected in the design, are pressure, temperature, viscosity, permeability, volume fraction, and filling time of the process. There are also a multitude of parameters that must be considered independently, such as the angle of attack of the nozzle, the orientation of the fibers, the paths of flow and shear rates, the stratification. In fact, the resin tends to flow more quickly in the fiber direction, thus the flow dynamic depends mainly on the type of fabric used and the number of overlapped layers. Sometimes it may be necessary to have a certain number of skins, not for structural reasons, but to obtain a homogeneous distribution of the resin. The thickness of the part to be manufactured can also affect the flow progress and the impregnation of the fibers, causing a high percentage of voids and dry spots. The thickness becomes a critical design constraint especially in the case of the inclusion of reinforcements and ribs.

The injection pressure determines the injection velocity of the resin into the mold, the hydraulic pressure and the holding and closing forces of the mold. Consequently, the injection velocity defines the filling time, which should not be too short to ensure an adequate impregnation of the fibers and, at the same time, the filling must be such as to avoid the risk of incurring in premature gelation of the resin. The injection pressure adjusts the distribution of the resin on the preform, which affects the formation of air voids in the matrix, the appearance surface and the mechanical properties of the finished product.

Another phenomenon in which this parameter is relevant, together with the viscosity, is the so-called "fiber wash", i.e. the movement of the reinforcement inside the mold during the injection phase. In this case, the surface treatment of the fibers and especially the choice of the binder play a fundamental role. If the binder dissolves too quickly in contact with the resin, then fibers under the injection pressure can move freely. The temperature is an extremely important process parameter and it is strictly related to the injection pressure and the viscosity of the resin. When the temperature increases, the filling time decreases and the working pressures are lower. When the temperature is low, the viscosity of the resin increases and it is necessary to increase the pressure to ensure the transfer of the resin itself [37].

That premised, after the identification and redesign of the composite stiffened panels, the manufacturing process of 6 composite flat panels was performed. The first step concerned the design of a suitable mold able to guarantee a uniform distribution of the resin during the injection phase, see Figure 64. According to the manufacturing process and design considerations, a well-established aerospace high strength (HS) fiber in a five-harness (5HS) woven fabric, Hexcel G0926 carbon fabric, and a suitable resin system RTM 6, were selected [38].

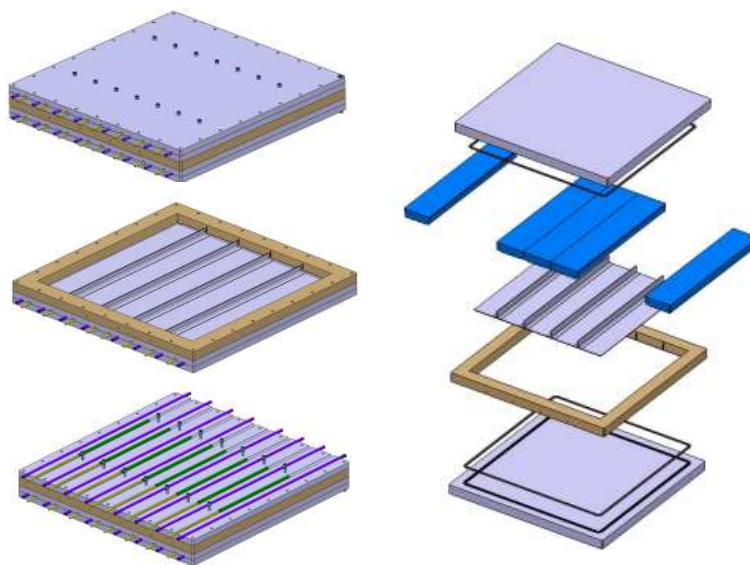


Figure 64 - Exploded view drawing of the mold used in RTM process

The fabrication phase was performed in collaboration with COMPOSITI AVANZATI srl, an industrial partner specialized in RTM process, located in Avetrana (TA); more details are available on www.compositiavanzati.it. Figure 65 shows the equipment used in the RTM process.



Figure 65 - Equipments used for RTM process

Relevant data about the manufacturing process are:

- Preforming: 30 minutes at 120 °C;
- Injection: resin temperature 80 °C, mould temperature 120 °C, curing 75' at 160 °C, pressure 900 KPa.

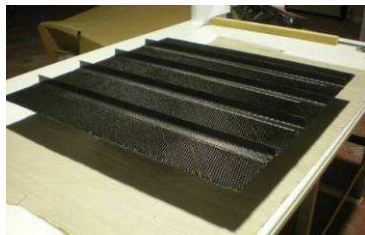


Figure 66 - Iso view of the preform



Figure 67 - Front and back views of the panels

4.3. Inspection Report

In order to ensure the good quality of all the panels fabricated, suitable Non Destructive Investigations (NDI) were identified and performed in collaboration with RAV AEROSPACE srl (Brindisi), an industrial partner of Italian team.

Two non-destructive inspections, ultrasonic based, were run. The reference standard used for calibration in both types of inspections was the step wedge RAVUTCFRP200PE with known defects made by the RAV and approved by AgustaWestland, because reference parameters were not available in our case. For instance, the test report of panel IT_ER_UNINA_4 is reported below.

- **Program:** AER Project
Description: Ultrasonic Non-Destructive Inspections for using manual (PE) and automatic (TT) methods.
- **Items ID:** IT_ER_UNINA_4.
- **Method 1:** Ultrasonic Inspection (Through Transmission mode) with water-column concept, automatic system ADG/Olympus.
The water-column concept eliminates the need for a wedge, thus providing the benefits of a phased array immersion-tank inspection. This concept, which uses a low-flow water supply and consumable gaskets, offers excellent surface conformance and optimized coupling conditions, even on rough surfaces.
Equipment: ADG ultrasonic system with Olympus OMNISCAN MX and probes of 5MHz Olympus V307-SU. The ultrasonic equipment and the probes have valid calibration certificates.
- **Method 2:** Manual Ultrasonic Pulse-Echo.
Equipment: Olympus OMNISCAN MX 2 with and probes of 5MHz Olympus V201-RM and coupling gel GE ZG-F. The ultrasonic equipment and the probes have valid calibration certificates.

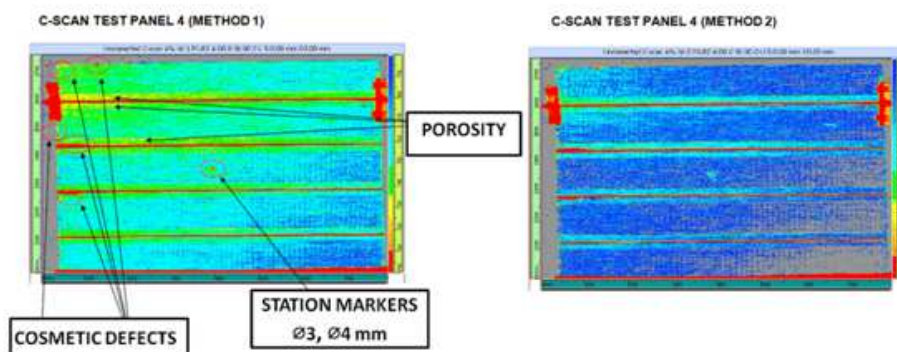


Figure 68 - C-SCAN TEST PANEL: IT_ER_UNINA_4

- **Result:**
 Since no reference parameters were available, the reference standard used for the calibration of both methods of inspections set by the company RAV Aerospace (Brindisi, Italy) and approved by Agusta Westland. Inspections showed small superficial porosities, less than 0.5 mm from the surface, along the longitudinal stiffeners. These results were also confirmed by NDI carried out by the French team. Hence, considering the scope of the ER Project we feel confident that these small and superficial defects will not affect the mechanical characteristics and the global quality of the panels.

4.4. Ballistic tests performed by US team, aimed to define the damage scenario

In agreement with AER Project, ballistic tests were performed by US partner on one of the panel provided by Italian team. Ballistic tests, based on a comparative analysis varying the speed and angle of inclination of the bullet, were intended to define a reference damage scenario to be applied on all the panels of AER Project. Figure 69 summarizes the ballistic tests performed on the panel IT_ER_UNINA_0. As illustrated, a 12.7mm bullet was used and 6 impacts at different speed (2538 f/s to 1530 f/s) and the angle of inclination (from 0 ° to 67°) of the projectile were performed.

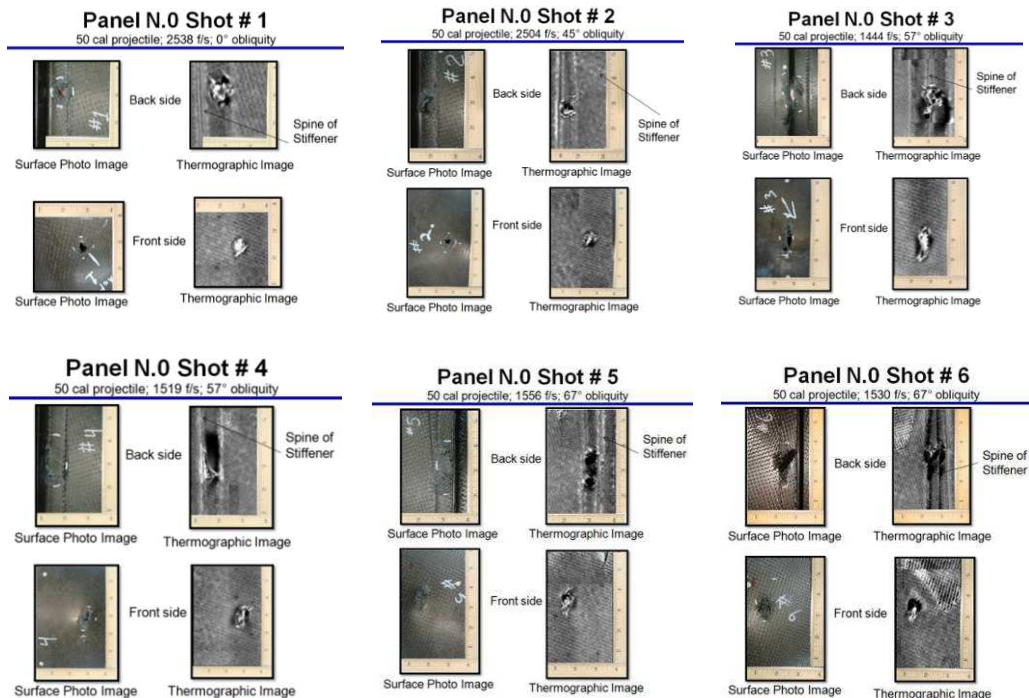


Figure 69 - Synthesis of the ballistic tests performed by US team on item IT_ER_UNINA_0

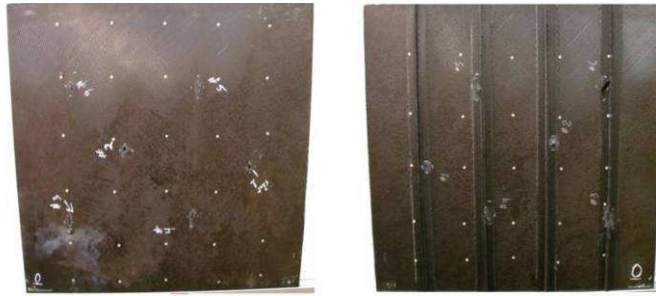


Figure 70 - Front and back views of the panel IT_ER_UNINA_0 after ballistic tests.

Partners of AER Project agreed that the impact condition to be considered as a reference was the number #5 (Figure 69), a bullet fired at a moderate speed (1556 f/s) with a high obliquity angle (67°). It was also agreed that the impact of the bullet shall take place directly on the stiffener, centered on it and that the cut-plan (removal of the damage for the execution of the ER) should have a diameter of 6 inches (152.4mm). Apparently, a hole with a size of 6 inches may seem to be excessive, as the scarfing probably would be extended on the two adjacent stiffeners, but this size was chosen because on the one hand there was the desire to produce a condition of damage representative but also invasive and challenging, in order to require a structural repair; while on the other hand it was added the constraint to have limited accessibility to the damaged part (access only from the surface free of stiffeners, the external side). The location of the damage is depicted in Figure 71.

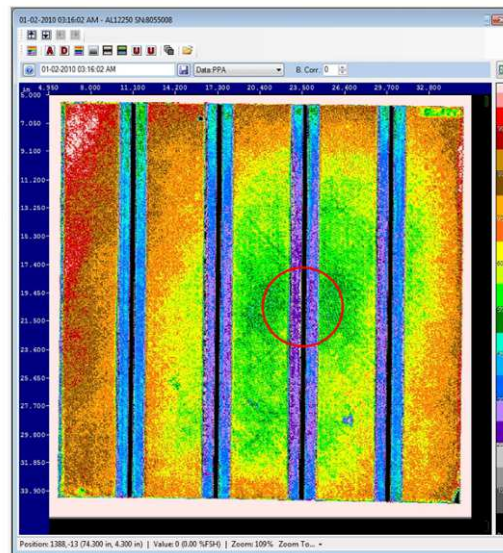


Figure 71 - Damage location proposed by US team.

4.5. Relevant considerations about the location of the damage and loading tests

Based on what reported in the previous paragraph, a 6-inches hole damage centered on the leg of the stiffener was performed by each partner of AER project and in the repair scenario a limited accessibility to the damaged part shall be taken into account. In agreement with these assumptions, before starting with design of the repair, other essential constraint related to test facilities came from the French team that was in charge of performing loading tests.

French team estimated that considering the space requested by the clamping tools (125mm on each side of the panel), the space available for the repair is about 500mm. The test machine will have a specific interface to clamp between the stiffener, a width of 880mm and 3 hydraulic actuators (200t).

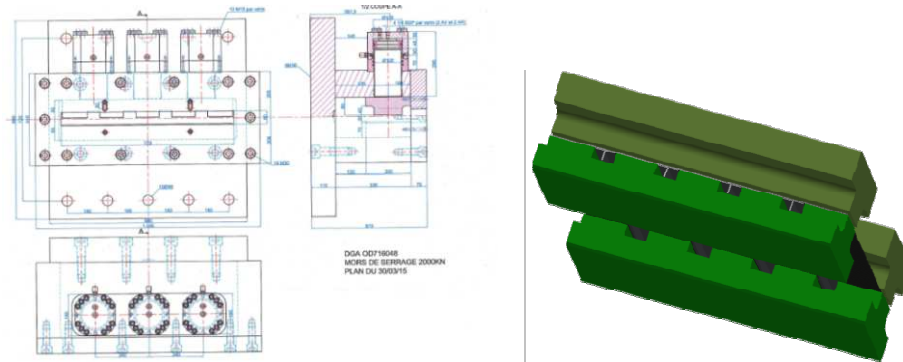


Figure 72 - Clamping tools

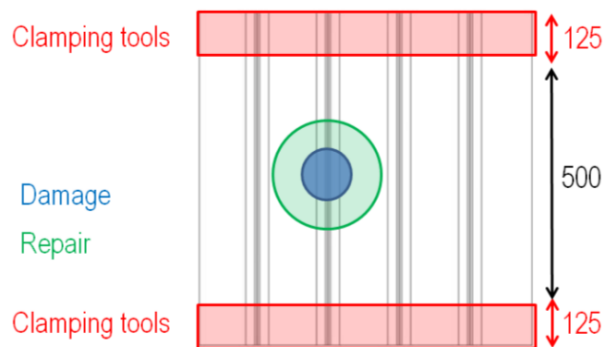


Figure 73 - Area available for Repair

Chapter 5 – Design and implementation of the repair for a Battle-Damaged Composite

Fixed-Wing Aircraft

As illustrated in previous chapter, the use of the FE method to study bonded joints with composite adherends brought a new level of understanding of these structures. The advantage of the method is the ability to determine the stresses within a body of arbitrary geometry. The inclusion of real joint features was a stumbling block for approach based on continuum mechanics because this method could not cope with complex geometries. On the other hand an exclusively experimental approach requires that the same experiments to be conducted for each new type of material. With the versatility of composites, the combinations are endless.

The feasibility study of the design and analysis of a scarf joint through FEM was demonstrated by numerous studies [35-39]. The majority of the models created to simulate adhesively bonded joints have not relied on lamina properties for the composite adherends and have subsequently made relevant assumptions.

The finite element modeling software additionally allows the lamina nature of the adherends to be simulated by modeling each lamina separately. This obviously requires material properties to be manually applied to each individual layer.

5.1. Finite Element Analysis and Modeling

Once relevant data concerning materials, geometry and type of damage to apply on the demonstrators were available, the design of the repair was developed by creating a 3-D FE model.

The model was implemented thanks to the extensive numerical investigation on scarf joints, previously conducted and illustrated in chapter 3. Table 14 shows the dimension of the analyzed scarf joint with relative geometry.

Quantity	Dimension
tp	2,96 mm
ta	0,37 mm
L	134 mm
LR	76.2 mm
Lt	33,8 mm
α	5°
Ply thickness	0,37 mm
Number of plies	8

Table 14: Panel Layout

The model was created using a bottom up approach. The two dimensional model was built as a skeleton based upon a Cartesian coordinate system (Figure 74). This was representative of the symmetrical through sample width. The skeleton was created through the input of key point coordinates, which act as nodes for creation of end points of lines.

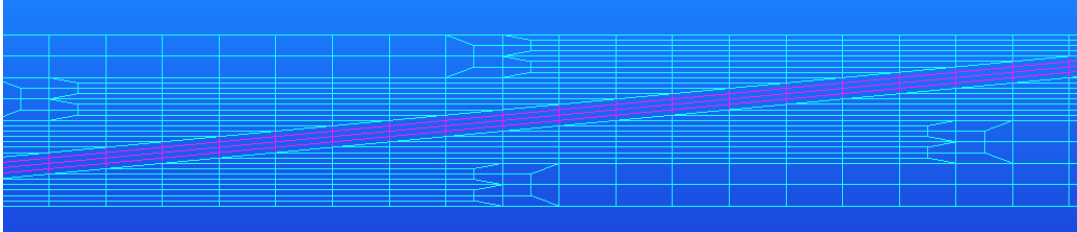


Figure 74 - FE model mesh detail

Line in violet represent the adhesive layer, while 3D solid blue elements constitute the composite parent laminate. The adherend plies were specified to be three-dimensional orthotropic materials with the adhesive specified to be an isotropic material. The properties of the adherends plies were based on room temperature properties for G0926/RTM6 carbon fiber fabric from Hexcel® [38] and from literature [40], while adhesive properties were obtained by FM®300-2 film adhesive data sheet [41]. These properties are provided in Table 15.

G0926/RTM6	E11	E22	G12	v12
	60000MPa	60000MPa	4300MPa	0,05
FM300-2	E	G	v	
	2268MPa	840MPa	0,35	

Table 15 - Material data

The base laminate chosen for this analyses consisted of 8 plies with a layup specified as follows: [+45°/ -45°/ 0°/ 90°]s.

Boundary conditions are simulated by fixing one end of the specimen, applying a constant load in the longitudinal direction on the other one, as simulating uni-axial tensile test and to ensure a perfect transfer of tensile load, a guide has been introduced at lower edge of the coupon, allowing only displacement along x-direction. In more detail, the presented study performed firstly elastic finite element analyses of scarf joints to investigate the stress concentration in composite-to-composite scarf joints, especially highlighting the influence of stacking sequence, laminate thickness, and adhesive yielding on the distribution of the stresses in the bondline. The analyses are then extended to a non linear elastic-plastic analysis of the scarf model in order to evaluate the stress and strain concentration under an incremental load until yielding point of adhesive is reached.

5.2. Elastic Analysis

At this stage the nonlinear shear behavior of the adhesive was not considered for this initial investigation into the adhesive stress. The average shear and peel stresses are related to the applied stress via the expressions σ_{av} (11) and τ_{av} (12).

For isotropic adherends, such as metallic materials, the above solutions have been confirmed to agree well with computational results. For composite laminates, however, the adhesive stresses can vary significantly along the scarf, because the in-plane stiffness of a composite laminate varies in the through-the-thickness direction. According to the simple first-order approximation suggested by Baker [30], the stress concentration factor can be expressed in terms of the ply percentage and stiffness ratios:

$$K_a = \frac{1}{P_0 + P_{45} \frac{E_{45}}{E_0} + P_{90} \frac{E_{90}}{E_0}} \quad (14)$$

where P and E denote respectively, the ply percentage and modulus of a given ply orientation, while the subscripts indicate the ply angle. For G0926/RTM6 laminate, the above theoretical first approximation yields to a stress concentration factor close to 1,7.

Linear static analysis was run using SOL101-MSC.Nastran and a particular focus was on the stresses along the mid-plane of the adhesive layer. Plot of the adhesive shear stress distribution within orthotropic adherend is provided in Figure 75.

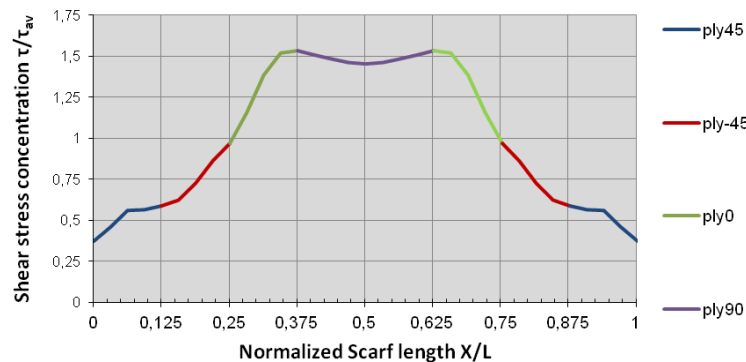


Figure 75 - Shear stress concentration of the scarf joint ($\alpha=5^\circ$)

It has been normalized by the average shear stress (τ_{av}) in the middle of the adhesive thickness. This plot confirms the existence of significant stress concentrations in the bondline of the scarf. High shear stresses occur at the ends of 0° plies and the adhesive shear stress concentration factor (K_a) is approximately 1,5, which is a value close to the empirical value of 1,7 calculated above. It means an error of about 22%. These stresses concentrations may cause shear failure (if the maximum shear stress criterion is applied) at a load much lower than if the average shear stress criterion is used. The last portion of the adhesive at the free

surface is incapable of carrying load, hence the shear stress tend to zero after the peaks. The peel stress (or normal stress) was taken perpendicular to the scarf bondline and are plotted in Figure 76. They are also normalized with respect to average shear stress (τ_{av}).

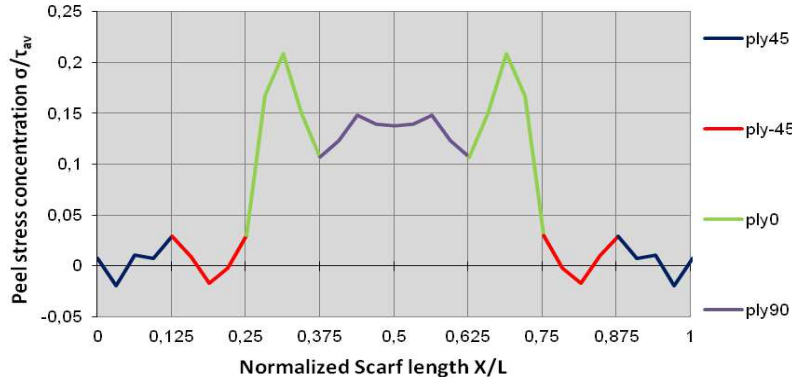


Figure 76 - Peel stress concentration of the scarf joint ($\alpha=5^\circ$)

At the mid-plane of adhesive layer a high peel-stress peak is noticed. Peel stresses, anyway, are lower than shear stress, which are more uniform.

Since the majority of structural adhesives can deform plastically prior to failure, particularly under shear deformation, predictions based on elastic analyses may be overly conservative. Therefore, it is important to perform an elastic-plastic analysis to account for the elastic-plastic deformation behavior of the adhesive in strength prediction.

5.3. Elastic-plastic Analysis

Elastic-plastic finite element analysis was performed to quantify the resulting stress redistribution as the adhesive reached plastic yielding. The geometry, material property and boundary conditions are identical to the these one applied in case of the elastic analysis. A summary is proposed in Tables 16-17.

Quantity	Dimension
tP	2,96 mm
tA	0,37 mm
L	53.8 mm
LR	76.2 mm
Lt	33,8 mm
α	5°
Ply thickness	0,37 mm
Number of plies	8
Stacking sequence	[+45°, -45°, 0°, 90°] _s

Table 16: Joint Geometry

G0926/RTM6	E11	E22	G12	v12
	60000MPa	60000MPa	4300MPa	0,05
FM300-2	E	G	v	Yield stress
	2268MPa	840MPa	0,35	50MPa

Table 17: Material data

The adhesive properties were considered at room temperature. Aimed at computational simplification, the adhesive stress-strain curve was idealized to be elastic-perfectly plastic with a yield stress of 50 MPa, as shown in Figure 77.

As previously seen, thanks to this idealization, only two more parameters were required for modeling the adhesive: the yield strength (τ_y) and the ultimate shear strain (γ_{ult}).

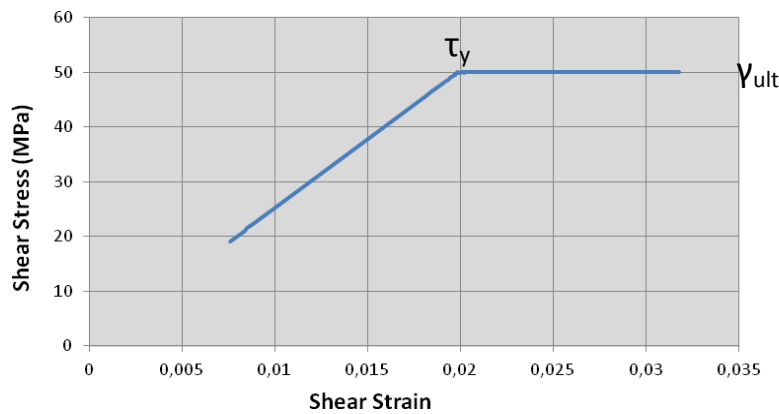


Figure 77 - Numerical Shear/Strain curve for FM300-2 film adhesive

An incremental elastic-plastic analysis was performed using SOL106- MSC.Nastran. Table 18 presents the applied load history.

Load history				
Case 1	τ_{av}/τ_y	0,20	10	MPa
Case 2	τ_{av}/τ_y	0,40	20	MPa
Case 3	τ_{av}/τ_y	0,60	30	MPa
Case 4	τ_{av}/τ_y	0,80	40	MPa
Case 5	τ_{av}/τ_y	0,88	44	MPa
Case 6	τ_{av}/τ_y	0,98	49	MPa
Case 7	τ_{av}/τ_y	1,005	50,25	MPa

Table 18: Load History

From the results of the elastic-plastic analysis, the normalized shear stress (τ/τ_y) and normalized shear strain (γ/γ_y) along the bondline are shown in Figure 78 and 79. It is clear that as the applied load increases the shear stress approaches the yield stress over the entire scarf.

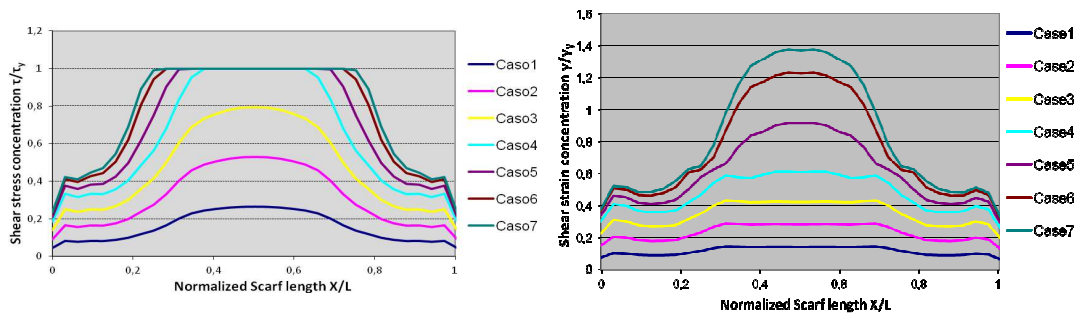


Figure 78 - Shear stress distribution along the mid-plane of adhesive layer.

Figure 79 - Shear strain distribution along the mid-plane of adhesive layer.

Although stresses would eventually become uniform as the adhesive undergoes plastic deformation, significant strain concentration still occur at the end of 0° plies. Consequently, the maximum strain in the adhesive bond may exceed the strain allowable before the average shear stress reaches the stress allowable.

5.4. FE Modeling of Progressive Failure for Bonded Joints

Research was aimed to assess the effectiveness of ER concepts, evolution of Aircraft Battle Damage Repair (ABDR), in case of a fixed-wing composite aircraft, subjected to battle-field damages.

A large representative and challenging damage condition that required a structural repair, was performed on a flat stiffened composite panel, representative of a lower wing skin, in order to investigate the performance of on-field repairs. The assessment involved a relative comparison of four models, representing pristine, damaged with simulated ballistic damage and repaired with a condition of full and a limited accessibility to the damaged composite structure. In case of the full access condition, a scarf repair based on adhesives and filler composite patch was taken into account, while for the limited access condition, a coupling of bonded patch and bolted substantiation was considered.

A FE predictive model that can be applied to the design of repairs for conventional (as reported in the SRM) and unconventional damages, was developed and implemented with the aim to investigate stress and strain concentration, the failure initiation and failure progression mechanisms of involved composite structures.

Numerical models are studied at a global scale of the composite stiffened panel. Linear and non linear analyses were conducted.

Hill criterion with a progressive failure analysis was implemented to describe the global behavior of the panel up to collapse. Load curves permitted to estimate the expected load and displacements.

5.4.1. Numerical approach

Finite element modeling was conducted through the design of four models (pristine, damaged, repaired with full- and limited- accessibility to the damaged part) as shown in Figure 80.

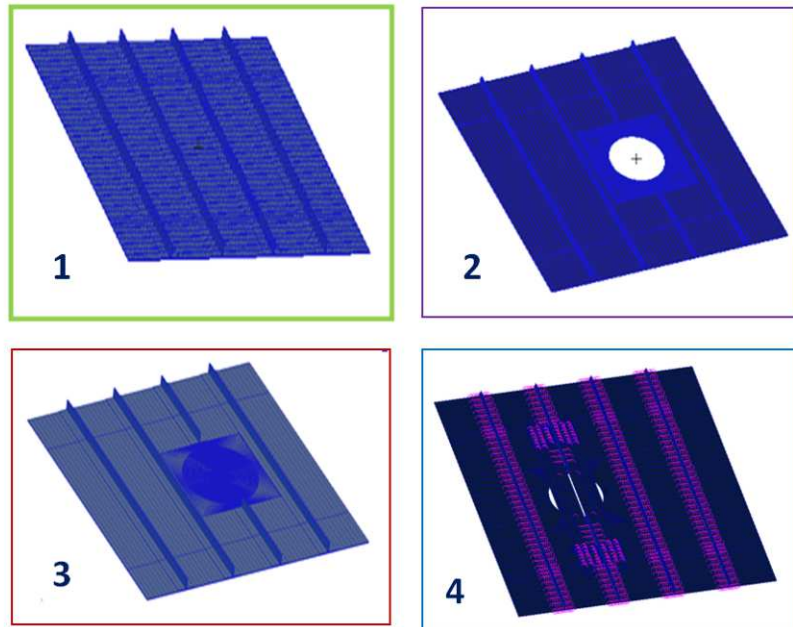


Figure 80 - FE models of specimens: pristine (1); damaged (2); full access repair (3); limited access repair (4).

As agreed by partners of AER Project, according to the constraints given by clamping tools that will be used French partner for performing the loading tests, boundary conditions were simulated using two Rigid Body Elements (RBE2). All degrees of freedom (DOFs) 123456 were locked on one edge of the panel, while the second edge was free to move only along the axial direction, the DOFs 23456 were locked. Two grid points were defined as independent grid points, transmitting corresponding DOFs to the dependent nodes located at the panel edges. Pre- and post-processing phase analyses were conducted using MSC.Patran, while the solver was MSC.Nastran, for linear analysis with SOL101 and for implicit non linear analysis with SOL400, in which Newton–Raphson method was used with a residual force of 0.1. Around current analysis, outcomes of using a linear analysis and displacements to be applied to a non linear analysis was discussed. In order to predict the damage initiation and the final failure of a repaired system, a linear static analysis was proved to be very useful. The numerical strategy implemented on each referenced model is outlined in Figure 81, in particular it underlines the use of results obtained by each analysis type to be introduced in the next one.

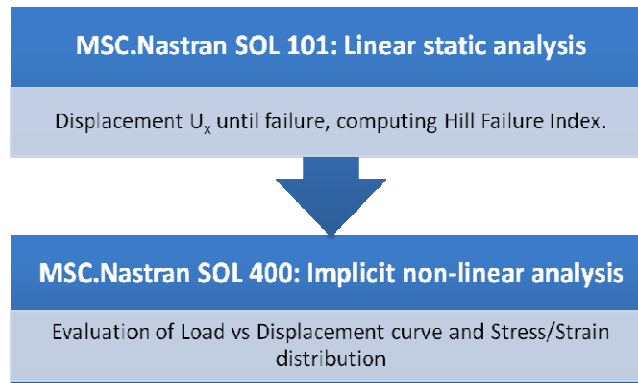


Figure 81 - Modeling strategy between each analysis

Linear static analysis is aimed at easily obtaining the panel displacement at failure, to be incorporated in a non linear analysis. Finally, by increasing the applied force until failure, the independent grid point displacement is recorded and used in the non-linear solver to consider geometric non linearity, called by SOL400 in Nastran. A displacement of 10 mm is applied at the independent node and an increment of 0.05 mm was used. The adhesive properties, considered as elastic-perfectly plastic with yielding stress of 50 MPa and thickness of 0.37 mm, plays an important role in the performance of the patched specimen.

5.4.2. Undamaged Panel

As known, undamaged specimen was manufactured by RTM process with Hexcel G0926/RTM6. Material properties are taken from Hexcel [35,38] and are given in Table 19. Geometry and FE model of the undamaged panel are reported in Figure 82.

G0926/RTM6	E11	E22	G12	ν_{12}	Xt=Yt	Xc=Yc	S12
	60000MPa	60000MPa	4300MPa	0,05	860MPa	700MPa	100MPa

Table 19: G0926/RTM6 datasheet from Hexcel

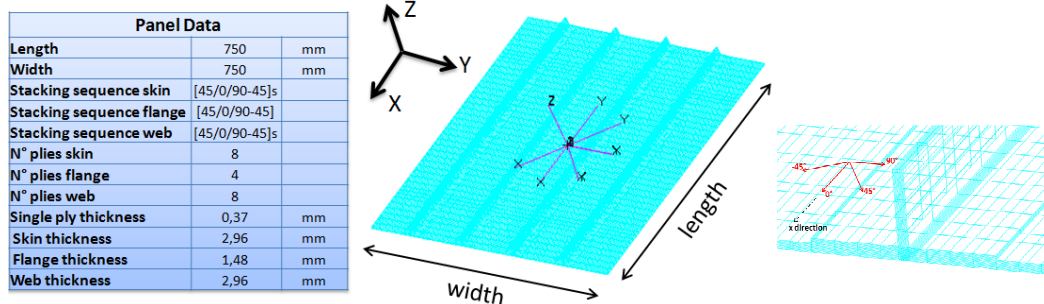


Figure 82 - Geometric data and FEM of the undamaged laminate

The model was created using a bottom up approach, starting from a 2D model, as illustrated in previous chapters. Concerning the boundary conditions, all degrees of freedom (DOFs) 123456 were locked on one edge of the panel, while the second edge was free to move only along the axial direction, the DOFs 23456 were locked. Both constraints take 125 mm of the edge length as specified by Partners of AER Project. The Hill criterion [14] was implemented in linear elastic analysis to evaluate Failure Index and respective displacement at failure.

$$\frac{\sigma_{11}^2}{X^2} + \frac{\sigma_{22}^2}{Y^2} + \frac{\sigma_{11}\sigma_{22}}{X} + \frac{\tau_{12}^2}{S^2} \quad (4)$$

σ_{11} and σ_{22} are stresses in the longitudinal and transverse directions of the ply. τ_{12} is the shear stress. X and Y indices stand for allowable tensile and compressive stresses respectively in the warp (X) and weft (Y) directions. The Hill failure criterion is an interactive failure criterion, it does not give the mode of failure but includes stress interactions. This makes it convenient to study a global behavior of a part as all failure modes are included in one expression. Various trial loads were analyzed until Hill Index was greater than one. Displayed results are X displacements along the panel length in (a) and finally Failure Indices (FI) in (b) for a load of 200 ton (Figure 83).

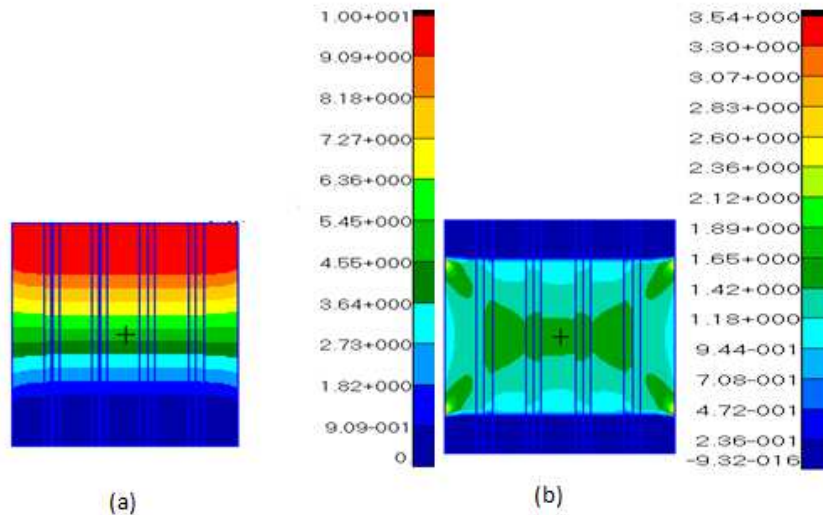


Figure 83 - Linear analysis results for the panel

Giving a look to the results of the linear analyses (SOL101) displayed in Figure 83, it can be noticed that the panel collapse for a load of about 200 ton, since $FI = 1.4$. Stresses concentrate at panel center where FI assumes the highest value. The longitudinal displacement of $U_x = 10\text{mm}$ is written down to be further introduced in the non linear analysis.

Linear analysis assumes a linear relationship between the load applied to a structure and the response of the structure. The stiffness of a structure in a linear analysis does not change depending on its previous state. Linear problems are solved in one step, and linear analysis can provide a good approximation of a structure response. It is important to highlight that predictions based on elastic analyses may under- or over-estimate displacement at failure, that is because linear behavior is restricted to small displacements, otherwise the stiffness of the structure changes and must be accounted for regenerating the stiffness matrix. Lastly, loads are assumed to be applied slowly as to keep the structure in equilibrium. Due to this reason, it is important to account for the non-linear behavior of the panel.

The displacements output from this model will be used as reference for the repaired and plate as the aim in any repair scheme is to restore a damaged component to a fully functional state.

➤ Progressive Failure Analysis (PFA)

Three dimensional finite element based progressive failure analysis method is used to study first ply failure and progression of failure of the models under in-plane geometrically non-linear deformations. In the progressive failure analysis of structures, geometric non-linear effects become prominent when the structure is subjected to large displacement and/or rotation.

Follow force effect due to a change in load as a function of displacement and rotation is one aspect of geometric non-linearity that must also be taken into account especially when the structures are subjected to out-of-plane loads resulting in large deformation. One of the aims of the presented study is to perform a non-linear progressive failure analysis through case studied. Therefore, a major objective of the present study is also to investigate the significance of geometrically non-linear analysis on the progressive failure response of composite laminates. For this purpose different ply and constituent based failure criteria and material property degradation schemes were implemented into a FE software as MSC.Patran and MSC.Nastran. By means of progressive failure analysis residual strength of the laminates can be determined. It is known that composite laminates with local damages can sustain operating loads much better than their metallic counterparts. Higher residual strength is a desirable property because especially in aerospace applications, the structure with local damage is expected to sustain the operating loads before the local damage is identified in a maintenance period. There are various methodologies used for progressive failure analysis in the literature but all of these examples are based on same procedure. A typical methodology for progressive failure analysis is shown in Figure 84.

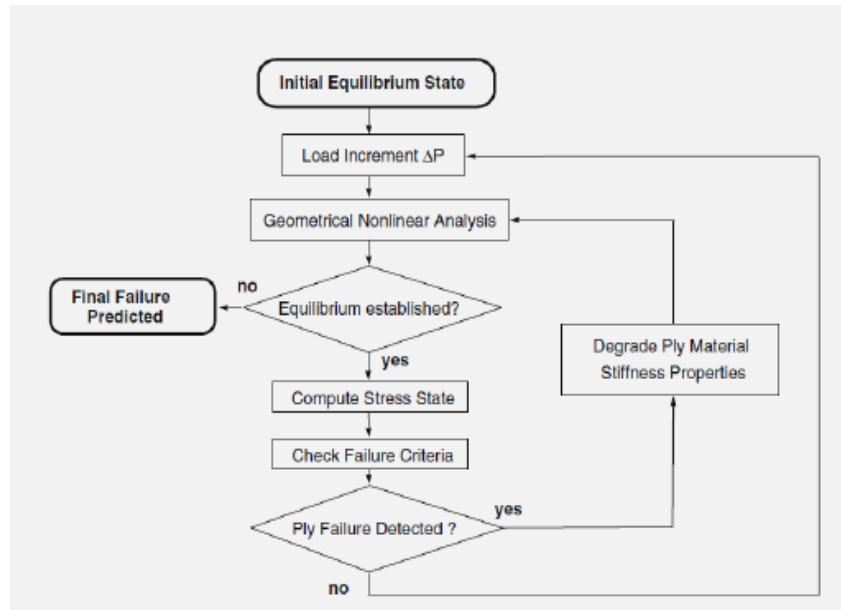


Figure 84 - Progressive failure analysis methodology

For an initial state, which is in equilibrium statically, load is incremented and finite element analysis is performed to calculate the displacements, strains and stresses in the composite structure. In general, one can perform geometrically linear or non-linear finite element analysis to determine the field quantities. Figure 84 shows a typical procedure in which geometrically non-linear finite element analysis is employed in the strain/stress recovery procedure. An incremental load is applied and then iteration is undertaken until a converged solution is achieved. Once the converged solution is achieved a failure criterion is invoked to detect local lamina failure and determine the failure mode. If no failure is detected at the particular load level, the load is incremented again and the whole process of establishing the equilibrium, stress recovery and check of the failure criterion is repeated at the current load level. If failure is detected at a particular load level, then a material degradation model is needed in order to determine new estimates of the local material properties and propagate the failure. After the degradation of the material properties of the damaged layer, a finite element analysis is conducted at the same load level without incrementing the load. Since the material properties are degraded locally due the failure induced, equilibrium must be re-established. Once the equilibrium is re-established, stress recovery and failure checks are performed as before. This loop continues until equilibrium cannot be established in geometrically non-linear finite element analysis. In the current study progressive failure analysis procedure is similar to the one defined in Figure 85. At an initial equilibrium state, finite element model is automatically sent to analysis in MSC.Nastran for the particular load and boundary condition case which is defined. After the completion of the analysis, the requested results are attached and depending on the failure criteria used, failure indices are calculated

based on the strains or stresses at the pre-defined location within the element. In the results presented in this study, failure indices are calculated based on the stresses at the Gauss point of solid elements.

Material degradation is the core of progressive failure analysis, especially for the estimation of ultimate failure. If failure does not cause an ultimate failure, the load on the failed material should be redistributed to the remaining undamaged material in some manner. For example, as mentioned by Tay et.al [42] in the element failure method that he proposed, the nodal forces of finite elements are manipulated to simulate the effect of damage while leaving the material stiffness values unchanged. However, in the most of studies in the literature, material property degradation has been performed by the stiffness reduction method [42-43]. Material property degradation proceeds throughout the structure according to the failure criterion implemented until no additional load can be sustained. The main idea in the stiffness reduction method is modeling failure of damaged material by reducing stiffness values. As an example, Tan et.al [42] has proposed a two-dimensional progressive failure method for a laminate with central hole under tensile/compressive loads. As shown in Equation (15), Tan used three internal state variables to reduce stiffness. Here E_{110} , E_{220} , G_{120} are undamaged material properties and E_{11} , E_{22} , G_{12} are damaged/degraded material properties.

$$E_{11} = D_1 E_{110} \quad E_{22} = D_2 E_{220} \quad G_{12} = D_6 G_{120} \quad (15)$$

The main challenge in material property degradation is to properly characterize the residual stiffness of the damaged material. At this point, material property degradation can be divided into three categories; sudden degradation, gradual degradation and constant stress at ply failure. In gradual degradation, associated material properties are degraded to zero gradually by using degradation factor between "0" and "1", while performing sudden degradation, after degrading associated material properties of an element according to a degradation model, compared to the intact element, the degraded element will take less load in the following iterations. This can be only achieved by using degradation factors less than one. The study is performed on the laminate model presented in previous section under a uniform tensile load, simulated with an enforce displacement of 10 mm. A material non-linear behavior was considered for the bonded repair specimens to examine the strength of the adhesive layer under the maximum load determined from the linear static analyses, where an elastic-perfect-plastic material model and Von-Mises yield criterion were used. For the adherends a geometric non-linear analysis, which is time consuming, was performed only for the axial tension load case to compare the results.

The failure analysis of composite laminates subjected to in-plane loads is complicated due to the fact that both material and geometric non-linearity become effective, when the loads are increased beyond the first ply failure. Material non-

linearity occurs due to damage accumulation, and geometric non-linearity become effective due to the large displacements which the structure undergoes after first ply failure and before the ultimate failure.

Another aspect of geometric nonlinear analysis involves follower forces. If the load is sufficient to cause large deformation in the structure, then in the deformed configuration, the load follows the structure to its deformed state. Capturing this behavior requires the iterative update techniques of nonlinear analysis.

In case of geometric nonlinearity, there are two distinct deformation types to consider:

- I. Large displacement, small strain: In large displacement small strain deformation type, the structure undergoes under large rotations as shown in Figure 85(a), but the strains remain small. In this deformation type, stiffness matrix is simply transformed to account for rotation. Therefore, large displacement small strain solutions are cheaper than the full large strain solutions.
- II. Large displacement, large strain: Large displacement, large strain deformation occurs when the strains also become large as shown in Figure 85(b). In such cases the whole element shape, hence the stiffness matrix, changes. Thus, stiffness matrix cannot be transformed by a rotation matrix.

In either case, the stiffness matrix is a function of the deformation, and the problem is non-linear.

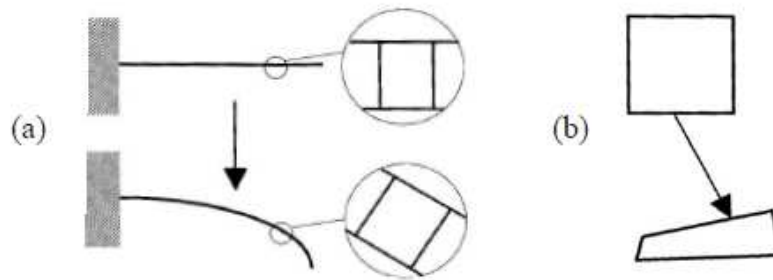


**Figure 85 - Example of (a) large displacement, small strain
(b) large displacement, large strain**

In this work SOL400 of Nastran solver (Implicit Nonlinear, Large deformation-large strain) was implemented into progressive failure analysis to evaluate effects of in-plane loads on the first ply failure and progression of failure in composite laminates. Throughout the study axial loads are assumed to have follower direction of the deformation.

➤ Non-linear Static Analysis

An implicit non-linear analysis SOL400, implemented in the MSC.Nastran solver, was performed in order to evaluate first ply and ultimate failure of the four FE models examined.

In the present study material property degradation factor is taken as "0.001". Displacement increment has been used for the purpose of comparing the load/displacement curves directly. Load is applied by enforced displacement at the free end of the laminate. An initial displacement of 0.02 mm is applied to the laminate and in each load step the displacement is incremented by an initial factor 0.05 mm. Increment type has been set as Adaptive .

Based on the results obtained with previous step (a displacement of 10 mm was applied at the independent node), the PFA was performed with SOL400 Implicit non linear - MSC.NASTRAN, in order to predict the first ply failure and progression of failure under in-plane geometrically non linear deformations.

Figure 87 shows the load-displacement curve of the pristine specimen subjected to tensile test up to failure. Results show that for the undamaged panel, the first ply failure is obtained at about 141 tons, while the ultimate failure is at 148 tons.

```

PARAM MRFOLLOW3 0
PARAM MRFOLLOW4 1
PARAM MRFOLLOW1 0
NLSTEP 1 1.
      GENERAL 30 1 10
      ADAPT .01 1.-5 .5 4 1.2 0
      6 2.-4
      MECH PV .01 PFNT
      .2
$ Elements and Element Properties for region : plies45
PSOLID 1 1 2 GAUSS
PSLDN1 1 1
      C8 SOLID L
$ Pset: "plies45" will be imported as: "psolid.1"
CHEXA 1 1 56553 56554 56552 56551

```

```

MATF 1 2
      CRI 3 860. 700. 860. 700. 860.
      700. 100. 100. 100.
+
$ Multipoint Constraints of the Entire Model
RBE2 1 133559 123456 1 2 3 4
      5
      6 7 8 42 43 44 45

```

Figure 86 - NLSTEP card and MATF card extracted by .bdf file

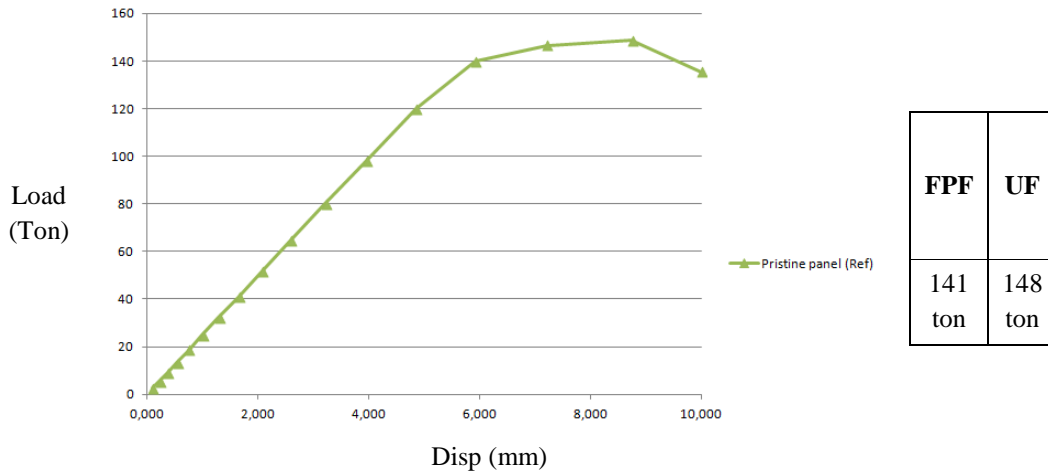


Figure 87 - PFA on the pristine specimen

5.4.3. Damaged, Repaired with full accessibility and Repaired with limited accessibility to damaged part

➤ **Damaged panel**

The damaged panel to test in tensile presents a 6 inches (152.4mm) hole located on the center of the stiffener, as reported in Figure 88. The damaged material was cut out leaving a circular hole, after a simulated ballistic impact in order to give external access to the damaged part. It is the configuration of the panel just before the repair is carried out.

The damaged panel was modeled to show the effect of the hole in the structure in terms of decay of the mechanical performance. The resulting mesh around the hole had a greater density to warrant accurate stress calculations around it. This area was more likely to have stress concentrations. Figure 88 depicts the mesh for this model and a detail of the elements around the hole.

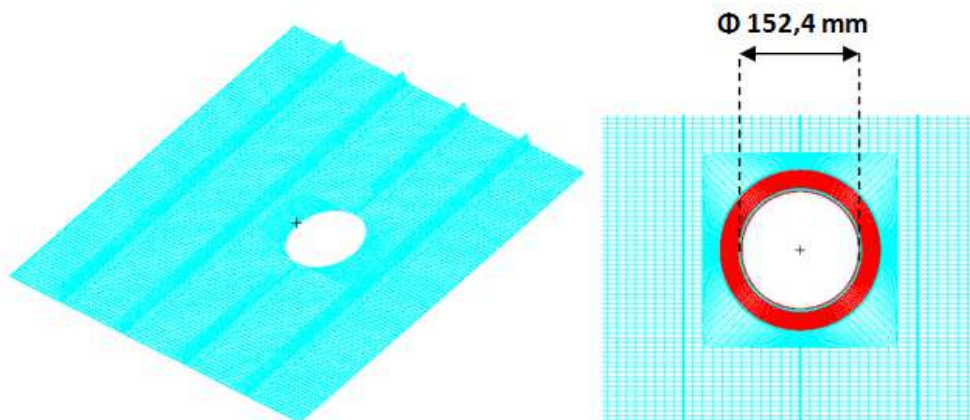


Figure 88 - Damaged panel and refined area around the hole.

First, a linear elastic analysis was conducted to characterize the stress state and to evaluate Hill failure index. The results of the linear elastic analysis were plotted in Figure 89 for the four sequence of orientation (0, 90 and ± 45), that correspond to plies direction around the circular hole along the highlighted line.

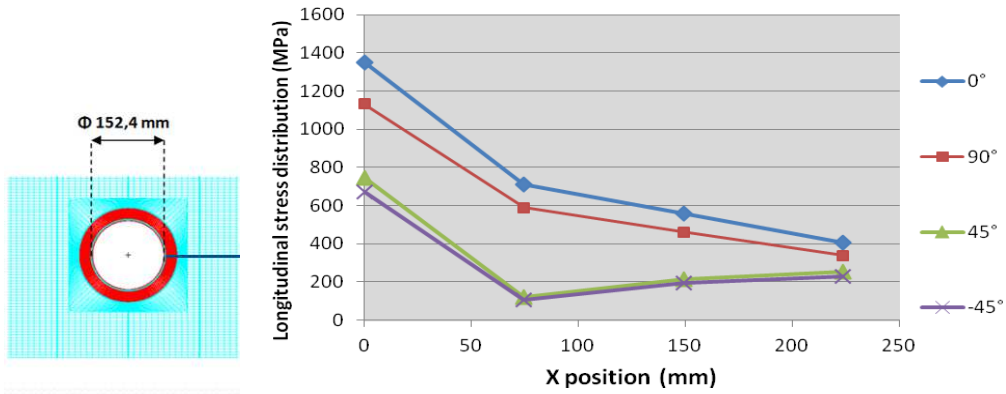


Figure 89 - Damaged Stress distribution of cracked hole composite subject to a tensile displacement of 10 mm

In Figure 90 Hill Failure index, computed by Nastran solver are presented.

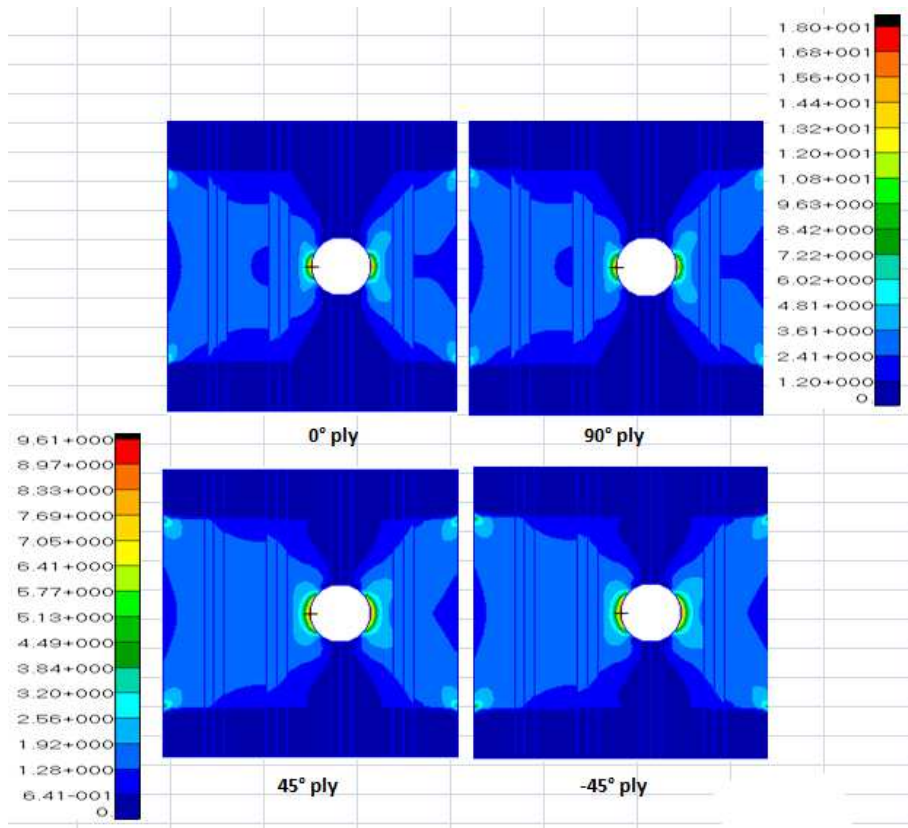


Figure 90 - Hill Failure Index.

Obviously, the hole creates regions of high stress concentrations, this reduces the load bearing capability of the laminate. Away from the hole, the stress distribution remains similar to the undamaged plate. It can be seen that the stress concentration reaches a maximum for fiber orientation angle of 0° , causing more of the force transfer to take place through the fibers. The 3D orthotropic damaged model provided a general guide to the plate overall response.

➤ **Repaired with full accessibility to the damaged part**

In this section the modeling strategy adopted for the repaired panel and the analysis of elastic response of the structure are presented.

The procedure followed for building this model started with the model geometry definition using geometric entities such as points, lines, surfaces and volumes. The nodes at the interfaces between the adhesive layers, the repair patches and the parent laminates were carefully merged to ensure continuity throughout the model. 3D solid elements (HEX8 and WEDGE6) were used throughout this model. For the composite adherends and repair patches, equivalent orthotropic properties were used. The mesh size, boundary and load condition used was exactly the same as for the 3D undamaged panel. Geometric data of the scarf are presented in Table 20, whereas the top view of the composite laminate with the scarf repair and a detail of tapered patches are illustrated in Figure 91.

Quantity	Dimension
Plies thickness	2,96 mm
Ad thickness	0,37 mm
Lt	33,8 mm
Scarf angle	5°
Ply thickness	0,37 mm
Number of patches	8

Table 20: Geometric data of the scarf repair

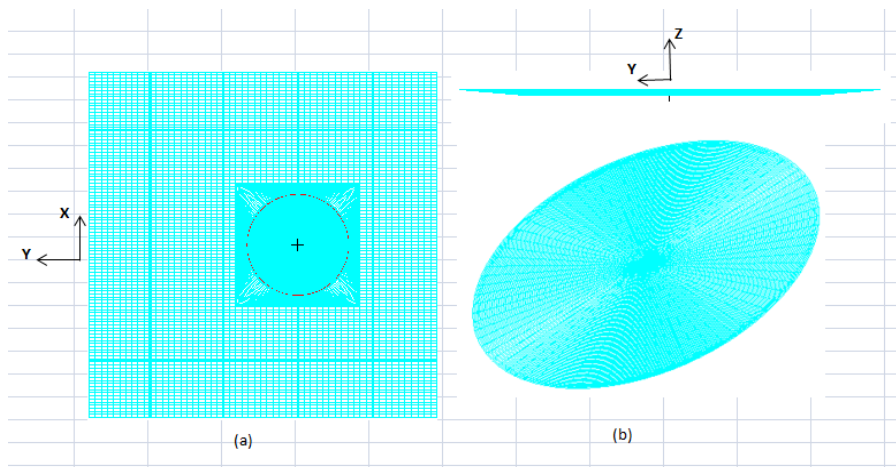


Figure 91 - Repaired Panel: (a) Top view; (b) Scarf detail

The tapered scarf is modeled as a series of steps and each step consists of the adhesive layer in between the repair and base adherend. Properties of adhesive FM®300-2 film adhesive [41] are shown in Table 21.

Adhesive	Properties			
	E	G	v	Yield stress
FM300-2	2268MPa	840MPa	0,35	50MPa

Table 21: Adhesive properties

The panel is subjected to an in-plane enforced displacement of 10 mm, as previously found in undamaged elastic analysis; the stresses in the mid-plane of repaired panel are shown in Figure 92.

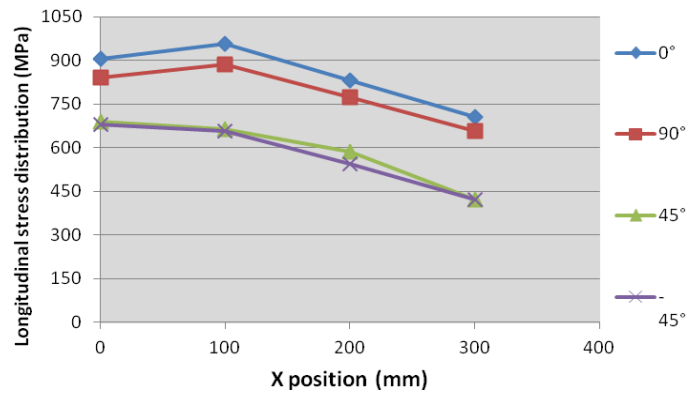


Figure 92 - Stress distribution of the repaired composite panel subject to a tensile displacement of 10 mm

It results interesting the comparison between stress distribution of the repaired panel and stress distribution of damaged panel found previously. Figure 93 shows the comparison between this stresses in case of the plies at 0°, the ones that are subjected to the higher stress value.

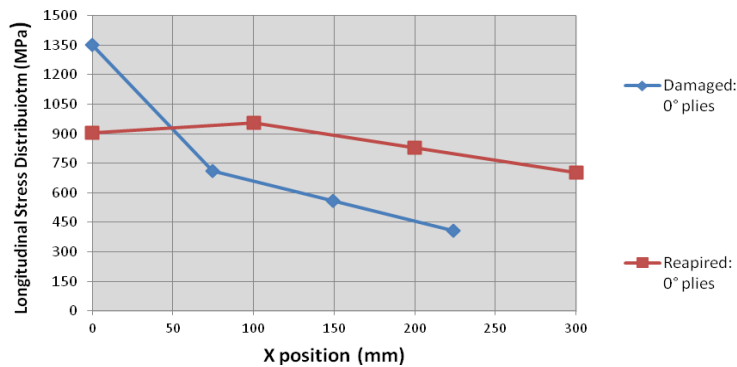


Figure 93 - Stress comparison between damaged and undamaged panels for 0° ply orientation.

Unlike the homogeneous adherends, the stress distribution in the laminated joints has an oscillating trend and locations of the peaks are in the vicinity of the 0° degree plies. However, a lower stress distribution can be noticed in the repaired panel, meaning probably an efficient repair was performed.

➤ **Repaired with limited accessibility to the damaged part**

Based on what agreed in AER Project, concerning the damage scenario, in particular the constraint of performing a repair with limited accessibility (access is only available through the hole created by the damage, external access only) and considering that design of the repair will be performed using strength allowable coming from literature, a bonded filler patch with a bolted repair substantiation was developed and implemented. The sole external repair concept is shown in Figure 94, it represents the repaired structure that will be tested by French partner within AER Project.

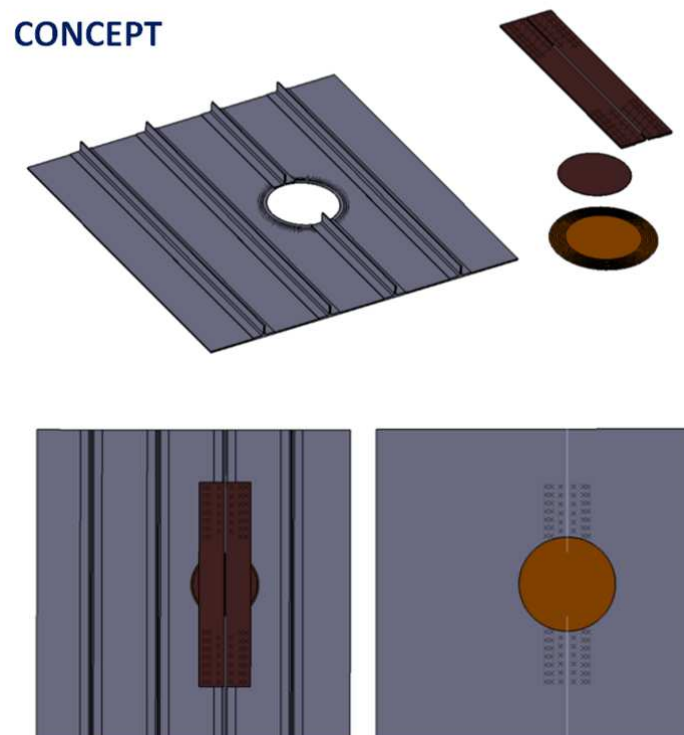


Figure 94 - Layout of repair configuration in case external access (only through damage hole)

The purpose of the exterior patch is to restore fuselage working skin continuity and to seal the structure from environmental ingress, whilst the aluminum bars are designed to restore the disrupted load path across the stiffeners and to ensure a solid base to perform the bonding. The sealed aluminum disk is needed to guarantee the application of the external patch by using a portable hot bonder, not

possible in presence of air leakages around the hole. The relevant property data of all the material used, are listed in Table 22.

Fiber : G0926 5H Satin Carbon Fiber Fabric by HEXCEL® (same fabric used for manufacturing, easy to store)				
Layup : the same of the parent material, including the addition of extra plies				
				EXTERNAL/SMOOTH SIDE
	Layup	Type of filler	D (mm)	t (mm)
	2nd extra p.	0	211,5	0,37
	1st extra p.	90	215,6	0,37
	6	45	211,6	0,37
	5	0	201,8	0,37
	4	90	191,9	0,37
	3	-45	182,0	0,37
	2	-45	172,1	0,37
	1	90	162,3	0,37
	AL2024	M	152,4	0,76
Adhesive				
<ol style="list-style-type: none"> 1) Resin system EC138/W341 by ELAN-TECH® compatible with RTM6 able to cure in 24h at RT or 1:00h at 70°C. (consistent thnk and easy to store) [http://www.cristex.co.uk/uploads/certification/Elantech_EC138_W340_W341_ing.pdf] 2. Cyanoacrylate based glue for fast metal parts bonding 3. 3M™ Scotch-Weld Epoxy Adhesive 100 Plus [http://multimedia.3m.com/mws/media/667050/3m-scotch-weld-epoxy-adhesive-dp100-plus-clear.pdf] 				
Doubler				
Nr. 2 metal bars (AL2024) 490mmx63mmx4.5mm				
Nr.1 circular sheet metal D=152.4mm,t=0.76				
Bolts				
Nr. 80 corrosion resistant rivets CR7773S-06-07W Protruding head Titanium Maxibolt® [http://fsrivet.com/6bFQM3N9IqgAHoP/1330038238Cherry_Titanium_Maxibolt.pdf]				

Table 22: Materials and components used for external access repair

The effectiveness of the proposed repair method was assessed via computational approach and Figure 95 shows the FE model developed.

The LBCs were the same used with previous FE models. Taking into account that only data from literature were available about the strength allowable, the following conservative assumptions were made:

- Composite patch and metal disk were not included in the simulation;
- Damaged stiffener was partially fixed to the skin by fasteners, in particular a lower percentage of RBE2 with respect to the reference panel was used where the fasteners are located.

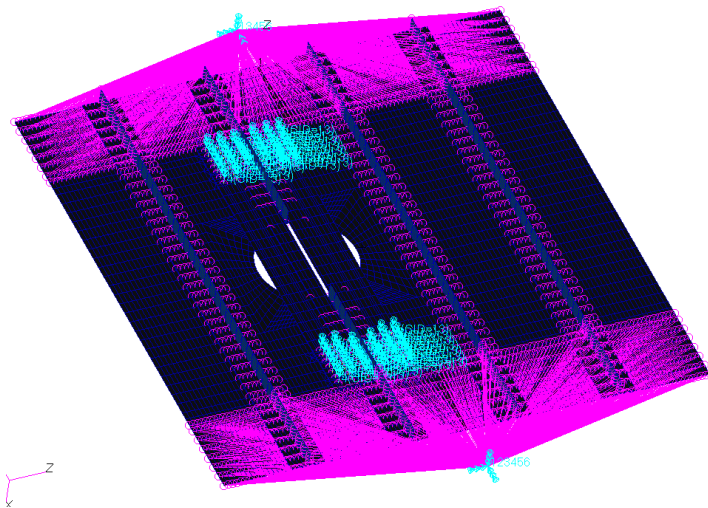


Figure 95 - FE model of the repaired with sole external accessibility

For the design of the bolted joint, it was assumed to have a MS>10% corresponding approximately to a load of 105 tons.

Fasteners were simulated using the utility available in MSC.Patran that implements the Rutman method [44]. In agreement with Boeing Design Manual, relevant checks on the fasteners concerning bolt-bending and shear, were performed by extracting the load applied on each bolt taken from a non linear analysis (SOL106-MSC.Nastran).

For what concerns the shear check, the critical load was a function of the load acting on the bolts and its diameter, while in case of the bolt-bending check, the critical load was function of the ultimate bearing strength values, the thicknesses of the involved parts and the diameter of the rivets.

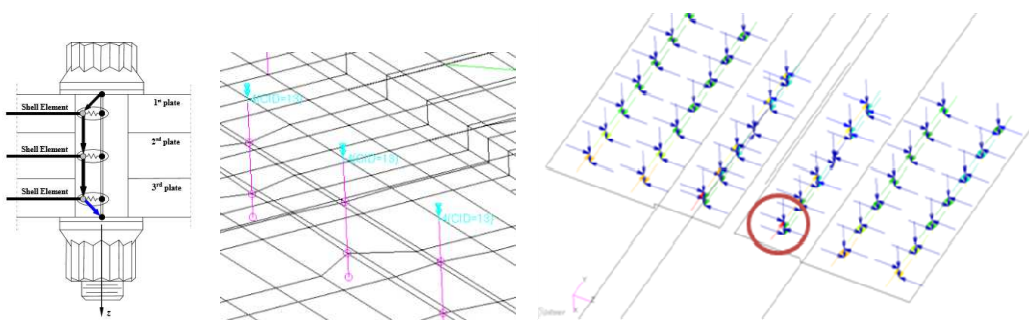


Figure 96 - Rutman-Fastener method to simulate the rivets and FEA to extract the loads acting on each bolt

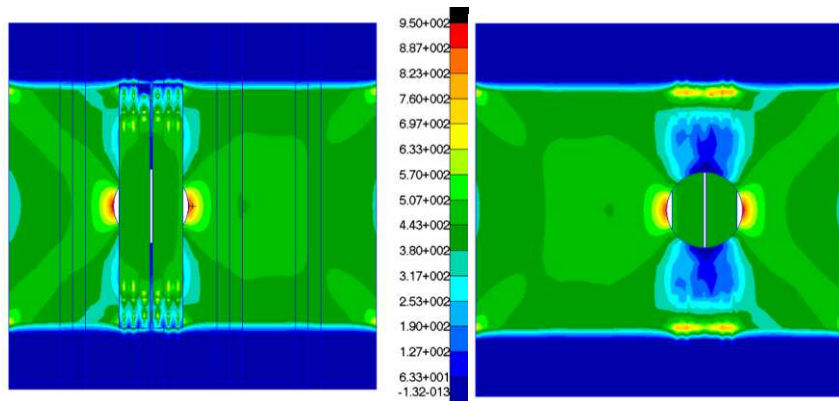


Figure 97 - FE Non Linear Analysis (SOL106 - MSC.Nastran) Stress Distribution - Max Principal (Layer 0°) for a tensile load of 105 tons

5.4.4. Results

In a load controlled progressive failure analysis, the ultimate failure load corresponds to the load level at which the edge displacement first increases indefinitely without increasing the load due to continuous failure caused by the degraded elements and at the end start reducing. Figure 98 shows the comparison between the failure loads obtained by running the SOL400 implicit non linear on the four models analyzed in this study: pristine, damaged and repaired with limited and full access to the damaged part.

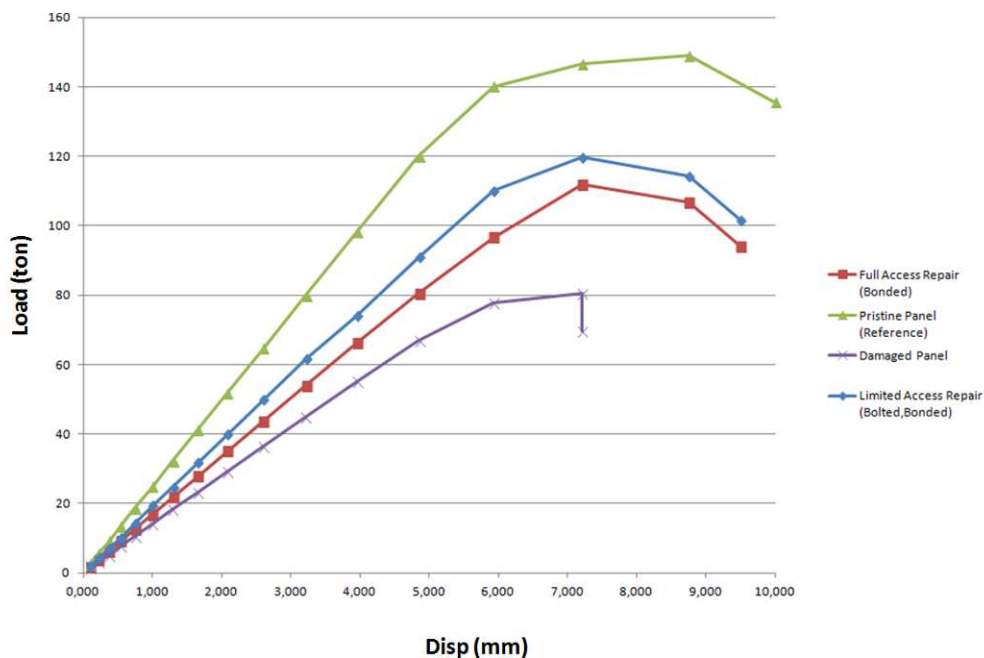


Figure 98 - Comparison of failure loads based on SOL400 for pristine, damaged and repaired panels.

Model		FPF/UF (ton)
1	Pristine Panel (reference)	141/148
2	Damaged Panel	77/80
3	Full Access Repair (Bonded Patch)	95/111
4	Limited Access Repair (Bonded composite patch, Bolted doublers)*	110/119

Table 23: Comparison of failure loads based on SOL 400 non-linear analysis

As shown in Figure 98, the stiffness of the damaged specimen was significantly lower than that of the pristine specimen, whereas the stiffness of the repaired specimen was increased significantly.

Table 23 shows that the damage would cause significant stiffness and strength reduction, by almost 50% for strength, under axial tension loadings. Full access composite patch repair could restore the static strength for about 67% of its initial state, while limited access repair with conservative assumptions could restore the static strength for about 78% of its initial state. Taking into account that pristine panel has a U.L. of 148 tons, both repair solutions will ensure a U.L. still included between the L.L. and U.L. of the pristine panel, 20% lower for the bolted joint repair and 25% lower for bonded joint repair

5.4.5. Implementation of the repair for COMPRIP project

As previously illustrated, since AER Project foresees experimental loading tests that will be performed by French team, during the development of project, the Dept. Of Industrial Engineering - Aerospace section identified and purchased a Portable Dual Zone Hot Bonder (Figure 99), certified by big aerospace companies as Boeing and Airbus, at the US retailer BriskHeat Corporation.

The Out-of-Autoclave equipment was identified by a market research based on costs and performance evaluations. Firstly, this equipment was used to perform some trials repairs (Figure 100), then once the damage scenario was set by partners of AER Project (paragraph 5.4.3) and design of the repair was developed, the definitive repair was implemented on the panel that will be tested by French team, following the design illustrated (Figures 101-102).



Figure 99 - ACR3 Dual Zone Hot Bonder portable kit

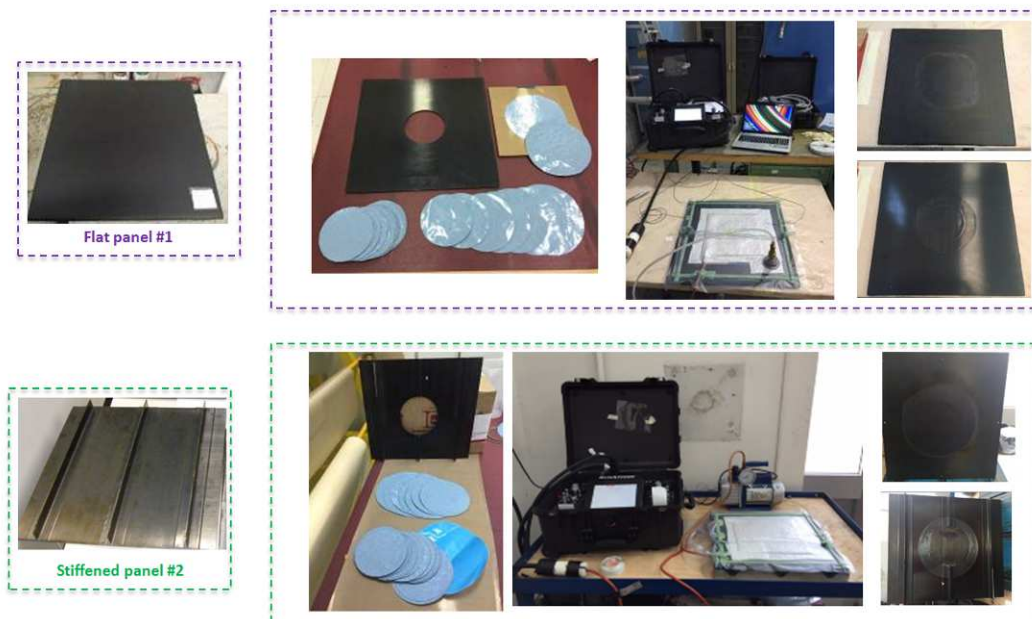


Figure 100 - Trials repairs



Figure 101 - Implementation of the AER Project repair (1)



Figure 102 - Implementation of the AER Project repair (2)

CONCLUSIONS AND FUTURE DEVELOPMENTS

The present work, based on a numerical-experimental approach, was aimed to assess the effectiveness of ER concepts in case of a fixed-wing composite aircraft, subjected to battle-field damage represented by a large and challenging damage condition that required a structural repair.

The activity was carried out within the research project called "COMPRIP", a contract between the Department of Industrial Engineering - Aerospace Section and Italian Ministry of Defense - Segretariato Generale della Difesa e Direzione Nazionale Armamenti - Direzione degli Armamenti Aeronautici e per l'Aeronavigabilità - Ufficio Tecnico Territoriale di Napoli.

All activities were carried out following decisions agreed in the frame of "*Aircraft Expedient Repair*" Program, by a Consortium including experts coming from Armed Forces of US, Germany, France and Italy. The objective of AER Project is to develop and exchange aircraft Expedient Repair techniques, procedures, and methodologies that will enhance the ER capabilities of the contributing participants individually and collectively, thus improving operational aircraft performance through restoring full operational capability of composite structures while reducing repair costs.

Thesis work started with an extensive review of literature on the type of damages and conventional/unconventional repair procedures of aircraft composite structures. Then, several FE investigations on bonded repairs were performed to define a set of guidelines to use in the design of bonded repairs. It is worth to point out that no Structural Repair Manual (SRM) was available in the test case.

Relevant aspects this study was the quite low sensitivity of adhesive stress to mismatched adherend layups and the reduction of peak stresses due to few over laminates adding. Furthermore, over laminate plies can have positive effect on repair durability giving environmental and impact protection. Another important influence from this investigation concerns how the stacking sequence of the composite adherends affects the scarf joints. The adhesive shear stress distribution along the scarf is not constant, local variations in adherend stiffness, corresponding to changes in ply orientation, result in peak shear and peel stresses in the adhesive bondline adjacent to the stiff plies of the adherends. This feature shows the potential for elastic tailoring of the scarf joint to dictate load transfer through adherend ply orientation. The stress components of a single scarf angle joint was shown to be dominated by shear. It was also shown that peak local stresses arise at stress concentrations around the termination of 0° plies, away from the adhesive centerline.

After this phase, following the decisions agreed by partners of AER Program, a set of structural demonstrators (flat composite stiffened panels representative of lower wing skins) were identified, redesigned and manufactured using RTM

process. The repair scenario identified concerned a large representative and challenging damage condition that required a structural repair.

Thus, once achieved a good confidence level with main aspects involved in a composite repair process, a versatile predictive model applicable to the design of repairs for conventional (as reported in the SRM) and unconventional damages, was developed and implemented with the aim to investigate stress and strain concentration, the failure initiation and failure progression mechanisms of involved composite structures.

The assessment involved a relative comparison of four FE models, representing pristine, damaged with simulated ballistic damage and repaired with a condition of full and a limited accessibility to the damaged composite structure. In case of the full access condition, a scarf repair based on adhesives and filler composite patch was taken into account, while for the limited access condition, a coupling of bonded patch and bolted substantiation was considered. Taking into account the conservative assumptions mainly due to strength allowable coming from literature, results have shown that the damage would cause significant stiffness and strength reduction, by almost 50% for strength, under axial tension loadings. Full access composite patch repair could restore the static strength for about 67% of its initial state, while limited access repair with conservative assumptions could restore the static strength for about 78% of its initial state. Taking into account that pristine panel has a U.L. of 148 tons, both repair solutions will ensure a U.L. still included between the L.L. and U.L. of the pristine panel, 20% lower for the bolted joint repair and 25% lower for bonded joint repair. After the numerical design of the repair, the limited access concept was implemented. If numerical predictions will be confirmed by experimental tests that will be performed by French partner, the main goal of AER project will be successfully achieved. This means that a battle-damaged aircraft can continue to fly after the ER, up the next scheduled maintenance, but with some limitations (i.e. limitation in manoeuvre and maximum speed).

Future work may be focused on geometric optimization of the repair in order to save more parental material, now in conflict with small scarf angle aimed to maximize structural efficiency, including more loading conditions.

A further development could be, in agreement with partners of AER Project to define a set of suitable experimental procedures to include in a shared document, precursor of an Expedient Repair Manual.

This aspect has an important industrial relapse in the case of an aircraft, remarkable in terms of cost, since the standard model developed guarantees a reduction of downtimes, resulting in an increase of the hours of airworthiness, a reduction of maintenance costs and/or replacement of damaged components

Acknowledgements

I would express my gratitude to my supervisor, prof. Leonardo Lecce. Nothing is more helpful than a good mentor to help you learn and grow in research and in daily life. Thank you for your support, continuous guidance, suggestions, astute critics and your patience.

A special thanks goes to Major Gennaro Abate (DAAA-UTT, Regional Technical Office for the Air Armaments Division) for the support provided during the project "COMPRIP".

My appreciation also goes to my colleagues at the department of Industrial Engineering - Aerospace section at the University of Naples Federico II to provide me with advices, support and assistance throughout my study. Thank you for teaching me that a good work can be achieved only via a team game and goals can be reached only with the contribution of all the colleagues.

A special thanks goes to my dear friend/colleague Giuseppe. Year by year, challenge after challenge, I recognize the luck to have met a sincere and positive brother as you. I wish you all the best.

Thank you to all of you!

References

1. D.Voyls, P. O'Connell. "An Overview of Aircraft Expedient Repair", 52nd AIAA/ASME/ASCE/AHS/ASC Structures, Structural Dynamics and Materials Conference, <http://dx.doi.org/10.2514/6.2011-1817>.
2. Robson, J. E.; "The repair of composite materials", PhD Thesis, 1993, Imperial College.
3. Heslehurst, R.B.; "Analysis and modelling of damage and repair of composite materials in aerospace", Numerical Analysis and Modelling of Composite Materials.
4. S.H. Myhre and C.E. Beck, "Repair Concepts for Advanced Composite Structures," Journal of Aircraft.
5. Volkersen O. Luftfahrtforschung 15:41-47 (1938).
6. Goland M, Reissner E.J.; Applied Mechanics, 1944.
7. Hall, S.R.; Raizenne, M.D.; Simpson, D.L.; "A proposed composite repair methodology for primary structures", 1989, pp. 479-483.
8. Gong X.J., Cheng P., Rousseau J., Aivazzadeh S.; "Effect of local stresses on static strength and fatigue life of patched composite panels".
9. Hashin, Z., "Failure Criteria for Unidirectional Fiber Composites," Journal of Applied Mechanics, June 1980, pp. 329-334.
10. M.N. Nahas, "Survey of Failure and Post-Failure Theories of Laminated Fiber-Reinforced Plastics and Composites", Journal of Composite Technology and Research, 1986.
11. M.J. Hinton, A.S. Kaddour and P.D. Soden, "A further assessment of the predictive capabilities of current failure theories for composite laminates: comparison with experimental evidence", Composite Science and Technology, (2004).
12. M.R. Garnish and V.M.K. Akula, "Review of degradation models for progressive failure analysis of fiber reinforced composites", Applied Mechanics Reviews, 2009.
13. S.W. Tsai, "A General theory of strength for anisotropic materials", Journal of Composite Materials, 1971.
14. R. Hill, "A Theory of Yielding and Plastic Flow of Anisotropic Metals", Proceedings of the Royal society of London, 1948.
15. L.J. Hart-Smith, "The first fair dinkum macro-level fibrous composite failure criteria". Proceedings 11th International Conference on Composite Materials, Vol. I, 1997, pp. 52-87.
16. R.F. Gibson, "Principles of Composite Material Mechanics", 2007.
17. Greenwood L., Boag T.G. and McLaren A.S., "Stress distributions in lap joints, Adhesion: Fundamentals and practice", 1969.
18. L.J. Hart-Smith, "Adhesive-bonded scarf and stepped-lap joints", report NASA-CR-112237, NASA, 1973.

19. Charalambides, M.N., Matthews, F.L.; Kinloch, A.J.; "Failure criterion for a double lap joint", *Computer-Aided Analysis of Composite Materials*, Imperial College, 1995.
20. Baker, A.A., "Repair techniques for composite structures", *Composite Materials in Aircraft Structures*, 1990.
21. Adams, R.D. and Wake, W.C. "Structural adhesive joints in engineering", 1984.
22. Baldan, A., "Adhesively-bonded joints and repairs in metallic alloys, polymers and composite materials", 2004.
23. Naveen Rastogi, B.P. Deepak, and Som R. Soni, "Stress Analysis Codes for Bonded Joints in Composite Structures," AIAA-1997-1341, *Collection of Technical Papers*.
24. Ojalvo I.U., Eidinoff H.L., *AIAA J*, 1978.
25. Tsai M.Y., Oplinger D.W., Morton J.J., *Eng. Appl. Sci.*, 1998.
26. Wah T., *Asme J., Eng. Mater. Technol.*, 1973.
27. Hart-Smith L.J., *NASA Contract Report*, 1973.
28. Adams R.D., Mallick V.J., *Adhesives*, 1992.
29. E.Beck, "Advanced Composite Structure Repair Guide," *Journal of Aircraft*, 1981.
30. Baker AA., "Joining and repair of aircraft composite structures", *Mech. Eng. Trans.*, 1996.
31. Oplinger D.W., "Mechanical fastening and adhesive bonding", *Handbook of composites*, 1998.
32. Harman A., Wang C.H., "Analytic and finite element stress predictions in two dimensional scarf joints", *Australian and International Aerospace Conference*, 2005.
33. ASTM D 5573-99, Standard practice for classifying failure modes in fiber-reinforced-plastic (FRP) joints. *Annual Book of ASTM Standards*, 2002.
34. Murray S. M., "Prepositioned Trailers for Aircraft Battle Damage Repair Support", *Air Force Institute of Technology, Wright Patterson Air Force Base, Ohio, Report No. AFIT/GLM/ENS-04-13*, March 2004.
35. Wang C.H., Gunnion A.J.; "On the design methodology of scarf repairs to composite laminates", *Composite Science and Technology, Science Direct*, 2006.
36. Gunnion AJ, Herszberg I. "Parametric study of scarf joints in composite structures". *Compos Struct* 2006;75:364–76
37. S. Laurenzi, M. Marchetti "Advanced Composite Materials by Resin Transfer Molding for Aerospace Applications" *Materials Science, Composite Materials, "Composites and Their Properties"*, book edited by Ning Hu, ISBN 978-953-51-0711-8, Published: August 22, 2012.
38. G0926/RTM6 Carbon fiber fabric Data Sheet, Hexcel Corporation.

39. Whitney, J.M.; "Structural analysis of laminated anisotropic plate", Technomic, Lancaster, PA, 1987.
40. Brunel J.E., Gresle B.; "Battle field damage repair of a helicopter composite frame-to-skin junction. Battlefield Technol.
41. FM® 300-2 Film Adhesve Tecnicl Data Sheet, Cyttec Engineered Materials.
42. T.E. Tay, G.Liu, V.B.C. Tan, X.S. Sun and D.C. Pham. "Progressive failure analysis of composites", Journal of Composite Materials, 2008.
43. M.R. Garnish and V.M.K. Akula. "Review of degradation models for progressive failure analysis of fiber reinforced composites", Applied Mechanics, 2009.
44. http://web.mscsoftware.com/events/vpd2007/na/presentations/tech_papers/8.p
45. Z.P. Marioli-Riga, D. Xenos. Reparability and cost analysis criteria for typical composite patch repairs.